

DETERMINATION OF EFFICIENCIES, LOSS MECHANISMS,
AND PERFORMANCE DEGRADATION FACTORS IN CHOPPER
CONTROLLED DC VEHICLE MOTORS

SECTION II

"THE TIME DEPENDENT FINITE ELEMENT MODELING OF
THE ELECTROMAGNETIC FIELD IN ELECTRICAL MACHINES -
METHODS AND APPLICATIONS"

Prepared for: NASA - Lewis Research Center and The Department of Energy

by: Electrical Engineering Department
University of Pittsburgh
Pittsburgh, PA 15139

Howard B. Hamilton, Principal Investigator
Elias Strangas, Research Assistant

FINAL REPORT

GRANT NSG #3163

DECEMBER 30, 1980

THE TIME DEPENDENT FINITE ELEMENT MODELING OF THE ELECTROMAGNETIC
FIELD IN ELECTRICAL MACHINES - METHODS AND APPLICATIONS

by

Elias G. Strangas

Dipl. Ing. in Electrical and Mechanical Engineering

National Technical University of Greece

M.S. in E.E., University of Pittsburgh

Submitted to the Graduate Faculty

of the School of Engineering

in partial fulfillment of

the requirements for the degree of

Doctor

of

Philosophy

University of Pittsburgh

1980

ACKNOWLEDGEMENTS

I would like to express here my gratitude to those people whose interest and contributions made this work possible. Dr. H. B. Hamilton suggested the topic, provided continuous guidance throughout the whole work and had very useful suggestions and observations regarding the final manuscript.

Very useful technical discussions and suggestions were contributed by Mr. E. F. McBrien, Mr. E. I. King, Mr. E. Wood, Mr. L. J. Long, Dr. M. Shah, Dr. S. J. Salon, and Mr. L. Montgomery. Dr. C. A. Hall's help with the time dependent finite element theory is greatly appreciated. I would also like to thank the members of the doctoral committee, Dr. Kusic and Dr. P. R. McCormick for their interest and constructive criticism.

This work was partially supported by NASA and the U. S. Department of Energy under Grant No. NSG - 3163.

ABSTRACT

Signature

Howard B. Hamilton

THE TIME DEPENDENT FINITE ELEMENT MODELING OF THE ELECTROMAGNETIC
FIELD IN ELECTRICAL MACHINES - METHODS AND APPLICATIONS

Elias G. Strangas, Ph.D.

University of Pittsburgh

A method is developed to calculate the field quantities at a cross section of an electrical rotating machine, and to use these quantities to calculate the machine parameters and performance. The method includes the effects of eddy currents and saturation and calculates the inductances, torque and losses due to eddy currents. It is applicable to cases which cannot be described by a constant set of parameters, but rather where these parameters become functions of time and field solution.

The method of time dependent finite elements is used, and a technique is developed to describe the airgap when the rotor is moving with respect to the stator. The solution techniques that can be applied to the resulting system of equations are investigated, and the method of the preconditioned conjugate gradient is described and applied. The underrelaxation method is applied to the calculations of the saturation levels in iron parts.

The solution of the magnetic potential at the cross section of the machine is used to calculate inductances through flux linkages, and torque through the application of the Maxwell stress tensor at a surface in the airgap. The techniques developed are used to calculate the performance of chopper controlled DC series machines used in electric vehicles and to predict torques and currents during the asynchronous starting of synchronous salient pole motors.

DESCRIPTORS

Asynchronous Starting	Chopper Controller
Conjugate Gradient Method	Damper Bars
DC Series Motors	Eddy Currents
Electromagnetic Fields	Finite Elements
Preconditioning	Saturation

TABLE OF CONTENTS

ACKNOWLEDGEMENTS	ii
ABSTRACT	iii
LIST OF FIGURES	viii
LIST OF TABLES	xii
1.0 INTRODUCTION.	1
1.1 Numerical Calculation of the Electromagnetic Field	2
1.2 The Calculation of Voltages, Inductances and Saturation of Iron Domains	3
1.3 The Asynchronous Starting of Synchronous Motors.	5
1.4 The Problem of Complex Waveform of the Input Voltage of Dc and AC Machines	6
1.5 The Continuous Modeling of the Electromagnetic Field - Incremental Inductances	7
1.6 Statement of the Problem	8
2.0 THE MAGNETIC VECTOR POTENTIAL AND THE QUANTITIES OF THE ELECTROMAGNETIC FIELD	10
2.1 The Magnetic Vector Potential	12
2.2 The Calculation of Induced Voltages and Eddy Currents	15
2.3 The Maxwell Stress Tensor	18
3.0 THE FINITE ELEMENT METHOD AS APPLIED TO THE ELECTROMAGNETIC FIELD CALCULATIONS.	23
3.1 The Variational Method.	23
3.2 Computing Considerations and the Formation of the System of Equations.	28
3.2.1 The Local Matrix and Vector	28
3.2.2 Boundary Values and Negative Coupling	30
3.2.3 Modeling the Airgap and Rotor Movement.	33

3.2.4	The Formation of the Global Matrix	37
3.3	Numerical Calculation of Torque	39
3.4	Calculation of the Permeability of Elements.	42
3.5	Calculation of Eddy Current Losses	45
4.0	SPARSE MATRIX ALGORITHMS APPLIED TO THE SOLUTION OF THE SYSTEM RESULTING FROM THE FINITE ELEMENT METHOD	48
4.1	Storage Techniques	49
4.2	Direct Methods of Solution	51
4.3	Iterative Methods of Solution.	52
4.4	The P-condition Number and the Preconditioning of a System.	54
4.5	The Conjugate Gradient Method.	55
4.5.1	Conjugate Directions	57
4.5.2	The Conjugate Gradient Algorithm	60
4.6	The Preconditioned Version of the Conjugate Gradient Method	62
4.6.1	Computer Considerations.	66
4.6.2	Determination of the Solution Technique for the Modeling of the Electromagnetic Field	67
5.0	THE OPERATION OF CHOPPER CONTROLLED DC SERIES MOTORS:	69
5.1	Calculation of Inductances and an Algorithm for the Calculation of Currents and Torque.	70
5.1.1	The Aitken Extrapolation	72
5.1.2	The Rotational Voltage	73
5.1.3	The Voltage Input and External Connections of the Machine	74
5.1.4	The Algorithm.	75
5.2	Application to an Electric Vehicle Machine	77
5.2.1	Characteristics of the Machine	78

5.2.2	Approximations and Assumptions	82
5.2.3	Results of the Computer Simulation	84
5.2.4	Airgap Radial Flux - Brush Positioning	90
6.0	THE STARTING OF SALIENT POLE SYNCHRONOUS MOTORS WITH DAMPER BARS.	97
6.1	The Electrical Equations of the Salient Pole Synchronous Machine	97
6.2	The Effect of Damper Bar Connections	102
6.2.1	Closed End Rings (Cage Winding).	102
6.2.2	Open End Rings (Grid Winding).	104
6.3	Calculation of Constants	106
6.3.1	External Connections	107
6.3.2	Self and Mutual Inductances of the Salient Pole Machine	107
6.4	The Algorithm and the Integration Scheme	116
7.0	CONCLUSIONS	128
	BIBLIOGRAPHY	131

LIST OF FIGURES

Figure No.		Page
2-1	Envelopes of the frame for the calculation of the conductivity of the magnetic materials	11
2-2	The grad Φ at symmetric points	16
2-3	The effect of eddy currents on the current distribution in a conductor	17
2-4	Stresses at a surface element	21
2-5	A surface on which the calculation of the torque can be carried out	22
3-1	For the determination of the periodicity conditions.	30
3-2	Modeling the air gap	34
3-3	Modeling the rotor movement in the global matrix	35
3-4	A collection of finite elements.	37
3-5	The calculation of torque in a machine	40
3-6	Max. error in μ versus solution number	43
3-7	Number of iteration in conjugate gradient versus solution number	43
3-8	For the calculation of the effective permeability of limited materials	45
4-1	A typical grid	49
4-2	Types of matrices	50
4-3	Storage of a generally sparse matrix	51
4-4	Steepest descent method.	56
4-5	Conjugate gradient method	60
4-6	A family of ellipsoids before and after preconditioning.	64
5-1	The external connections to a chopper controlled DC series motor	75

Figure No.		Page
5-2	Friction and windage losses	79
5-3	Dimension of rotor and stator.	80
5-4	Dimensions of the field winding	81
5-5	Dimensions of slot and armature conductors	81
5-6	The grid for the electric vehicle motor	85
5-7	Solid frame	86
5-8	Laminated frame	86
5-9	Voltage waveform	87
5-10	Torque waveform	88
5-11	Current waveform	89
5-12	Effect of brush position on resultant field distribution	92
5-13	M.V.P. on rotor surface brushes at 0°	93
5-14	Flux density on rotor surface brushes at 0°	93
5-15	M.V.P. at stator surface	94
5-16	Flux density at stator surface B	94
5-17	The magnetic field, brushes shifted 30 electrical degrees.	95
5-18	M.V.P. on rotor surface brushes at 30° electrical.	96
5-19	Flux density on rotor surface brushes at 30° electrical	96
6-1	Salient pole synchronous machine	99
6-2	Damper winding with closed rings	103
6-3	Damper winding with open rings	105
6-4	Equivalent circuit for the supply of the motor	107
6-5	The grid for a six pole generator.	110
6-6	Current in phase a, $\theta = 0$	111

Figure No.		Page
6-7	Current in phase b, $\theta = 90^\circ$ electrical	111
6-8	Current in the field.	112
6-9	Current in damper bar 1	112
6-10	Current in damper bar 2	113
6-11	Current in damper bar 3	113
6-12	Current in damper bar 4.	114
6-13	Current in damper bar 5	114
6-14	The algorithm for the starting of a synchronous machine . .	115
6-15	RMS values of armature current	118
6-16	Average value of torque	118
6-17	Slip = 0.15	119
6-18	Slip = 0.25	120
6-19	Slip = 0.45	121
6-20	Slip = 0.5	122
6-21	Slip = 1.0	123
6-22	Field at a cross section, Step 1.	124
6-23	Field at a cross section, Step 2.	124
6-24	Field at a cross section, Step 3.	124
6-25	Field at a cross section, Step 4.	124
6-26	Field at a cross section, Step 5.	125
6-27	Field at a cross section, Step 6.	125
6-28	Field at a cross section, Step 7.	125
6-29	Field at a cross section, Step 8.	125
6-30	Field at a cross section, Step 9.	126

Figure No.		Page
6-31	Field at a cross section, Step 10126
6-32	Torque at various slips127

LIST OF TABLES

Table No.	Page
5-1 Parameters of a DC Machine	80
5-2 Test and Simulation Results	89

1.0 INTRODUCTION

Availability of modern, high speed digital computers with large storage capacity and speed of operations has had a dramatic impact on the methods of treating electrical machinery problems. Sophisticated numerical techniques, yielding accurate results, have replaced the approximate analytical approaches of the past.

The modern techniques are based upon rigorous mathematical analysis methods; also they have stimulated the further development of the methods. A case in point is the problem of calculating the electromagnetic field of a machine. Initially only the field in small regions was calculated by rather crude means based on the fundamental magnetomotive force and flux waves. Then, the finite difference method emerged, providing a powerful tool with capability and accuracy exceeding that of the earlier methods. Following this, the finite-element approach to machine analysis was introduced, providing a still more capable analysis technique.

In addition to the fact that numerical solutions are more elegant, fast, and accurate than analytical calculations or hand flux mapping, they are able to yield solutions to new problems which, because of their complexity, could not be treated with the old methods. A typical example discussed in this dissertation, is that of the performance of motors operated from a controller which produces a complex voltage waveform. An analytical treatment of such a problem requires many simplifications which introduce relatively large errors and which do not provide accurate knowledge of the internal conditions of the machine. The problem of starting a synchronous motor, although entirely different, has the

same characteristics as the operation of a machine from a controller, since the varying saturation and speed result in continuously changing operating conditions and parameters.

1.1 Numerical Calculation of the Electromagnetic Field

The first numerical techniques applied to the solution of the electromagnetic field in a machine were derived not from a mathematical theory which would provide an approximation to the exact solution of the field, but instead from the development of an equivalent circuit that used capacitors and resistors to represent conductivities and reluctances. The voltages calculated from this circuit were equivalent to the value of the magnetic vector potential in a cross section of the machine. Later, the mathematical method of finite differences was used to provide the systems of equations that would yield the field quantities. Erdelyi and Fuchs^{(1,2)*} presented a series of papers using this method for the calculation of the field distribution in DC machines, accounting for saturation in the iron regions. They later applied their technique to synchronous machines.⁽³⁻⁵⁾ This approach resulted in flux plots from which self and mutual inductances could be calculated as well as steady state, transient and subtransient reactances. Demerdash and Hamilton^(6,7) demonstrated that by using an effective permeability which yields the same energy in the field as does the integral $\int B dH$ over one half of a

*Parenthetical references placed superior to the line of text refer to the bibliography.

period, one may assume a sinusoidal flux density and magnetomotive force and solve the problem in the frequency domain. Salon⁽⁸⁾ used the finite difference method to calculate eddy currents in generator rotors by solving for the field distribution in the time domain. He used the solution in the frequency domain to calculate voltages, currents and inductances and to solve a plethora of problems related to the operation of synchronous cylindrical rotor generators.

In 1971, Chari⁽⁹⁾ introduced the finite element method to the solution of electromagnetic fields. Although much more complicated to program than the finite difference method, it was proved superior for the modeling of boundaries and contours of materials and for giving detailed information about the field in specific areas of interest. Demerdash and Niehl⁽¹⁰⁾ demonstrated in 1977 the superiority of this method in accounting for the saturation of iron. In 1975, Foggia, Sobonnadiere and Silvester⁽¹¹⁾ presented a time dependent solution for the saturated eddy current case. A theoretical analysis of the time dependent finite element method is found in the thorough treatment of the subject by Douglas and Dupont⁽¹²⁾, where the nonlinearity is taken into consideration with the use the of Crank-Nicolson-Galerkin approximation.

1.2 The Calculation of Voltages, Inductances and Saturation of Iron Domains

The solution of the electromagnetic field in an electrical machine requires knowledge of the current densities in the conductors. This

presents difficulties since what is known in most cases are the voltages at the terminals of the machine, rather than the currents. When the performance of the machine is to be determined, one has to resort to the use of self and mutual inductances. These are calculated by injecting currents into the conductors, solving the electromagnetic field and from that calculating the voltages induced in all of the windings. In DC machines this is quite straight forward. In AC machines it is simpler to use the "two Reaction" Theory and to calculate d- and q- axis parameters for various current and saturation levels. This is a model developed from the Blondell-Park transformation and results in a system of differential equation, which can be used to predict the machine performance.

The above approach contains certain unavoidable approximations. Firstly, the inductances are considered constant, whereas they actually depend upon the saturation level and thus are functions of the currents. Secondly, the two reaction theory presupposes linearity, so that superposition can be possible, which is not the case when saturation is present. Thirdly, the effect of eddy currents and skin effect on the inductances and the field solution is neglected, but usually this cannot be done without significant loss of accuracy.

In the time domain solution, one can do away with inductances by incorporating in the system of equations resulting from the finite element method, the dependence of the current on the applied and induced voltages⁽⁸⁾. This technique, however convenient, increases drastically both the storage requirements and the number of the operations needed for the solution of the resulting system of equations.

1.3 The Asynchronous Starting of Synchronous Motors

The main consideration in the design of a synchronous motors is obviously the performance during synchronous operation, while the starting performance often receives less attention. A synchronous motor is usually started by connecting across the line or through an auto transformer. Only in the case of very large motors are they brought up to near synchronous speed by a smaller "pony" motor before the armature is energized. In the case of direct starting, the field excitation terminals are not energized, but are connected through a resistor of comparatively large ohmic value for the starting up period and the field is energized at near synchronous speed. The torque developed during the start-up is that of an asynchronous motor, but due to the dissymmetry of the rotor it contains an oscillation of twice the slip frequency (120-0 Hz for a supply of 60 Hz). These torque oscillations can be in resonance with the connected load, resulting in severe stresses on the shaft and gear teeth used to connect motor and load. Also, the currents induced in the damper bars may increase the temperature to the point that the bars and pole faces are overheated and distorted.

These problems have been recognized and addressed for a number of years. As early as 1930, Linville⁽¹³⁾ wrote a classic paper in which he derived equivalent circuits for rotor and stator; resolved the starting currents and magnetomotive forces into forward and backward components and applied the Blondell-Park equations to calculate currents and torque.

Since then, numerous studies have been conducted to cover both the mechanical and electrical aspects of asynchronous starting⁽¹⁴⁻²⁵⁾. The

majority are along the lines of Linvill's work. Barret⁽²⁶⁾ recently (1980) presented a technique for predicting the starting performance of a motor with solid, salient poles, by calculating, in the time domain, the magnetic field using the finite element method in the airgap and an analytical one in the rotor iron.

The technique of developing equivalent circuits for the rotor and stator, in the d- and q- axis, has been refined with the use of numerical tools, and more lumped elements have been added; some, time and slip dependent to account for the space harmonics of the magnetic field and skin effect. Goodman⁽¹⁶⁾ included higher current harmonics and corresponding inductances in the model of the machine for which he calculated the torque during asynchronous starting. The work of Jovanovski⁽²⁷⁻³⁰⁾, strongly supported by experimental results, gives an insight in the current distribution in the damper winding, both in the case of squirrel cage and grill connections of the damper bars.

1.4 The Problem of Complex Waveform of the Input Voltage of DC and AC Machines

This problem is of relatively recent origin, since it is only in the last few years that controllers have been developed utilizing solid state components (thyristors or transistors) for supply, switching or chopping to yield a lower voltage level. However, some analytical work⁽³¹⁾ was done as early as 1912 on the operation of DC series motors from an AC power supply. The performance of DC series motors when controlled by pulses was extensively examined by Franklin^(32, 33)

with the aid of analytical tools. In this treatment the inductance and resistance of the machine was assumed to be constant, independent of frequency and saturation. A simple model of the machine was developed, which describes the operation under various speeds, pulse widths and periods.

Such a model, although useful to describe the machine from a user's viewpoint does not appear to accurately predict the performance of a machine. Recently, DeWolf⁽³⁴⁾, and Hamilton et al⁽³⁵⁾ demonstrated that the inductance and apparent resistance of a DC machine are functions of the current level and the frequency, and noted the need for a model which would encompass this phenomena. The external manifestation of the eddy currents is an increased resistance resulting from eddy current losses in both conductors and in iron portions in the magnetic circuits and the saturation effect is that of changing inductance as the currents change.

1.5 The Continuous Modeling of the Electromagnetic Field - Incremental Inductances

In both cases, of synchronous motor starting and of complex input waveforms, the problems associated with predicting, from design parameters, the performance of the machine stem from the nonlinearities involved. These nonlinearities are caused by the eddy currents induced in the solid iron parts and the conductors and by saturation of the magnetic circuit. At any instant, the rate of change of induced voltages and of currents will depend on the input voltages and also on these nonlinearities to an extent that can be determined only by the knowledge

of the electromagnetic field at that instant. Incremental, or small signal, inductances can be calculated from the voltages induced in conductors due to small changes of currents. These inductances, together with terminal voltages, can be subsequently used to predict currents and voltages after a small time increment, and this process can be repeated and the machine performance calculated for any desired length of time.

1.6 Statement of the Problem

As has been discussed in the previous articles, the performance of a machine under continuously changing operating conditions poses a problem, both to the user and the designer which cannot be treated using traditional tools. The main causes of such an inability of conventional methods to deal with this problem are the presence of nonlinearities, namely the eddy currents in conductors and solid iron portions of the machine and the magnetic saturation of the iron of the magnetic circuit.

In this dissertation this problem is addressed to as basically a transient problem from the viewpoint of the calculation of the electromagnetic field. The method of time dependent finite elements is utilized to model the field in the time domain, and both mathematical models and computer techniques are developed to solve efficiently the resulting systems of equations and to calculate parameters which describe the performance of the machine, as currents in conductors, induced voltages and torque.

While doing so, it becomes clear that electric machinery problems which appeared to be entirely unrelated, can be treated with the same

techniques. Two such transient problems are discussed in this dissertation, the asynchronous starting of synchronous motors and the operation of a chopper controlled DC machine, and essentially the same techniques are used on both to predict their performance. Such a uniform way of analyzing the operation of a machine gives a deeper understanding of the principles on which the theory of electrical machinery is based, and at the same time makes possible the calculation of such parameters as the proper shift of the brushes in a DC machine and the current distribution in the damper bars of a synchronous motor.

2.0 THE MAGNETIC VECTOR POTENTIAL AND THE QUANTITIES OF THE ELECTROMAGNETIC FIELD

The solution of the electromagnetic field inside an electrical machine is a difficult task, even when one is to use numerical techniques, because of the fact that the field is three dimensional and the geometry changes with time. In order to simplify the problem, the machine is assumed to be infinitely long and all the currents parallel to its axis. These assumptions mean that the field is two dimensional at any cross section of the machine, and simpler techniques can be used for its solution. The field in the end region cannot be considered two dimensional, at least at cross sections perpendicular to the axis of the machine. It has to be calculated separately, and the portion of the inductances due to it - the "end-turn inductances" - evaluated. The currents and voltages can be subsequently adjusted by taking these end-turn quantities into consideration.

A similar problem is encountered when dealing with the eddy currents both in solid iron portions of the machine and in laminated steel. The eddy currents induced have to travel a distance longer than twice the length of the machine, since they have to form a loop by following a route transverse to the axis of the machine, as is shown in Figure 2-1. The conductivity assigned therefore to iron portions must not be the actual but a corrected one equal to:

$$\sigma_{\text{corr}} = \sigma \cdot \frac{l_1 + l_3}{l_1 + l_2} \quad (2-1)$$

where σ is the actual conductivity of the medium, σ_{corr} the corrected one and ℓ_1 and ℓ_2 defined in Figure 2-1.

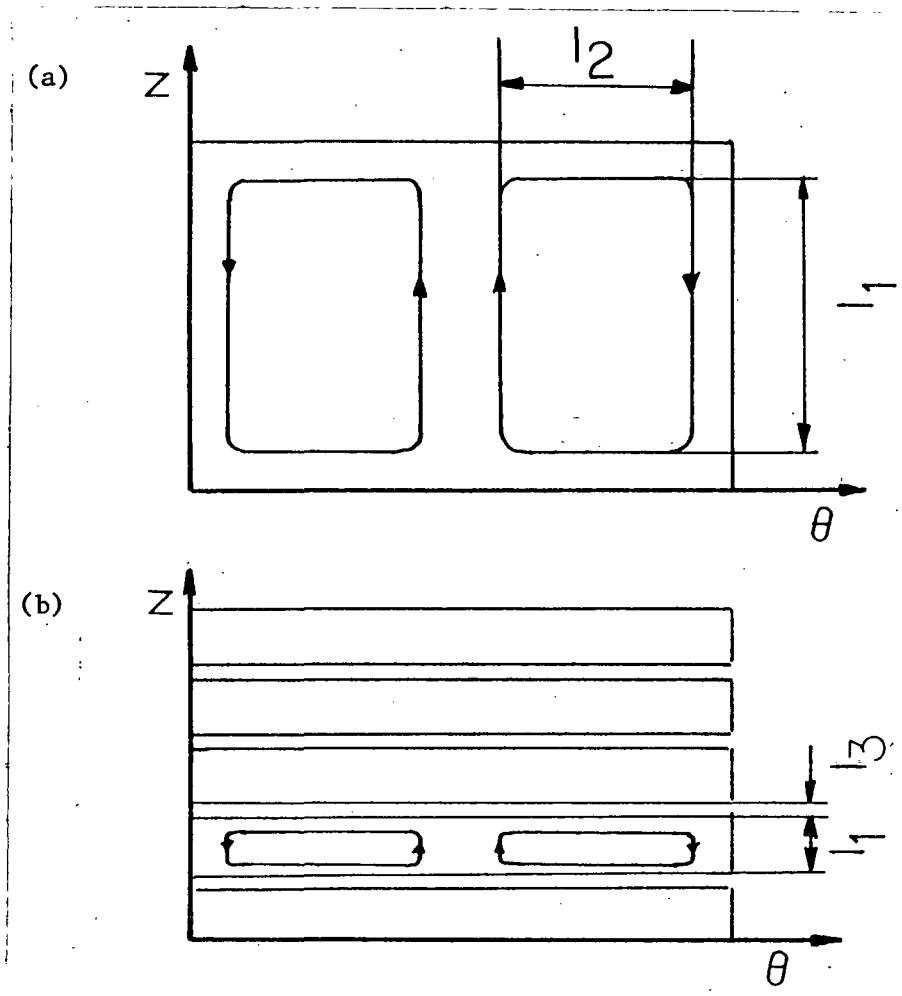


Figure 2-1 Envelopes of the frame for the calculation of the conductivity of magnetic materials in (a) solid iron and (b) laminations.

2.1 The Magnetic Vector Potential

From Maxwell's equations⁽³⁶⁾, in a domain without electric charges or polarized media, and neglecting displacement currents:

$$\nabla \times B = \mu (J + \nabla \times M) \quad (2-2)$$

where μ is the magnetic permeability of the medium, B is the magnetic flux density, J is true density, M the magnetic moment density and $\nabla \times M$ the atomic magnetization currents. In the absence of permanent magnets this term can be dropped, and equation (2-2) becomes:

$$\nabla \times B = \mu (J) \quad (2-3)$$

Also, from Maxwell equations:

$$\nabla \cdot B = 0 \quad (2-4)$$

Equation (2-4) implies that B can be written as the curl of a function:

$$B = \nabla \times A \quad (2-5)$$

where A is defined as the magnetic vector potential. In terms of A , equation (2-3) can be written as:

$$\nabla \times \left(\frac{1}{\mu} \nabla \times A \right) = J \quad (2-6)$$

The current density J may be either a known quantity, as is the case of applied currents in conductors, or unknown as is the case of eddy currents.

Again, from Maxwell equations:

$$\nabla \times E = - \frac{\partial B}{\partial t} \quad (2-7)$$

From equations (2-7) and (2-5):

$$\nabla \times E = - \frac{\partial}{\partial t} (\nabla \times A) \quad (2-8)$$

Thus, E and $-\frac{\partial}{\partial t} A$ differ by a function, the curl of which is zero. This function, therefore, can be written as a gradient of another function ϕ :

$$E = - \frac{\partial}{\partial t} A + \text{grad } \phi \quad (2-9)$$

This last equation means that the actual electric field which can be measured by any suitable method, can be considered to be due to the rate of change of the magnetic field (as given by the first component of the right hand side of eq. 2-9), and to an applied electric scalar potential ϕ (the second part of the right hand side of eq. 2-9).

On the other hand, the current densities can be calculated from the strength of the electric field as:

$$J = \sigma E \quad (2-10)$$

where σ is the conductivity of the medium.

From the above equations, it is clear that when instead of the true current densities, the applied electric field is known, equation (2-6) can take the form:

$$\nabla \times \left(\frac{1}{\mu} \nabla \times A \right) = - \sigma \left(\frac{\partial}{\partial t} A - \text{grad}\Phi \right) \quad (2-11)$$

The first term of the right hand side of eq. (2-11), $-\sigma \frac{\partial A}{\partial t}$, is the density of the eddy currents, while the second part, $-\partial \text{grad}\Phi$, is the superimposed current density due to a voltage, either applied, or present due to electrostatic phenomena.

In the two dimensional case addressed here, equations (2-6) and (2-11) can be further simplified, since the only component of the current densities present is the z component, parallel to the axis of the machine. This means that the z component of the flux density, B_z , vanishes from equation (2-4), and from (2-5):

$$B_x = \frac{\partial}{\partial y} A_z \quad (2-12)$$

$$B_y = - \frac{\partial}{\partial x} A_z \quad (2-13)$$

and,

$$\nabla \times \left(\frac{1}{\mu} \nabla \times A \right) = - \nabla \left(\frac{1}{\mu} \nabla \cdot A_z \right) \cdot \bar{k} \quad (2-14)$$

\bar{k} being the unit vector in the z direction.

Equations 2-7 and 2-12 then become:

$$\nabla \left(\frac{1}{\mu} \nabla A_z \right) = J_z \quad (2-15)$$

$$\nabla \left(\frac{1}{\mu} \nabla A_z \right) = \sigma \left(\frac{\partial}{\partial t} A_z - \frac{\partial \Phi}{\partial z} \right) \quad (2-16)$$

These two equations can be solved over the entire cross-section of the machine. Knowledge of the value of A_z makes it possible to calculate flux densities, induced voltages, eddy currents, losses, forces and torque.

2.2 The Calculation of Induced Voltages and of Eddy Currents

If a conductor is located in an electromagnetic field and is either moving with respect to the field, or the field quantities are changing with time, an electrical field results in the conductor, of magnitude:

$$E = - \frac{\partial A}{\partial t} + \text{grad}\Phi \quad (2-9)$$

$\text{grad}\Phi$ is the component of the field strength due to charges or external connections, whereas the induced voltage is $-\frac{\partial A}{\partial t}$. If the field solution holds for a length ℓ the voltage along this length will be:

$$V = \ell (\text{grad}\Phi)_z \quad (2-17)$$

If that part of the machine which was called a conductor above, is a line in the iron of the rotor or stator parallel to the axis of the machine, this voltage must be zero. This can be shown with the aid of Figure 2-2. Assume A and A' to be lines symmetric with respect to the axis of a two pole machine, and parallel to it. Due to the symmetry the voltages, currents and magnetic vector potentials at A and A', and B and B' will be opposite. On the other hand, all points at every cross section are connected together; therefore, they have the same potential. It follows that this voltage should be zero. This means that the eddy current density in solid portions of rotor stator are given by

$$J_{\text{eddy}} = -\sigma \frac{\partial A}{\partial t} \quad (2-18)$$

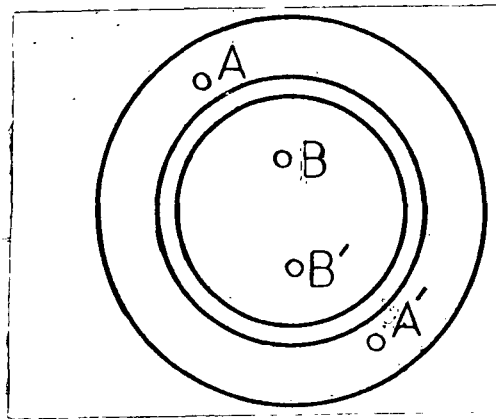


Figure 2-2 The grad ϕ at symmetrical points.

In an actual conductor, the value of grad ϕ is not identically zero. The field strength is given again by equation 2-9. When the current

density is constant over the cross section of the conductor, E is also constant. The $\text{grad}\phi$, since it is externally applied, it is also uniform over the cross section.

In the case of solid conductors of relatively large cross sectional area, eddy currents can be induced, and the resulting skin effect can be pronounced. The skin effect can be treated in the same fashion as eddy currents. These eddy currents sum to zero and the total current remains the same as if there were no eddy currents, with an increased apparent resistance.

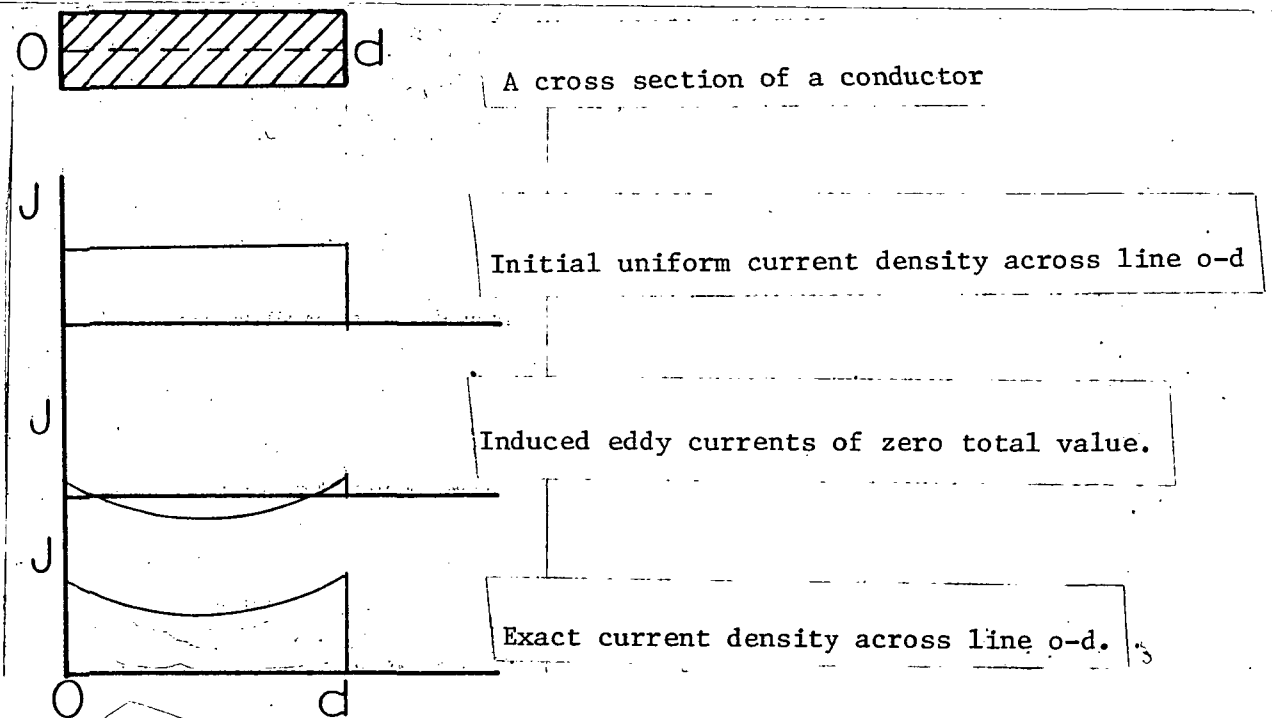


Figure 2-3 The effect of eddy currents on the current distribution in a conductor

In order to account for these eddy currents, revisions are needed in the way in which the magnetic vector potential is calculated:

Total current in a conductor, of cross-section S , is given by:

$$I = \int_S J \, dS = -\sigma \int_S \frac{\partial A}{\partial t} \, dS + \sigma \int_S \text{grad } \Phi \, dS \quad (2-19)$$

$$I = -\sigma \frac{\partial}{\partial t} \int_S A \, dS + \sigma \text{grad } \Phi \, S \quad (2-20)$$

If the total current is known, the current density in a conductor takes the form:

$$J = -\sigma \frac{\partial A}{\partial t} + \sigma \text{grad } \Phi \rightarrow J = -\sigma \frac{\partial A}{\partial t} + \frac{I}{S} - \frac{\sigma}{S} \cdot \frac{\partial}{\partial t} \int A \, dS \quad (2-21)$$

and the average induced voltage in the conductor is:

$$V_{\text{ind}} = - \left[\frac{\partial}{\partial t} \int_S A \, dS \right] \cdot \frac{l}{S} \quad (2-22)$$

These last equations can be simplified when numerical methods are used, as will be shown later.

2.3 The Maxwell Stress Tensor⁽³⁶⁾

In field theory it should be possible to calculate the net force on a given volume element within a magnetic field, using only the field conditions on the surface of the volume. This implies that the field is

a stress transmitting medium in the same sense that a string tying two weights together is the medium that transmits a force from one weight to the other.

Following this procedure and considering that the force of a given volume is transmitted through the surface of this volume, the transmitting force can be formulated in terms of a quantity known as the Maxwell stress tensor, T . The $\alpha\beta^{\text{th}}$ component of this tensor, $T_{\alpha\beta}$, is constituted so that the α^{th} component, dF_{α} , of the force, dF , transmitted across a surface element, dS , and whose component is the β^{th} direction is dS_{β} , is given by:

$$d F_{\alpha} = \sum_{\beta=1}^3 T_{\alpha\beta} dS_{\beta} \quad (2-23)$$

When the following restrictions are imposed for the medium through which the forces are transmitted:

1. B is linear, i.e. permeability is not a function of the field.
2. No permanent magnets are present.
3. There is no magnetorestriction.

then the stress tensor components take the form:

$$T_{\alpha\beta} = H_{\alpha} B_{\beta} - \frac{\delta_{\alpha\beta}}{2} H_{\gamma} B_{\gamma} \quad (2-24)$$

where $\delta_{\alpha\beta}$ is the Kronecker delta.

The matrix corresponding to this tensor is:

$$T = \frac{1}{\mu} \begin{bmatrix} \frac{1}{2} (B_x^2 - B_y^2 - B_z^2) & B_x B_y & B_x B_z \\ B_x B_y & \frac{1}{2} (B_y^2 - B_z^2 - B_x^2) & B_y B_z \\ B_x B_z & B_y B_z & \frac{1}{2} (B_x^2 - B_y^2 - B_z^2) \end{bmatrix} \quad (2-25)$$

This tensor can be reduced to three components by transformation to principal axes. These axes are oriented so that one is parallel to the vector B and the two other are perpendicular to each other and the first axis:

$$T = \frac{1}{\mu} \begin{bmatrix} B^2 & 0 & 0 \\ 0 & B^2 & 0 \\ 0 & 0 & B^2 \end{bmatrix} \quad (2-26)$$

To illustrate, assume such a system of axes. One will be parallel to B and the other perpendicular to B , in the plane defining by B and the normal to the surface element as shown in Figure 2-4. It is seen from this figure that the magnetic field bisects the angle between the normal to the surface, and the direction of the resultant and force acting on the surface.

In the application to electrical machines, the main concern is the torque acting on the rotor of the machine, rather than forces. A surface on which such a calculation can be carried out, is a cylinder lying in the air gap and enclosing the rotor as shown in Figure 2-4.

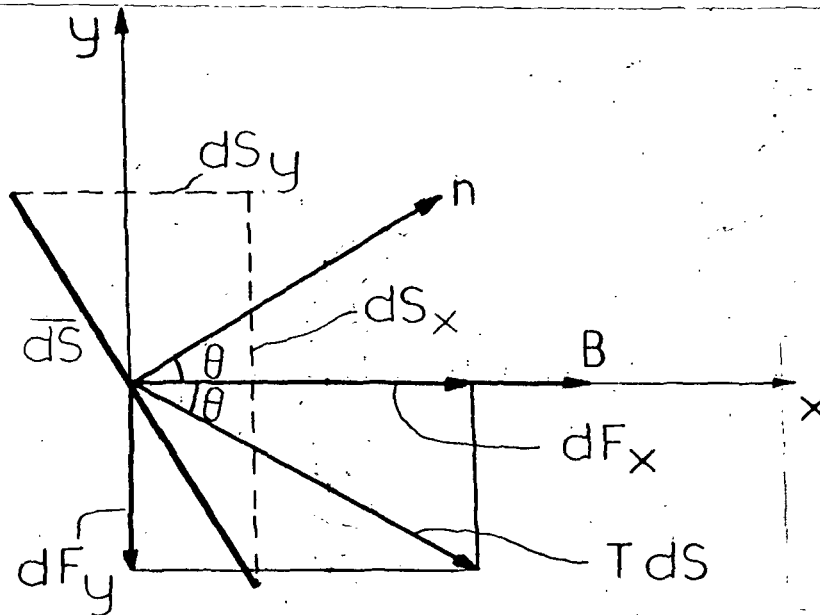


Figure 2-4 Stresses at a surface element.

From the solution of the magnetic vector potential in the cross-section of the machine, the flux density can be calculated everywhere in the machine. In the two dimensional case, equation (2-23) and (2-25) become:

$$d F_{\alpha} = \ell \cdot \sum_{\beta=1}^3 T_{\alpha\beta} dS_{\beta} \quad (2-27)$$

$$T = \frac{1}{\mu} \begin{bmatrix} \frac{1}{2}(B_x^2 - B_y^2) & B_x B_y \\ B_x B_y & \frac{1}{2}(B_y^2 - B_x^2) \end{bmatrix} \quad (2-28)$$

The torque on the rotor, M , can then be calculated by integrating over the surface of the cylinder by:

$$M = \oint \vec{r} \cdot d\vec{F}$$

(2-29)

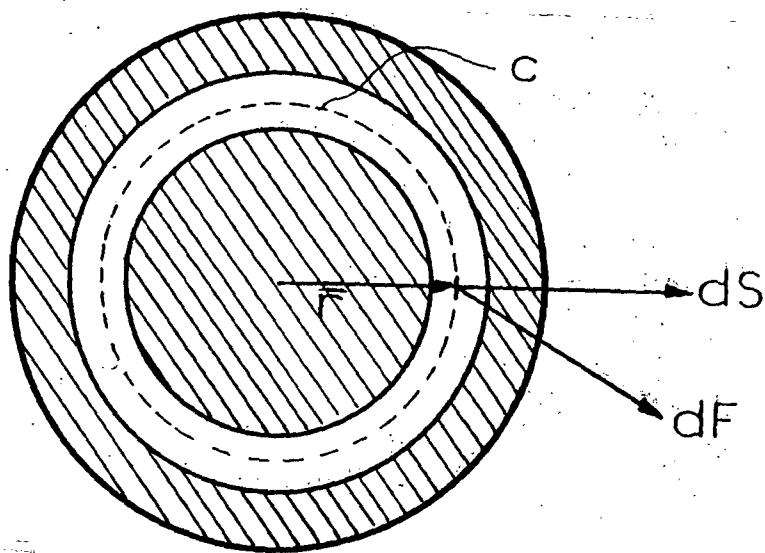


Figure 2-5 A surface on which the calculation of the torque can be carried out.

3.0 THE FINITE ELEMENT METHOD AS APPLIED TO THE ELECTROMAGNETIC FIELD CALCULATIONS

Since 1970, considerable research has been devoted to applying the Finite Element Method to the solution of equations 2-15 and 2-16 at the cross-sections of electrical machines and to utilizing the result for the prediction of their performance. A general overview of the applications and of the theoretical background is given by Chari⁽³⁷⁾. What follows is a brief description of the general method, the mathematical analysis and the techniques that utilize the solution to calculate the field quantities and machine parameters. Both the time independent and time dependent solutions are discussed, since the electrical machinery problems are solved in the time domain.

3.1 The Variational Method

Consider a class of problems characterized by equations of the form:

$$A(x) \cdot u(x) = f(x) \quad x \in \Omega \quad (3-1)$$

where $u(x)$ satisfies the boundary conditions:

$$\frac{\partial u}{\partial n} = 0 \quad (\text{or } u=0) \text{ on the boundary } \partial\Omega$$

and A is a strongly elliptic 2nd order partial differential operator, i.e. it can be written as:

$$A(x) = \sum_{|\alpha|, |\beta| \leq 2} (-1)^{|\alpha|} D^\alpha a_{\alpha\beta}(x) D^\beta \quad (3-2)$$

where the operator D^α is defined as

$$D^\alpha u(x) = \frac{\partial^{\alpha_1}}{\partial x_1^{\alpha_1}} \frac{\partial^{\alpha_2}}{\partial x_2^{\alpha_2}} \dots \frac{\partial^{\alpha_n}}{\partial x_n^{\alpha_n}} \quad (3-3)$$

A bilinear form $B(u,v)$ can be associated with A , where:

$$B(u,v) = \int \sum_{|\alpha|, |\beta| \leq 2} a_{\alpha\beta}(x) D^\alpha v D^\beta u \, dx \quad (3-4)$$

It is possible now to replace the original problem of solving (3-1) with the equivalent variational one of finding a u , such that:

$$B(u,v) = (f,u) \quad \forall u \in H_0^2(\Omega) \quad (3-5)$$

where the operation (\cdot, \cdot) denotes the $L_2(\Omega)$ inner product and $H_0^2(\Omega)$ is a Hilbert space of second order.

The Galerkin method for the solution of (3-5) can be now described.

Identify a subspace, $S_h(\Omega)$ of $H_0^m(\Omega)$, spanned by a system of linearly independent functions $\{\phi_i(x)\}_{i=1}^G$. Each element of $S_h(\Omega)$ is of the form:

$$V(x) = \sum_{i=1}^G c^i \phi_i(x) \quad (3-6)$$

where C^i $i = 1, \dots, G$ are constants.

The Galerkin approximation to $u(x)$ is then a function

$$U(x) = \sum A^i \phi_i(x) \quad (3-7)$$

which satisfies:

$$B(U, V) = (f, v) \quad \forall v \in S_h(\Omega) \quad (3-8)$$

Thus, by introducing (3-7) in (3-8) a system of linear equations is obtained:

$$\sum K_{ij} A^j = f_i \quad (3-9)$$

where

$$K_{ij} = B(\phi_i, \phi_j) \quad (3-10)$$

$$f_i = (f, \phi_i)$$

For the time dependent case, equation (3-1) becomes:

$$\frac{\partial u(x, t)}{\partial t} + A(x) \cdot u(x, t) = f(x, t) \quad (3-11)$$

$$u(x, 0) = u_0(x)$$

and the Galerkin approximation at every t becomes:

$$u(x, t) = \sum A^i(t) \cdot \phi_i(x) \quad (3-12)$$

which satisfies:

$$\left(\frac{\partial U(t)}{\partial t}, V\right) + B(U(t), V) = (f(t), V) \quad (3-13)$$

$$t \in (0, T]$$

and the initial condition

$$(U(0), V) = (u_0, v) \quad (3-14)$$

Again, by introducing (3-12) into (3-13) it is possible to obtain a system of first order differential equations:

$$\sum_{j=1}^G [G_{ij} \dot{A}^j(t) + K_{ij} A^j(+)] f_i(t) \quad (3-15)$$

where:

$$G_{ij} = (\phi_i, \phi_j)$$

$$K_{ij} = B(\phi_i, \phi_j) \quad (3-16)$$

$$f_i = (f, \phi_i)$$

The system of linear equations (3-8) can be solved using various methods; an overview of these methods is given in the following chapter. The system of first order differential equations, (3-15) requires further consideration.

In the case of linear coefficients, the Crank-Nicholson-Galerkin approximation can be used. To start, a partition P of the time interval $(0, T)$ is introduced, composed of the set $\{t_0, t_1, \dots, t_R\}$ where

$0 = t_0 < t_1 < \dots < t_R = T$ with $t_{n+1} - t_n = \Delta t_n$; also the sequence $\{u^n\}_{n=0}^R$ is introduced to denote the value of the function $U(x,t)$ at all the points of the partition P . Then, a family of finite-difference Galerkin approximations is introduced, associated with $\theta (0 \leq \theta \leq 1)$ which represents solutions to:

$$\left(\frac{u^{n+1} - u^n}{\Delta t}, v \right) + (1-\theta) B(u^{n+1}, v) + \theta (u^n, v) = (f(+), v) \quad (3-17)$$

Expansion of (3-18) using (3-14) yields:

$$\sum_j [G_{ij} + \Delta t(1-\theta)K_{ij}] A_j^{n+1} = \sum_j (G_{ij} - \Delta t \cdot \theta \cdot K_{ij}) A_j^n + \Delta t f_i \quad (3-18)$$

which for every n is a system of linear equations that can be solved with the same methods used for (3-9). In nonlinear cases, the differential operator (3-2) becomes a function of the solution u . Denoting

$$B(w; u, v) = \int_{|\alpha|, |\beta| \leq 2} \sum a_{\alpha\beta}(x, w) D^\alpha v D^\beta u \, dx \quad (3-19)$$

then, a two level predictor corrector version of the previously described Crank-Nicholson-Galerkin approximation is given by:

$$\left(\frac{W_{m+1} - U_m}{\Delta t}, v \right) + B(U_m; \frac{1}{2} (1+\theta) W_{m+1} + \frac{1}{2} (1-\theta) U_m, v) = 0 \quad (3-20)$$

$$\left(\frac{U_{m+1} - U_m}{\Delta t}, v \right) + B\left(\frac{1}{2} (1+\theta) W_{m+1} + \frac{1}{2} (1-\theta) U_m; \frac{1}{2} (1+\theta) U_{m+1} + \frac{1}{2} (1-\theta) U_m, v\right) = 0 \quad (3-21)$$

Such an approach requires the solution of two systems of linear algebraic equations, for W_{m+1} and U_{m+1} , at each time step.

3.2 Computing Considerations and the Formulation of the System of Equations

Throughout this investigation, linear triangular elements have been used, since they can be easily defined over any domain, and simple enough to be handled in a computer program. The details of the calculations associated with them are presented herein.

3.2.1 The Local Matrix and Vector of a Linear Triangular Element

Assume a triangle with vertices at (x_1, y_1) , (x_2, y_2) , (x_3, y_3) . The linear interpolation functions ϕ_i :

$$\phi_i = a_i x + b_i y + c_i \quad (3-19)$$

should be 1 at the point i and zero at the other two points. From this consideration, the constants a_i , b_i , c_i can be calculated as:

$$\begin{bmatrix} a_1 & b_1 & c_1 \\ a_2 & b_2 & c_2 \\ a_3 & b_3 & c_3 \end{bmatrix} = \begin{bmatrix} x_1 & x_2 & x_3 \\ y_1 & y_2 & y_3 \\ 1 & 1 & 1 \end{bmatrix} \quad (3-22)$$

From equation (2-5), the quantities $B(\phi_i, \phi_j)$ are given by:

$$\begin{aligned} B(\phi_i, \phi_j) &= \int \frac{1}{\mu} \frac{d}{dx} \phi_i \frac{d}{dy} \phi_j = \frac{1}{\mu} \int a_i a_j ds \\ &= \frac{1}{\mu} a_i a_j \frac{\Delta}{2} \end{aligned} \quad (3-23)$$

where:

$$\Delta = 2 \int ds = x_1 (y_2 - y_3) + x_2 (y_3 - y_1) + x_3 (y_1 - y_2) \quad (3-24)$$

Defining the integrals over an element:

$$\begin{aligned}
 I_1 &= \int x \, ds = (x_1 + x_2 + x_3) \Delta/6 \\
 I_2 &= \int y \, ds = (y_1 + y_2 + y_3) \Delta/6 \\
 I_3 &= \int xy \, ds = [(x_1 + x_2 + x_3)(y_1 + y_2 + y_3) + (x_1 y_1 + x_2 y_2 + x_3 y_3)] \Delta/24 \\
 I_4 &= \int x^2 \, ds = (x_1^2 + x_2^2 + x_3^2 + x_1 x_2 + x_2 x_3 + x_3 x_1) \Delta/12 \\
 I_5 &= \int y^2 \, ds = (y_1^2 + y_2^2 + y_3^2 + y_1 y_2 + y_2 y_3 + y_3 y_1) \Delta/12
 \end{aligned} \tag{3-25}$$

Then,

$$\begin{aligned}
 (\phi_1, \phi_j) &= \int (a_1 x + b_1 y + c_1) (a_j x + b_j y + c_j) \, ds = \\
 &= [a_i a_j I_4 + b_i b_j I_5 + c_i c_j I_0 + (a_i b_j + a_j b_i) I_3 \\
 &\quad + (c_i a_j + c_j a_i) I_1 + (b_i c_j + b_j c_i) I_2] \tag{3-26}
 \end{aligned}$$

and for f constant over the element:

$$(\phi_i, f) = \int (a_i x + b_i y + c_i) f = f(a_i I + b_i I + c_i) \Delta/2 \tag{3-27}$$

If:

$$\begin{aligned}
 G_{ij} &= -\sigma (\phi_i, \phi_j) \\
 K_{ij} &= B (\phi_i, \phi_j) \\
 f_i &= (f, \phi_i)
 \end{aligned} \tag{3-28}$$

the local matrix has as its ij^{th} entry the term $G_{ij} + \Delta t(1-\theta)K_{ij}$ and the local vector has as the i^{th} entry the term $f_i + (G_{ij} - \Delta t\theta K_{ij})A_i^n$.

3.2.2 Boundary Values and Negative Coupling

It is a characteristic of electrical machines that at points having the same radius and differing in angle by one pole pitch, the flux densities are of equal value and opposite direction, and that the flux lines (equipotential lines) run parallel to the outer shell, which means that the whole shell surface is at a constant magnetic potential. By assigning zero values to the potential of the points of this surface, the potential at points shifted by one pole pitch assumes opposite values, with the result that calculation of the potential of points of the machine which lie outside an angle corresponding to a pole pitch is redundant.

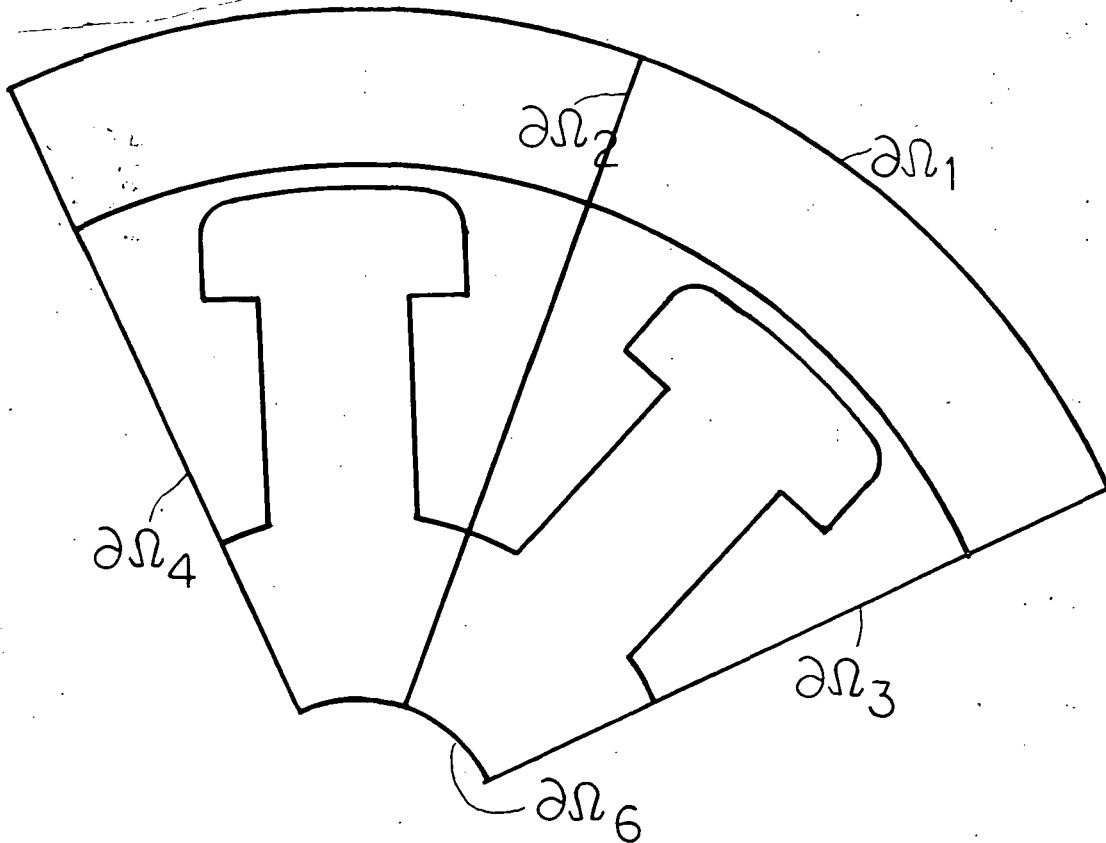


Figure 3-1. For the determination of the periodicity conditions.

In Figure 3-1 the value of A at $\partial\Omega_1$ and $\partial\Omega_6$ is zero. This results:

$$A(r) \partial\Omega_3 = - A(r) \partial\Omega_2 = A(r) \partial\Omega_4 \quad (3-29)$$

This case is treated by constructing compatible boundaries at $\partial\Omega_2$ and $\partial\Omega_3$, i.e. the grid is such that the nodes at the two boundaries correspond one-to-one and the corresponding ones have the same radius.

Assume an element having distribution functions ϕ_1, ϕ_2, ϕ_3 and values at the nodes of A_1, A_2 and A_3 . The solution inside the element is then given by:

$$A = A_1 \phi_1 + A_2 \phi_2 + A_3 \phi_3 \quad (3-30)$$

The ij^{th} entry of the local matrix is:

$$a_{ij} = -\sigma(\phi_i, \phi_j) + (1-\theta) \Delta t_n B(\phi_i, \phi_j) \quad (3-31)$$

and the i^{th} entry of the local vector is

$$S_{i-t_i} = (f, \phi_i) + [-\sigma(\phi_i, \phi_j) - \theta \Delta t_n B(\phi_i, \phi_j)] A^n \quad (3-32)$$

When the value of the magnetic vector potential at one point, A_1 , is the opposite of that at another point, A_1' , equation (3-30) becomes:

$$A = -A_1' \phi_1 + A_2 \phi_2 + A_3 \phi_3 = A_1' (-\phi_1) + A_2 \phi_2 + A_3 \phi_3 \quad (3-33)$$

which means that a new shape function $\phi_1' = -\phi_1$ can be used, and since:

$$B(\phi_i, \phi_j) = -B(-\phi_i, \phi_j) = -B(\phi_i, -\phi_j) \quad (3-34)$$

$$(\phi_i, \phi_j) = -(-\phi_i, \phi_j) = -(\phi_i, -\phi_j) \quad (3-35)$$

the local matrix and vector become

$$\Lambda = \begin{bmatrix} a_{11} & -a_{21} & -a_{13} \\ -a_{21} & a_{22} & -a_{23} \\ -a_{31} & a_{32} & a_{33} \end{bmatrix} \quad (3-36)$$

$$V = \begin{bmatrix} -s_1 \\ s_2 \\ s_3 \end{bmatrix} - \begin{bmatrix} t_{11} & -t_{13} & -t_{13} \\ -t_{21} & t_{22} & t_{23} \\ -t_{31} & t_{32} & t_{33} \end{bmatrix} \begin{bmatrix} A_1^n \\ A_2^n \\ A_3^n \end{bmatrix}$$

when $A_1 = -A_1'$ and $A_2 = -A_2'$, it follows easily from the previous considerations that:

$$\Lambda = \begin{bmatrix} a_{11} & a_{12} & -a_{13} \\ a_{21} & a_{22} & -a_{23} \\ -a_{31} & -a_{32} & a_{23} \end{bmatrix} \quad (3-37)$$

$$V = \begin{bmatrix} -s_1 \\ -s_2 \\ s_3 \end{bmatrix} - \begin{bmatrix} t_{11} & t_{12} & -t_{13} \\ t_{21} & t_{22} & -t_{23} \\ t_{31} & -t_{32} & t_{33} \end{bmatrix} \begin{bmatrix} A_1^n \\ A_2^n \\ A_3^n \end{bmatrix} \quad (3-38)$$

3.2.3 Modeling the Airgap and Rotor Movement

For the purposes of this study and the computer programs developed, the rotor and the stator are considered defined by coaxial cylindrical surfaces and include iron, copper, insulation and also air regions. Also, of course the airgap is defined by two coaxial cylindrical surfaces. The air gap links two regions which move with respect to each other with the passage of time. For this reason, the whole domain - rotor, stator and air gap - cannot be discretized in a unique, time independent fashion. If the air gap is excluded, the remaining two regions (rotor and stator), although moving in space, can have unique discretizations and global matrices, since they are independent of the position of the domain and its movement.

In Figure 3-2 the discretization of the air gap is shown for three consecutive time instants. Assuming a discretization of the rotor and stator such that the number of points on their surfaces interfacing the gap are equal, S_1 is defined as the point on the stator slice modeled, which is the leftmost on the surface interfacing the gap, and R_1 the corresponding point on the rotor surface. G_1 is then defined as the midpoint between S_1 and R_1 . Figure 3-2(a) then, is enough to define a discretization of the airgap for this initial position of rotor and stator. It must be noted that the points at the right hand side of the boundary of the slices, S_N , G_N and R_N are to be coupled with S_1 , G_1 and R_1 .

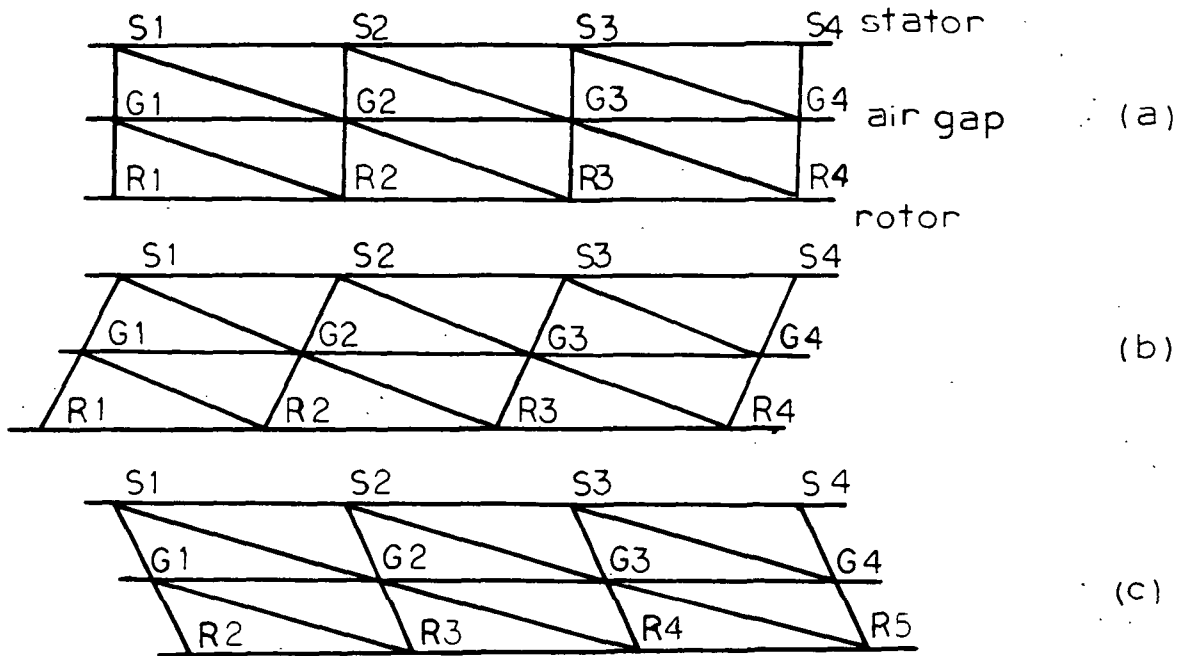


Figure 3-2 Modeling the air gap

As the rotor moves, the elements of the air gap are reconstructed but are still defined by the same nodes. It is evident that the rectangles and elements of the air gap will be skewed for a period of time, but after the angle of point R2 has become closer to the angle of S1, the nodes defining the elements of the air gap must change, in the fashion shown in Figure 3-2(c). The negative coupling will remain as before, since the solution is sought for the initial slices of the rotor and stator.

The initial relative position of the rotor and stator slice is shown in Figure 3-3(a). As in Figure 3-3(b), after a short time R2 corresponds to S1 and corresponding to -S1 is point -R2. After some time lapse the slice of the rotor modeled is shifted completely outside the corresponding slice of the rotor. The correspondence of point will

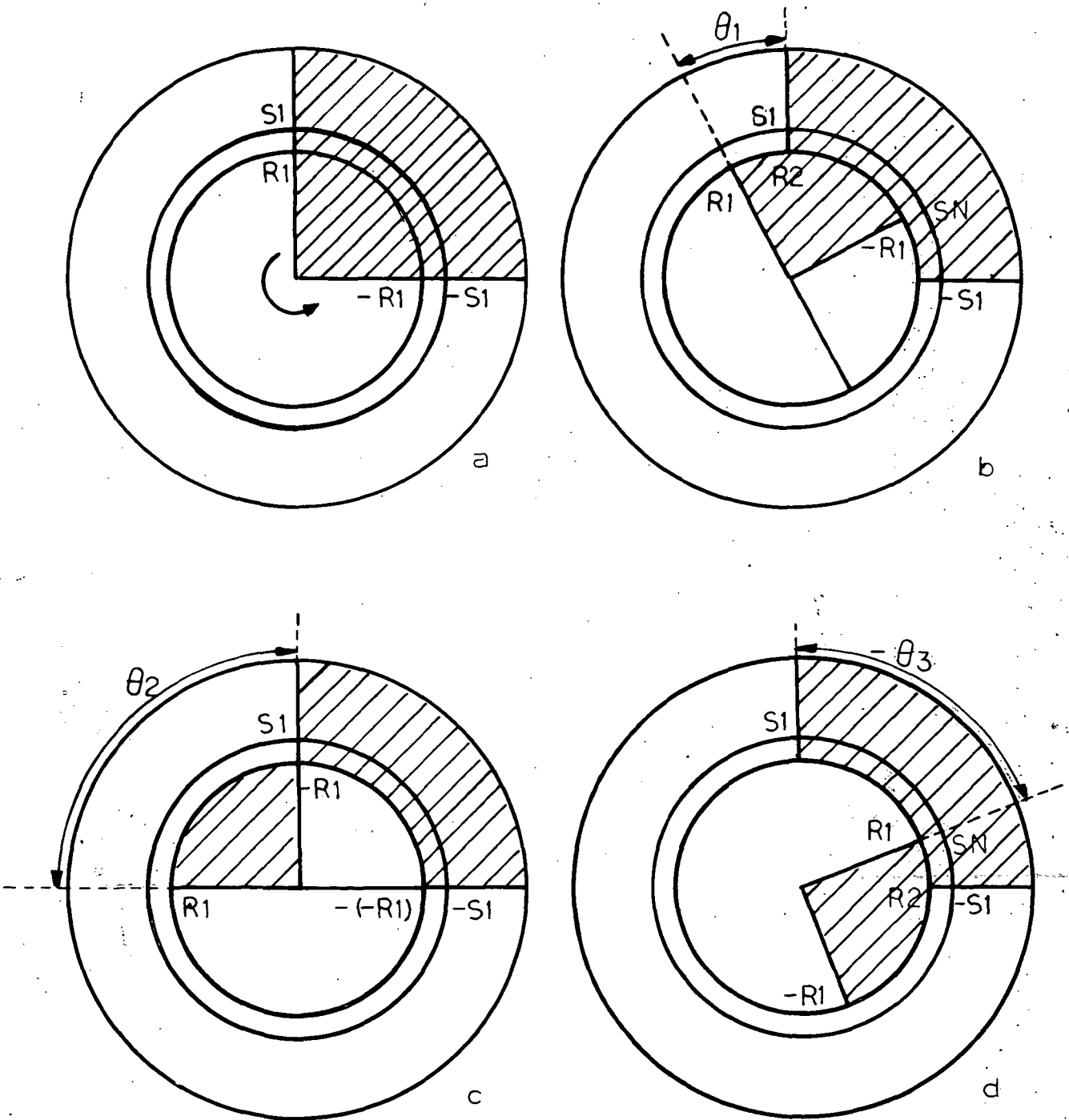


Figure 3-3 Modeling the rotor movement in the global matrix

be as shown in Figure 3-3(c) and it will be necessary to solve for the opposite of the values of the rotor surface.

Such a movement results in changes in geometry of the gap, which in turn causes changes in the nodes and the local matrices of the gap elements. These changes do not markedly affect the global matrix; they only affect the entries related to the points at the surfaces of the rotor and stator, and the points in the air gap.

Programming this movement in a computer is not as complicated a problem as it first appears. The treatment is based on a pointer, which shows which point on the rotor surface is corresponding to S1 and whether it is coupled positively or negatively to the gap points. If at time zero, an angle of zero is assigned to all the points at the right side of the rotor and stator slices, and the angle of the points at the left hand side is α , and if δ is the minimum angle between two consecutive points on the rotor surface, then the pointer moves down the rotor-air gap interface when the angle of point R1 exceeds $\alpha + \delta/2$ (for clockwise movement) and changes sign every time it reaches the point which was originally the rightmost.

The local matrices of the airgap elements are formulated taking the negative couplings into account. Such a technique makes it unnecessary to solve in the whole rotor domain, which for a six pole machine would give a matrix prohibitively large to manipulate within a reasonable computer time.

3.2.4 The Formulation of the Global Matrix

In every time step of the solution, the permeability of many of the materials and the conductivity of some of them may change. In order to avoid unnecessary calculations, the values of G_{ij}/σ and μK_{ij} in equations (3-28) must be stored, since they are independent of σ and μ . Each 3x3 local matrix is symmetric, therefore, only six of its nine entries have to be stored. After every time step, μ and possibly σ are recalculated for each element, and subsequently the local matrices. The global matrix is then assembled, taking into consideration the negative couplings of boundaries. The following example illustrates the way the matrix is assembled.

Assume local matrices and vectors for the elements in Figure 3-4.

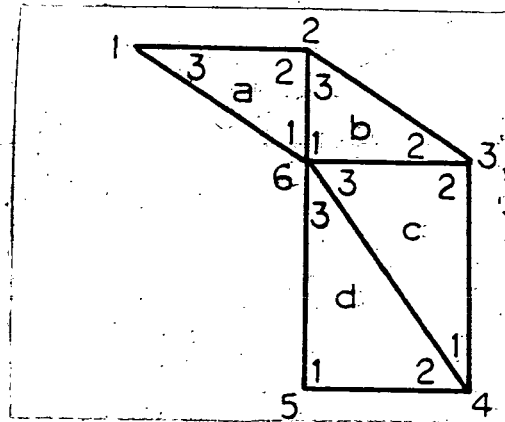


Figure 3-4. A collection of finite elements; the node numbering outside the elements is global, inside is local

$$\lambda^{(a)} = \begin{bmatrix} a_{11} & a_{12} & a_{13} \\ a_{21} & a_{22} & a_{23} \\ a_{31} & a_{32} & a_{33} \end{bmatrix} \quad v^{(a)} = \begin{bmatrix} a_1 \\ a_2 \\ a_3 \end{bmatrix}$$

$$\lambda^{(b)} = \begin{bmatrix} b_{11} & b_{12} & b_{13} \\ b_{21} & b_{22} & b_{23} \\ b_{31} & b_{32} & b_{33} \end{bmatrix} \quad v^{(b)} = \begin{bmatrix} b_1 \\ b_2 \\ b_3 \end{bmatrix}$$

(3-39)

$$\lambda^{(c)} = \begin{bmatrix} c_{11} & c_{12} & c_{13} \\ c_{21} & c_{22} & c_{23} \\ c_{31} & c_{32} & c_{33} \end{bmatrix} \quad v^{(c)} = \begin{bmatrix} c_1 \\ c_2 \\ c_3 \end{bmatrix}$$

$$\lambda^{(d)} = \begin{bmatrix} d_{11} & d_{12} & d_{13} \\ d_{21} & d_{22} & d_{23} \\ d_{31} & d_{32} & d_{33} \end{bmatrix} \quad v^{(d)} = \begin{bmatrix} d_1 \\ d_2 \\ d_3 \end{bmatrix}$$

The global matrix and vector become:

$$\Lambda = \begin{bmatrix} a_{33} & a_{23} & 0 & 0 & 0 & a_{13} \\ a_{32} & a_{22} + b_{33} & b_{23} & 0 & 0 & a_{12} + b_{13} \\ 0 & b_{32} & b_{22} + c_{22} & c_{12} & 0 & b_{12} + c_{23} \\ 0 & 0 & c_{21} & c_{11} + d_{22} & d_{12} & c_{13} + d_{23} \\ 0 & 0 & 0 & d_{21} & d_{11} & d_{13} \\ a_{31} & a_{21} + b_{31} & b_{21} + c_{32} & c_{31} + d_{32} & d_{13} & a_{11} + b_{11} + a_{33} + d_{33} \end{bmatrix}$$

(3-40)

$$V = \begin{bmatrix} a_1 \\ a_2 + b_3 \\ b_2 + c \\ c_1 + d_2 \\ d_1 \\ a_1 + b_1 + c_3 + d_3 \end{bmatrix} \quad (3-41)$$

3.3 Numerical Calculation of Torque

As discussed in the previous chapter, the torque can be computed in the air gap, half way between the rotor and the stator surfaces. For an element in that area with nodes at magnetic potential of A_1 , A_2 and A_3 , the potential over the surface can be given by:

$$A = A_1 \phi_1 + A_2 \phi_2 + A_3 \phi_3 \quad (3-42)$$

$$\phi_i = a_i x + b_i y + c_i \quad i = 1, 2, 3 \quad (3-43)$$

where a_i , b_i , c_i are given by eq. (3-22). From equations (3-42), (2-12) and (2-13), the flux density components inside the element can be calculated:

$$\begin{aligned} B_x &= A_1 b_1 + A_2 b_2 + A_3 b_3 \\ B_y &= -(A_1 a_1 + A_2 a_2 + A_3 a_3) \\ B_z &= 0 \end{aligned} \quad (3-44)$$

The stress tensor in Cartesian coordinates is:

$$T = \frac{1}{2\mu_0} \begin{bmatrix} B_x^2 - B_y^2 & 2B_x B_y \\ 2B_y B_x & B_y^2 - B_x^2 \end{bmatrix} \quad (3-45)$$

Then the forces applied on an elementary surface, dS , with components dS_x and dS_y are:

$$dF_x = T_{xx} dS_x + T_{xy} dS_y = \frac{1}{2\mu_0} [(B_x^2 - B_y^2) dS_x + 2B_x B_y dS_y] \quad (3-46)$$

$$dF_y = T_{yx} dS_x + T_{yy} dS_y = \frac{1}{2\mu_0} [2B_y B_x dS_x + (B_y^2 - B_x^2) dS_y]$$

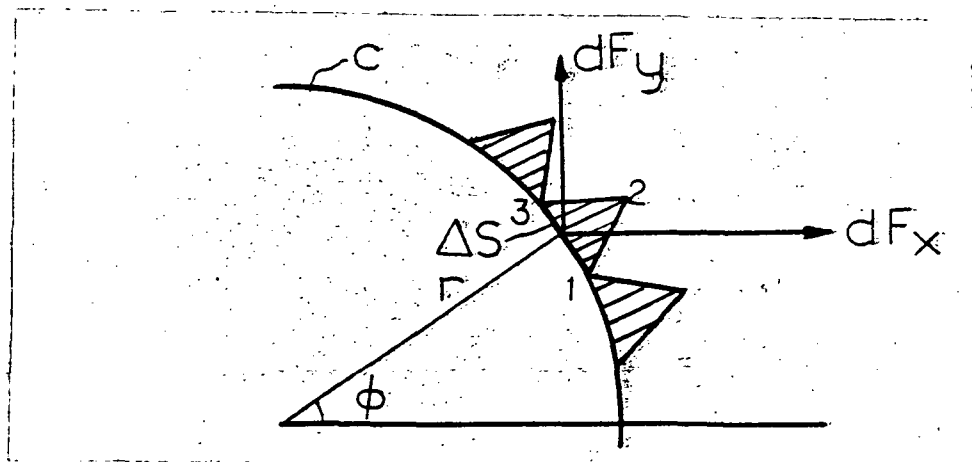


Figure 3-5 The calculation of torque in a machine

The torque contributed by this elementary surface is:

$$dM = r \cdot \sin \phi \cdot dF_x - r \cdot \cos \phi \cdot dF_y = y dF_x - x dF_y \quad (3-47)$$

and the total torque is given by the integral over the whole rotor surface, thus:

$$M = \oint_c dF = \frac{1}{2\mu_0} \left[\oint_y (B_x^2 - B_y^2) dS_x + 2 \oint_y B_x B_y dS_y + \oint_x B_x B_y dS_x + \oint_x (B_x^2 - B_y^2) dS_y \right] \quad (3-48)$$

The rotor surface is represented by small linear segments, ΔS . The values of B_x and B_y are constant on each segment, therefore:

$$M = \frac{1}{2\mu_0} \sum_{\Delta S \in c} \left[(B_x^2 - B_y^2) \int_{\Delta S} y dS_x + 2B_x B_y \left(\int_{\Delta S} y dS_y + \int_{\Delta S} x dS_x \right) + (B_x^2 - B_y^2) \int_{\Delta S} x dS_y \right] \quad (3-49)$$

Equation (3-49) defines an algorithm by which the torque can be computed from the knowledge of the magnetic vector potential at the nodes of a grid, as calculated from the finite element method:

1. On an element, calculate B_x and B_y from (3-44)
2. Calculate the torque contributed by the linear segment of the surface, ΔS , defined by the element
3. Repeat steps 1 and 2 over the whole slice of the rotor that is modeled, adding the torque contributions.
4. Multiply the result by the number of poles.

3.4 Calculation of the Permeability of Elements

The permeability of each element is assumed to have a constant value over the element but it is also assumed to change (for magnetic materials) with a passage of time, depending on the flux density in the element. The simplest way to deal with this characteristic is to calculate the flux density from equations (3-44) and calculate the permeability from that and the saturation curve of the material. The solution (with the same force vector) is then repeated, and the permeabilities are recalculated. This procedure is repeated until the permeabilities calculated in the previous iteration are close enough to the new one. Various methods have been devised which accelerate this iterative technique, the simplest of them being the underrelaxation method. In this, instead of the newly calculated value of permeability, μ_{new} , a linear combination is used, of μ_{new} and the previously calculated permeability μ_{old} .

$$\mu = \alpha \mu_{\text{new}} + (1-\alpha)\mu_{\text{old}} \quad (3-50)$$

$$0 < \alpha \leq 1 \quad , \quad \text{usually} \quad 0.9 \leq \alpha \leq 1$$

This method appears to be rather slow in the time independent problem, but gives good results for the time dependent problem and for iterative solution of the system of equations resulting from the finite element method, as Figures (3-6) and (3-7) show:

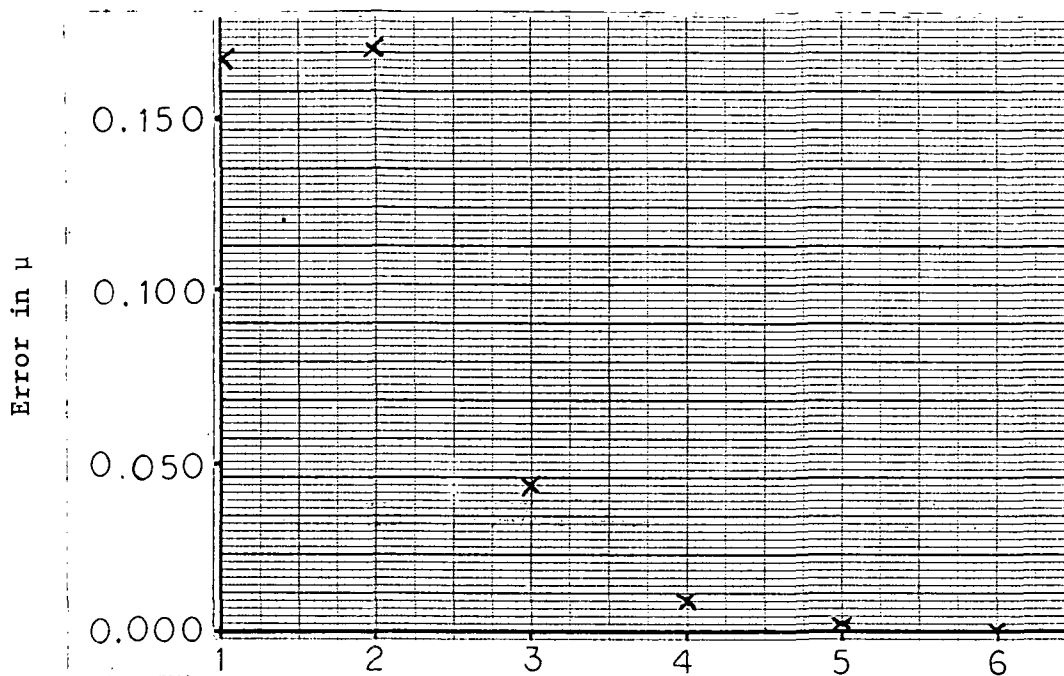
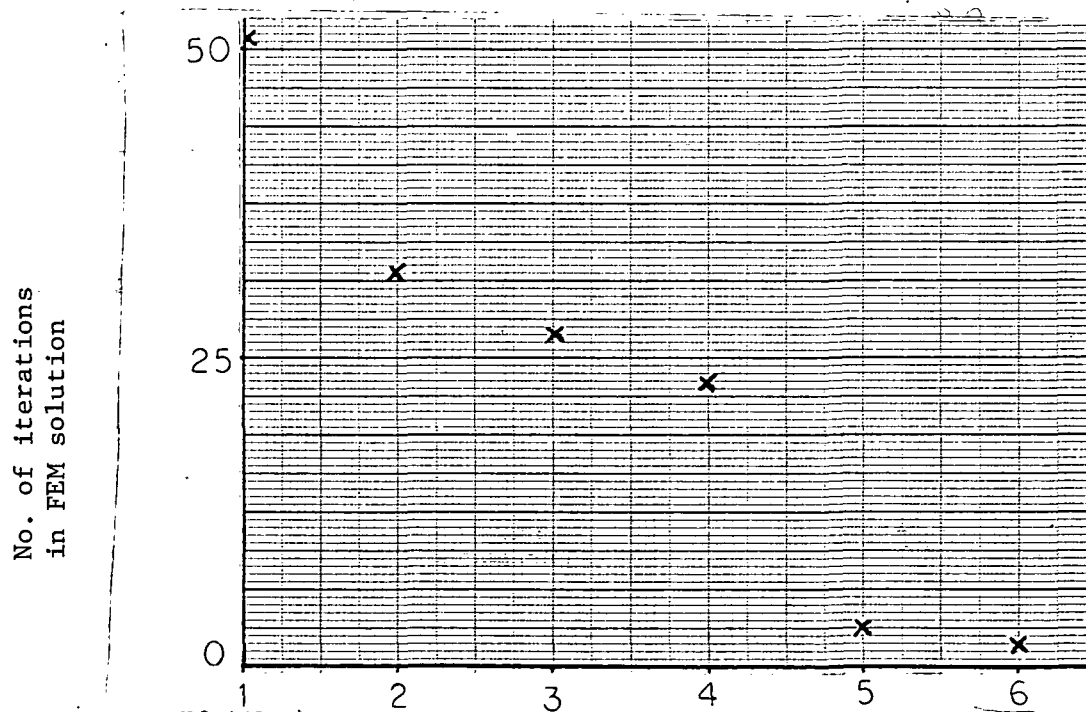
Figure 3-6 Error in μ versus solution number

Figure 3-7 Number of iterations in conjugate gradient versus solution number

The case of laminated materials requires some special considerations. The effective permeability of such a material will be less than the permeability of iron, while the saturation level will be based on the flux density in the iron only, and not on the average flux density. The value of H will be the same in both iron and air. Assuming a stacking factor s, an iron permeability μ , air permeability μ_0 , the average flux density B can be obtained using Figure 3-8:

$$B = s \cdot \mu \cdot H + (1-s) \cdot \mu_0 \cdot H \quad (3-51)$$

$$B = [s \cdot \mu + (1-s) \mu_0] H$$

From which the effective permeability will be

$$\mu_{\text{eff}} = [s \cdot \mu + (1-s) \mu_0] \quad (3-52)$$

Conversely, when the average flux density is known from the solution of the electromagnetic field, as given in (3-42), the flux density in the iron, B_{iron} , can be calculated from (3-49)

$$B = s \cdot B_{\text{iron}} + (1-s) \mu_0 H$$

$$B = s B_{\text{iron}} + (1-s) \mu_0 B_{\text{iron}} / \mu \quad (3-53)$$

$$B_{\text{iron}} = B / [s + (1-s) \mu_0 / \mu]$$

This value of the flux density in the iron, based on the previous value of the permeability, can be used to calculate a new value of the permeability

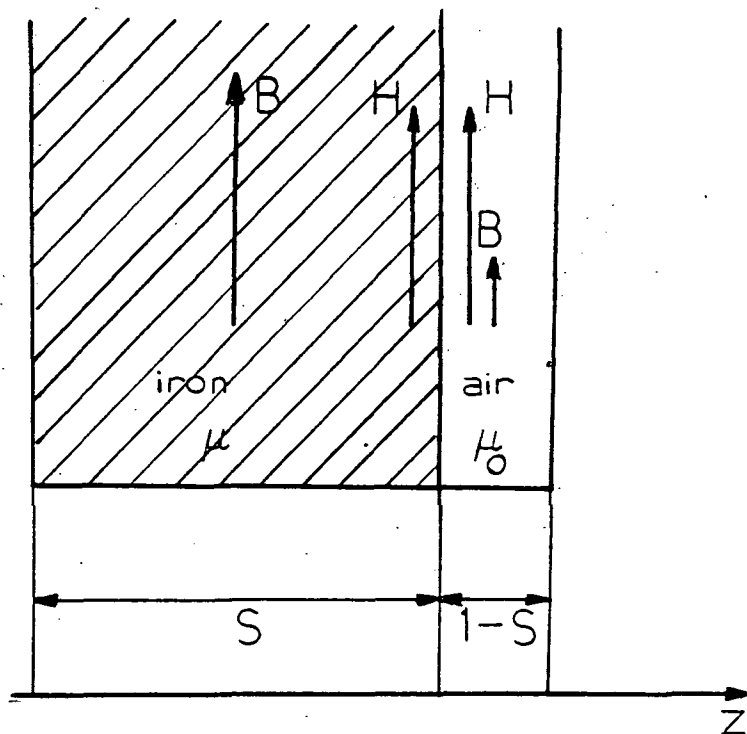


Figure 3-8 For the calculation of the effective permeability of laminated materials.

3.5 Calculation of Eddy Current Losses

The losses due to eddy currents are of importance, particularly these in the iron portion of the machine. There, the current density is:

$$J = -\sigma \frac{\partial A}{\partial t} \quad (2-18)$$

and it can be calculated for each element from equation (3-40) and (3-41):

$$\begin{aligned}
 J &= -\sigma \left(\phi_1 \frac{\partial A_1}{\partial t} + \phi_2 \frac{\partial A_2}{\partial t} + \phi_3 \frac{\partial A_3}{\partial t} \right) \\
 &= \frac{-\sigma}{\Delta t_n} \left[\phi_1 (A_1^{n+1} - A_1^n) + \phi_2 (A_2^{n+1} - A_2^n) + \phi_3 (A_3^{n+1} - A_3^n) \right] \quad (3-54)
 \end{aligned}$$

The losses in this element can be calculated from:

$$dW = \frac{1}{\sigma} J^2 dV dt \quad (3-55)$$

where dW is the Joule loss in an element of volume dV . For the case of two dimensional field, the losses in an element during the time step Δt_n are:

$$\Delta W = \frac{\sigma}{\Delta t_n} \ell \int \left[(A_1^{n+1} - A_1^n) \phi_1 + (A_2^{n+1} - A_2^n) \phi_2 + (A_3^{n+1} - A_3^n) \phi_3 \right]^2 dS \quad (3-56)$$

where ℓ is the length of the machine and the integral extends over the cross section.

In case of current carrying conductors, equation (2-18) becomes,

$$J = -\sigma \left(\frac{\partial}{\partial t} A_z - \frac{\partial \phi}{\partial z} \right) \quad (2-9)$$

$$J = -\sigma \frac{\partial}{\partial t} A_z + I_o \quad (3-57)$$

where I_0 is the current flowing in the conductor due to external sources.

Then equation (3-56) becomes:

$$\Delta W = \frac{\Delta t}{\sigma} \int \left\{ \frac{\sigma}{\Delta t} [(A_1^{n+1} - A_1^n) \phi_1 + (A_2^{n+1} - A_2^n) \phi_2 + (A_3^{n+1} - A_3^n) \phi_3] + I_0 \right\}^2 dS \quad (3-58)$$

4.0 SPARSE MATRIX ALGORITHMS APPLIED TO THE SOLUTION OF THE SYSTEM RESULTING FROM THE FINITE ELEMENT METHOD

The system of linear equations derived from the application of the finite element method to an elliptical differential equation possesses certain properties, which can be utilized so that the solution is carried out in an efficient and accurate way.

From the structure of the grid used in the finite element method, it is evident that every node is coupled directly only to the ones with which it is in the same element. In Figure 4-1, for example, node 1 is coupled to nodes 2, 3, 4, 5 and 6, not to 7, 8, 9 or any other in the grid. As a result, the only possibly non-zero entries in the first row of the global matrix will be (1,1), (1,2), (1,3), (1,4), (1,5), and (1,6), no matter how large the total grid may be. Such a construction creates a global matrix of very large order (equal to the number of nodes), but also very sparse (very small percentage of non-zero entries). Theoretical considerations also guarantee that this matrix is symmetric and positive definite.

The computational techniques which can be used to solve this system of linear equations can be classified as either direct or iterative. Direct methods reach a solution after a fixed and predetermined number of computations, while in iterative methods, an initial guess solution is successively improved through a repetition of rather simple matrix-vector operations. These iterations are stopped when a specified accuracy is reached.

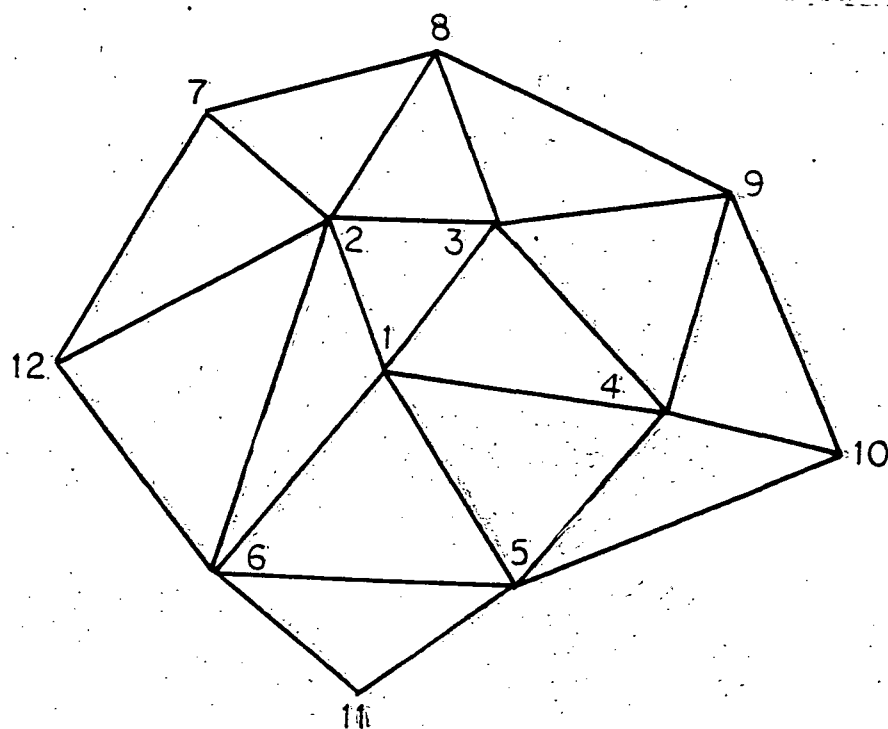


Figure 4-1 A typical grid

4.1 Storage Techniques

The structure of the global matrix is of importance for the determination of the method of storage. Two types of matrices can be encountered; broadly classified as the banded and the generally sparse matrix (see Figure 4-2). In a banded matrix a pattern of non-zero terms occurs along the diagonal and both the storage scheme and the algorithm used for the solution can take advantage of this characteristic in order to decrease the storage area and increase the solution speed.

The matrix is always stored in a compact fashion. This means that besides the non-zero entries, none, or only a few zero entries are stored. Markers are used to point to the first and last non-zero elements in

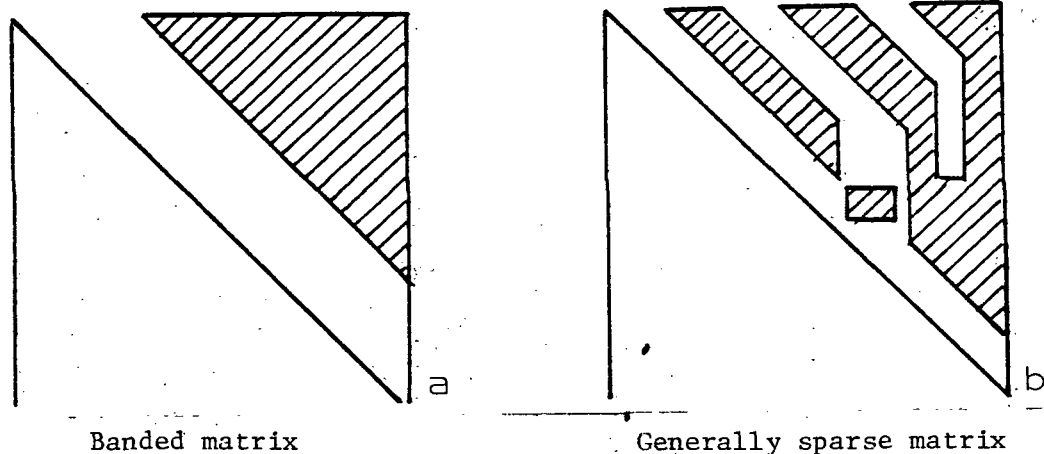


Figure 4-2 Types of matrices

each row in the case of a variable bandwidth matrix, whereas for a constant bandwidth matrix, the number of vectors used is equal to half the bandwidth and each contains the entries of the matrix which lie on lines parallel to the diagonal.

In the case of a generally sparse matrix, the storage scheme becomes more complicated. Three vectors are used to store the values of the matrix entries and the location of each within the matrix. One vector is used to store the non-zero entries in the order that one would find them in the matrix while moving from left to right within a row, scanning rows from top to bottom. Another vector of integer values is used to point to the first entry of each row. A third integer vector indicates the column in which each entry lies. Since the matrix is symmetric, only the upper triangular part must be stored.

In Figure 4-3 an example is given of the storage scheme for a matrix 6x6. Vector A contains the values of the entries, vector JA

shows the row to which each entry belongs and vector IA points to the location of the first entry of each row. This storage method is very efficient from the storage space viewpoint, but the handling of the matrix requires many manipulations of the local index vectors, thus increasing the execution time.

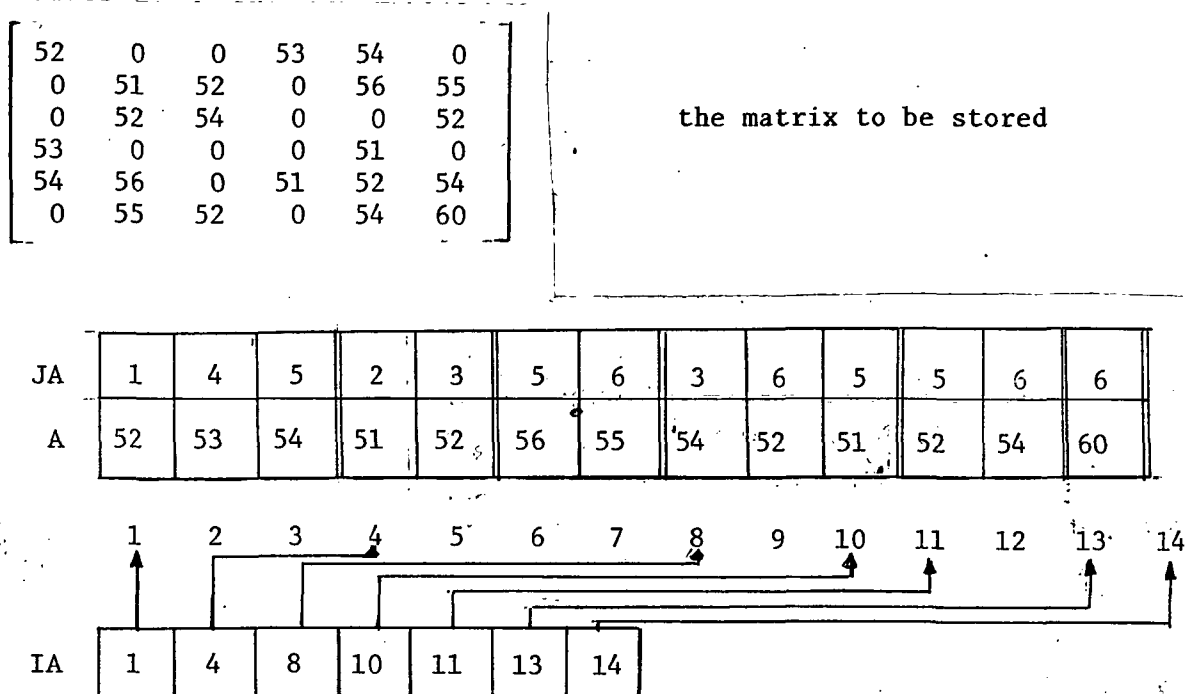


Figure 4-3 Storage of a generally sparse symmetric matrix

4.2 Direct Methods of Solution

A direct solution process can almost always be divided into three subprocesses:

1. Triangularization of the matrix by factorization or elimination.

2. Back substitution on the right hand side.
3. Iterative refinement to improve accuracy.

Triangularization becomes more complicated, and the data handling more time consuming, as the form of the matrix departs from the constant bandwidth structure. It usually requires the storage on magnetic disk of the rows of the matrix - including some zero entries - and the consecutive retrieval of a number of these rows at a time, so that the Gaussian elimination or the Choleski factorization can be carried out. The number of the zero entries that have to be stored also increases when the matrix is not banded.

4.3 Iterative Methods of Solution

These methods have the advantages over the direct methods in that their programming is simpler and that they efficiently utilize the sparsity of the matrix. The simplest iterative method, and the most widely used, is the Successive Over Relaxation and its variations. For a system of equations:

$$A \cdot u = b \quad (4-1)$$

with

$$A = D - L - U \quad (4-2)$$

where U and L are upper and lower triangular matrices respectively and D is a diagonal matrix, the following equation is applied:

$$u^{n+1} = U^{-1} + \omega D^{-1} \cdot (L \cdot u^{n+1} + U u^n - D u^n + b) \quad (4-3)$$

where u^n is the n^{th} approximation to the solution and ω is a real number between 1 and 2. This method is always convergent for symmetric positive definite matrices. The optimal selection of the parameter ω is of practical interest, since it should minimize the spectral radius of the iteration matrix. For matrices possessing a special property A⁽³⁹⁾, the spectral radius is minimized for an ω given by

$$\omega = 2 / (1 + \sqrt{1 - \mu^2}) \quad (4-4)$$

where μ is the spectral radius of the related Jacobi matrix $D^{-1}(L+U)$. However, in practical problems, seldom is a matrix obtained having property A. An increased convergence rate can be achieved by Successive Line Over Relaxation (SLOR), where the computational molecule groups points along rows or columns of the mesh, thus forcing the system to have property A. When two rows or columns are included, the method is called the Successive Two Line Overrelaxation (S2LOR), and when both columns and rows are included in a form of a peripheral block, the method becomes the Successive Peripheral Overrelaxation (SPOR). These last three methods (SLOR, S2LOR and SPOR) require for their implementation, a fairly regular grid, where the nodes are arranged in columns, rows, or circular patterns and the construction of the global matrix is

based on the shape of the grid. On the other hand, SOR, although relatively slow, does not require a regular grid and is often used for large irregular domains.

4.4 The P-condition number and the Preconditioning of a System^(40,41)

The asymptotic convergence of a system of linear equations with a symmetric positive definite coefficient matrix, has been shown to depend inversely on the P-condition number of the coefficient matrix, defined as the ratio of the maximum eigenvalue to the minimum eigenvalue of a positive definite matrix. Thus, to improve convergence, it is required that the P-condition number of the matrix be very small. When this does not happen it is desirable to "prepare" the system so that its condition number is minimized. This means that instead of solving the system of equations (4-1), it would be easier to solve system:

$$Q \cdot A \cdot u = Q \cdot b \quad (4-5)$$

where Q is a non-singular matrix and the condition number of the resulting system is less than that of the original system. One such matrix is $(I - \omega L)^{-1}$, and the system (4-5) can be rewritten as:

$$[(I - \omega L)^{-1} \cdot A \cdot (I - \omega L^T)^{-1}] [(I - \omega L^T) \cdot u] = (I - \omega L)^{-1} b \quad (4-6)$$

Denoting:

$$\begin{aligned} v &= (I - \omega L^T) \cdot u \\ d &= (I - \omega L)^{-1} \cdot b \\ B &= (I - \omega L)^{-1} \cdot A \cdot (I - \omega L^T)^{-1} \end{aligned} \quad (4-7)$$

then B can be shown to be also a symmetric positive definite matrix. A minimum of the value of the P-condition number exists for ω between 1 and 2, whereas for $\omega = 0$, the system reverts back to its original form.

4.5 The Conjugate Gradient Method^(42,43)

In gradient methods in general, instead of solving the system of equations (4-1) as is, a variational method is derived based on the observation that the solution of (4-1) is the same vector that maximizes the quadratic functional:

$$F(u) = -\frac{1}{2} u^T \cdot A \cdot u + u^T \cdot b \quad (4-8)$$

This functional defines a family of similar ellipsoids in a Euclidean n -space with center at $A^{-1}b$. The solution, therefore, can be attempted by proceeding to this center, using a sequence of displacements, achieving after each, a better approximation of the maximum:

$$u^{(n+1)} = u^{(n)} + \sigma_n p^{(n)} \quad (4-9)$$

where $u^{(n)}$ is the n^{th} approximation, $p^{(n)}$ is the direction followed in the n^{th} step and σ_n is a real number selected so that $F(u^{(n+1)})$ is minimized. At the n^{th} step a residual, $r^{(n)}$, can be calculated as:

$$r^{(n)} = b - A \cdot u^{(n)} \quad (4-10)$$

The way that the direction vector $p^{(n)}$ is determined defines the method used. The most obvious choice is the direction normal to the surface of the ellipsoid, i.e. $p^{(n)}$ is chosen to be $-r^{(n)}$. This technique defines the steepest descent method and it is illustrated for a two dimensional case in Figure 4-4.

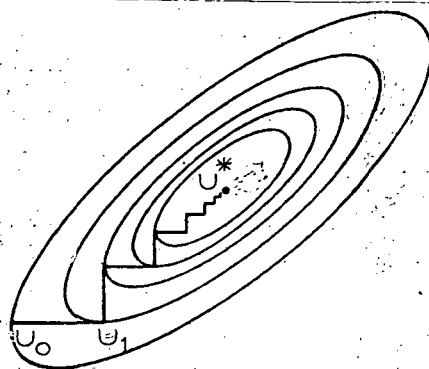


Figure 4-4 Steepest descent method.

This is an iterative technique, and the rate of convergence and number of iterations depend on the form of the equations and the accuracy desired.

A better method results when advantage is taken of the property of quadratic functionals, that the center of the ellipsoid lies on a plane conjugate to a given cord.

4.5.1 Conjugate Directions

Given a symmetric matrix A , two vectors, d_1 and d_2 , are A -orthogonal, or conjugate with respect to A if:

$$d_1^T \cdot A \cdot d_2 = 0 \quad (4-11)$$

If a set of vectors d_0, \dots, d_k are A orthogonal, then these vectors are linearly independent. A solution then, u^* , of $Au=b$, or equivalently that maximizes $(-1/2 u^T A u - u^T b)$, can be expanded in terms of n vectors $d_0 \dots d_{n-1}$ (A is a $n \times n$ positive definite matrix) as:

$$u^* = \sigma_0 d_0 + \dots + \sigma_{n-1} d_{n-1} \quad (4-12)$$

Multiplying by A and taking the scalar product with d_i , yields σ_i as:

$$\sigma_i = \frac{d_i^T \cdot A \cdot u^*}{d_i^T \cdot A \cdot d_i} = \frac{d_i^T \cdot b}{d_i^T \cdot A \cdot d_i} \quad (4-13)$$

The last equation indicates that the coefficients σ_i of equation (4-12) can be evaluated without knowing u^* , which, however can then be calculated from (4-12). Thus:

$$u^* = \sum_{i=0}^{n-1} \frac{d_i^T \cdot b}{d_i^T \cdot A \cdot d_i} d_i \quad (4-14)$$

The basic idea imbedded in (4-14) is that when a set of d_i 's is selected, the unknown vector u^* can be calculated from it. This expansion of u^* can be considered as the result of a process of n steps, where at the i^{th} step, $\sigma_i d_i$ is added.

Viewing the procedure in this way, the conjugate direction method can be formulated in n steps; the k^{th} of which is described by equation (4-15):

$$u_{k+1} = u_k + \sigma_k d_k \quad (4-15)$$

where:

$$\sigma_k = - \frac{r_k^T \cdot d_k}{d_k^T \cdot A d_k} \quad (4-16)$$

and

$$r_k = A \cdot u_k - b \quad (4-17)$$

This holds true because the difference between an initial guess, u_0 , and the solution, u^* , can be written as:

$$u^* - u_0 = \sigma_0 d_0 + \dots + \sigma_{n-1} d_{n-1} \quad (4-18)$$

Multiplying by A and taking the scalar product with d_k , as in (4-13) yields:

$$\sigma_k = \frac{d_k^T \cdot A \cdot (u^* - u_0)}{d_k^T \cdot A \cdot d_k} \quad (4-19)$$

Following the iterative process (4-15) from u_0 up to u_k , one obtains:

$$U_k - U_0 = \sigma_0 d_0 + \sigma_1 d_1 + \dots + \sigma_{k-1} d_{k-1} \quad (4-20)$$

and because of the A-orthogonality of the vectors d_k :

$$d_k^T A \cdot (u_k - u_0) = 0 \quad (4-21)$$

Substituting (4-21) in (4-19) produces:

$$\sigma_k = \frac{d_k^T \cdot A \cdot (u^* - u_k)}{d_k^T \cdot A \cdot d_k} = \frac{r_k^T d_k}{d_k^T \cdot A \cdot d_k} \quad (4-22)$$

An important property of the conjugate direction method is that in each step the functional (4-8) is maximized on the line:

$$u = u_{k-1} + \alpha d_{k+1}, \quad (4-23)$$

where α is a real number, as well as in the linear space $u_0 + B_k$, where B_k is a linear combination of d_0, \dots, d_{k-1} meaning that the remainder, r_k is perpendicular to the space B_k as shown in Figure 4-5.

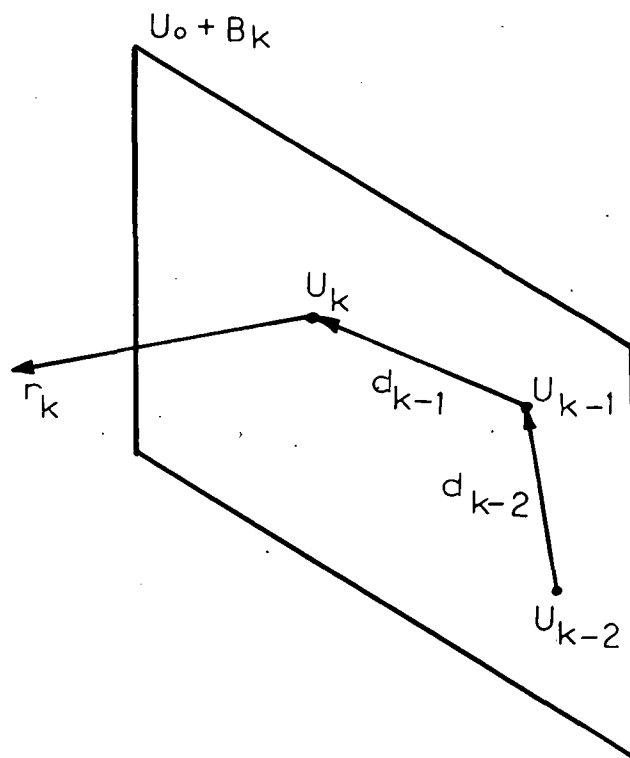


Figure 4-5 Conjugate direction method

4.5.2 The Conjugate Gradient Algorithm

The conjugate gradient method is obtained from the conjugate direction method by selecting the successive direction vectors as a conjugate version of successive gradients which are obtained as the method progresses. Thus, the directions are not specified before the solution starts; they are determined sequentially at each step of the iteration. At step k one evaluates the current negative gradient vector

and adds to it a linear combination of the previous direction vectors in order to obtain a new conjugate direction vector along which to move.

The distance to move in this direction is given, as before, by equation (4-22), while the coefficients τ_k which will give the new vector d_{k+1} from equation (4-24),

$$d_{k+1} = -r_{k+1} + \tau_k d_k \quad (4-24)$$

are given by equation:

$$\tau_k = \frac{r_{k+1} \cdot A \cdot d_k}{d_k^T \cdot A \cdot d_k} \quad (4-25)$$

The algorithm derived from the previous considerations can be described by the following steps:

1. Start with the initial guess u^0 , with initial remainder $r^0 = b - Au^0$, and initial conjugate direction $d^0 = -r^0$
2. $\sigma_n = r_n^T d_n / (d_n^T \cdot A \cdot d_n)$
3. $u_{n+1} = u_n + \sigma_n d_n$
4. $r_{n+1} = r_n - \sigma_n A \cdot d_n$
5. $\tau_{n+1} = -r_{n+1}^T A \cdot d_n / (d_n^T \cdot A \cdot d_n)$
6. $d_{n+1} = r_{n+1} - \tau_{n+1} d_n$
7. If $|r_{n+1}|$ is less than the maximum allowed error, stop.

Otherwise continue from step No. 2.

The last step of the algorithm is of particular importance when the coefficient matrix is of large order. From the theory of the conjugate direction method it is clear that the solution will be reached after a number of iterations equal to the order of the matrix. But, because the method is based on gradients, the algorithm makes good uniform progress towards the solution at every step, in contrast to the case of arbitrary conjugate directions, where the progress may be slight until the final few steps. In the conjugate gradient method, therefore, the progress is quite good at the first steps, whereas the last steps improve the solution only slightly, making the last iterations unnecessary when the desirable accuracy has already been achieved. A measure of the distance of an approximation from the exact solution is the gradient. When the solution is obtained, the gradient vanishes and a norm of it can be used to evaluate its length and be compared to the desired accuracy.

A very important advantage of the conjugate gradient method is the very simple formulae which are used to determine the new direction vector. This simplicity makes the method only slightly more complicated than the steepest descent method.

4.6 The Preconditioned Version of the Conjugate Gradient Method^(40,41)

When the matrix A in the functional (4-8), is ill conditioned, the ellipsoids, as in Figure (4-4), become long and thin, and thus the normals to the surface become coplanar. Preconditioning reshapes these ellipsoids, so that they take a less prohibitive form, thus enabling the

solution algorithm to lead more rapidly to a good approximation. An example is given here of the effect of preconditioning on the form of the quadratic functionals and the shape of the corresponding ellipsoids:

Assume the system of equations:

$$\begin{bmatrix} 1 & -0.98 \\ -0.98 & 1 \end{bmatrix} \begin{bmatrix} x_1 \\ x_2 \end{bmatrix} = \begin{bmatrix} 1 \\ 1 \end{bmatrix} \quad (4-26)$$

The solution of this system is equivalent to maximizing the functional:

$$\frac{1}{2} \begin{bmatrix} x_1 & x_2 \end{bmatrix} \begin{bmatrix} 1 & -0.98 \\ -0.98 & 1 \end{bmatrix} \begin{bmatrix} x_1 \\ x_2 \end{bmatrix} - \begin{bmatrix} x_1 & x_2 \end{bmatrix} \begin{bmatrix} 1 \\ 1 \end{bmatrix} = c \quad (4-27)$$

or

$$x_1^2 - 1.96 x_1 x_2 + x_2^2 - 2x_1 - 2x_2 = 2c \quad (4-28)$$

The ellipsoids corresponding to equation (4-28) are shown in Figure 4.6(a).

When preconditioning is applied, the system of eq. (4-26) becomes:

$$\begin{bmatrix} 1 & 0 \\ .98\omega & 1 \end{bmatrix} \begin{bmatrix} 1 & -0.98 \\ -0.98 & 1 \end{bmatrix} \begin{bmatrix} 1 & .98\omega \\ 0 & 1 \end{bmatrix} = \begin{bmatrix} 1 & 0 \\ .98\omega & 1 \end{bmatrix} \begin{bmatrix} 1 \\ 1 \end{bmatrix} \quad (4-29)$$

and the corresponding functional is:

$$x_1^2 + 2 \cdot 0.98(1-\omega)x_1x_2 + (0.98^2 - 2 \cdot 0.98\omega + 1)x_2^2 - 2x_1 - 2(1-0.98\omega)x_2 = 2c \quad (4-30)$$

which has as corresponding ellipsoids for $\omega = 1.05$ the ones in Figure 4-6(b), and for $\omega = 1$ the ellipsoids in Figure 4-6(c) which are circles.

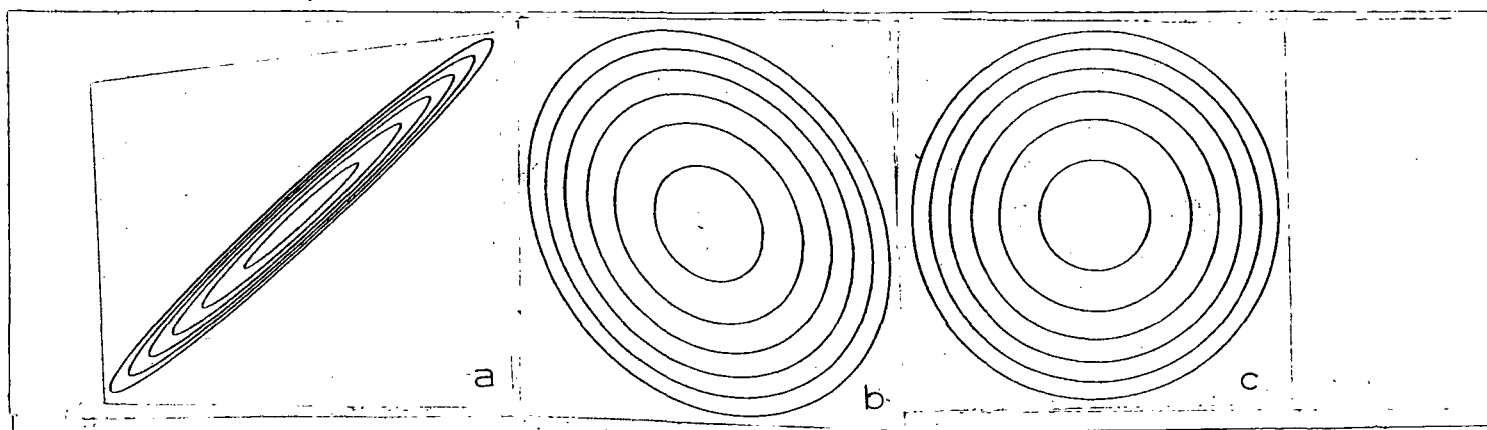


Figure 4-6 A family of ellipsoids before and after preconditioning

When preconditioning is used, the arithmetic operations per iteration are increased drastically, but, due to the faster convergence, the overall speed is improved. The matrix $B = (J - \omega L)^{-1} A (I - \omega L^T)^{-1}$ is never calculated, since such a transformation would destroy the sparseness of the matrix and make storage requirements prohibitively large. Instead, back-and-forward substitution is used every time the matrix B is to be multiplied by a vector. The algorithm described in section 4.3.2 remains essentially the same, while certain manipulations are added to

account for the preconditioning. The system has to be prepared so that the entries along the diagonal become one. The final algorithm takes the following form:

1. Prepare the system by multiplying both sides with matrix G:

$$G_{ij} = 0 \quad \text{for } i \neq j$$

$$G_{ii} = \frac{1}{\sqrt{A_{ii}}}$$

(4-31)

Thus the system becomes:

$$(G \cdot A \cdot G) \cdot (G^{-1} \cdot u) = G \cdot b$$

Using for simplicity the same symbols for system (4-27) as for (4-1), but noting that the diagonal is now the unity matrix:

2. Calculate $v_0 = (I - \omega L^T) u_0$

3. Calculate $d = (I - \omega L)^{-1} b$

4. Calculate the remainder of the system:

$$B \cdot v = d \quad \text{as:}$$

$$v_0 = d - B \cdot v_0 = d - (I - \omega L)^{-1} \cdot A \cdot (I - \omega L^T) v_0$$

5. Find the first conjugate direction as:

$$d^0 = -r^0$$

and store it in the place of d .

6. Calculate $\sigma = r \cdot d / (d^T \cdot B \cdot d)$

$$\text{as } \sigma = r \cdot d / [d \cdot (I - \sigma L)^1 \cdot A \cdot (I - \omega L^T)^{-1} \cdot d]$$

7. Calculate the new approximation to the solution:

$$v := v + \sigma \cdot d$$

8. Calculate the new residual

$$r := r - \sigma \cdot B \cdot d = r \sigma \cdot (I - \omega L)^1 \cdot A \cdot (I - \omega L^T)^{-1} \cdot d$$

It must be noted here that $B \cdot d$ has already been calculated in step 6.

9. $\tau = -r \cdot d / d^T \cdot B \cdot d$

10. The new direction vector, d , can be calculated as

$$d = r + \tau \cdot d$$

11. The distance of the current approximation to the solution, V , from the exact one can be checked by finding the norm of the remainder. If it is larger than the desired accuracy, the algorithm is repeated from step one. Otherwise, the solution, u , is calculated in the next step:

12. $u = (I - \omega L^T)^1 \cdot v$ and $u := G \cdot u$

4.6.1 Computer Considerations

The preconditioned conjugate gradient method requires the storing of four vectors, v , r , d and $B \cdot d$. Involved in the preparation of the matrix are two matrix-matrix multiplications and two scalar-vector products for the determination of A , u and B in step 1. In step 2, a matrix-vector product is involved, and in step 3 one back substitution.

At the exit (step 12), a back substitution is required, as well as a scalar-vector product. In each iteration, a back substitution, two inner products and three scalar-vector products are involved in computational effort.

As later discussed, often solutions are required using the same stiffness matrix A and entirely different force vectors b . In these cases the initial multiplication is not repeated; instead the values of G are stored in the diagonal of the matrix A , while the adjusted values of L are stored in the lower triangle of the same matrix. Therefore, only vectors d and u have to be multiplied by G and G^{-1} respectively.

When the saturation level of the iron parts in the machine is to be determined, the linear system is solved repeatedly with the entries of the matrix changing slightly, and the force vector remaining constant. These conditions cause the solution vector of the previous repetition an excellent guess for the following. This policy drastically decreases the number of iterations required for each solution.

4.6.2 Determination of the Solution Technique for the Continuous Modeling of the Electromagnetic Field.

The fact that the solution at each time step is close to the solution of the previous time step makes iterative solutions more attractive than direct ones, since the number of iterations is decreased by the introduction of a good guess solution. The storage requirements are less restrictive in the iterative techniques, since no space needs to be allowed for fillings during the triangularization. This is of special importance in this case, since the grid is quite irregular and the

number of fillings would be large. The simplicity of programming is also a significant factor in deciding in favor of an iterative scheme.

Among the iterative techniques which are commonly used, SOR, is the simplest and usually the first choice. The matrix from the finite element method, though, does not possess the property A, and it is difficult to find the optimal parameter ω . When the grid is regular, the matrix takes a very convenient form, making the variations of SOR very attractive. However, the limitation of a regular grid deprives the finite element method of the ability to utilize a fine mesh only where it is necessary, while using a coarser grid where the solution does not vary greatly in space.

The electromagnetic problem has the peculiarity that the entries of the local matrices of neighboring elements can differ by two or three orders of magnitude when the material is magnetic in one element and non-magnetic in the other since these entries are inversely proportional to the magnetic permeability. Such vast differences in numbers which are added together in the global matrix, make the global matrix ill conditioned. This characteristic makes it necessary, when SOR is used, to alternate between SLOR and SPOR⁽¹⁻⁵⁾. Preconditioning appears to be an elegant way of rectifying or improving this situation.

Reid⁽⁴³⁾ has shown that the conjugate gradient method in its original form ($\omega=0$) is a powerful algorithm, and with the further application of preconditioning, both in this work and other⁽⁴⁰⁾; it has been proven both fast and convenient, especially in the case of time dependent solution of electromagnetic fields.

5.0 THE OPERATION OF CHOPPER CONTROLLED DC SERIES MOTORS

Both experimental work and problems noted with the application of DC motors have made it clear that there exists a discrepancy between the analytically calculated inductance of DC machines and that observed when the motors are driven by a chopper. Also, recent experimental work (34,35) has shown that a single value of inductance cannot be assigned to the machine; rather, both apparent resistance and inductance vary greatly with the frequency of the current which is used to measure them and with the value of the DC current on which the AC current is superimposed. These effects are attributed to the combined phenomena of magnetic saturation of the iron parts of the machine, eddy currents in both solid and laminated iron and the eddy currents and skin effect in solid conductors in the machine.

These phenomena cannot be adequately described by a small set of equations except in an incomplete and empirical form. Instead, the solution of the field inside the machine should be sought at every instant, and the values of the inductances and other parameters should be calculated from it and be used to calculate the quantities of interest to the designer and analyst.

When the inductances are known as a function of input and time, the currents can be calculated as well. The theory of the two axes cannot be applied for the calculation of the torque since voltages are induced in parts of rotor and stator which are not part of the windings. Instead, the theory of the Maxwell stress tensor is used, as applied to a discretized grid (section 3.3). The radial flux density at the air gap can

be calculated in order to determine the optimal location of the brushes for linear commutation and the electromagnetic field can be solved based on that position of the brushes.

5.1 Calculation of Inductances and an Algorithm for the Calculation of Currents and Torque

In the absence of eddy currents, the small signal, or incremental inductance around an operating point of the machine, can be found by first solving the electromagnetic field for the actual current at that operating point, obtaining in this way both the values of the magnetic vector potential inside the machine and the permeabilities of all the elements which correspond to that current level. Then, the current changed by a small increment, the field calculated again and the flux linkage (with all windings) calculated. The ratio of these flux linkages to the change in current gives the incremental self and mutual inductances, on which the calculation of the actual change of current can be based, for a small time step, provided the changes in time and current are relatively small (so that the slope of the saturation curve remains constant for this change), the change of currents calculated on the basis of this incremental inductance will be accurate. Thus

$$L_{incr} = \frac{\Delta\lambda}{\Delta I_{incr}} \quad (5-1)$$

$$\Delta I = V / \frac{L_{incr}}{\Delta t} \quad (5-2)$$

where ΔI_{incr} is a small change of current, $\Delta\lambda$ the corresponding change

in flux linkages, V the induced voltage, and ΔI the actual change in current.

However, when eddy currents are present and of a magnitude which greatly affects the performance of the machine, the current change, ΔI , cannot be based on the same formulae described above.

The reason is that in this case, the machine, in addition to the current carrying winding, has an infinite number of other windings representing the paths that the eddy currents can follow. These windings are not open circuited; rather each is short circuited through the resistance corresponding to that current path. Each of these windings has a self inductance and a mutual inductance with every other current path, as well as with the real winding of the machine. Even in the case when all these current paths are replaced by a finite number of circuits, in order to make the problem less formidable, the number of independent windings required is still too large to give an inductance matrix which can be handled efficiently.

If, in some way, the current change had been known (either measured or calculated), then a value of inductance could be obtained, depending not only on the saturation level, but also on the actual change of current, ΔI , and the time step, Δt :

$$L_{incr} = - \frac{V}{\frac{\Delta I}{\Delta t}} \quad (5-3)$$

Equation (5-3) can be used in an iterative way in order to calculate the change of current from the finite element solution. Initially

a "guess" change of current is applied and the field is solved, assuming this change to be the exact one for the time step examined. From the solution, the voltage induced in the winding is calculated and a value of the incremental inductance is obtained from (6-3). It is then substituted in equation (5-2) to yield a corrected value of the change in current. The process is then repeated to yield a closer approximation to the correct incremental inductance. The iterations are stopped when the values of inductance obtained from two consecutive iterations are sufficiently close.

This process can be very slow, with the values of inductances approaching asymptotically the final value, but for the calculations of each, the field has to be solved. When the field is solved in an iterative way, however, the previous solution is a good approximation to the next, decreasing the amount of the iterations needed for convergence. The number of iterations for the inductance calculations can be decreased if the Aitken extrapolation⁽⁴⁴⁾ is used to accelerate the convergence.

5.1.1 The Aitken Extrapolation

When the differences between successive values of the incremental inductance form a geometric progression, of ratio α :

$$\frac{L_2 - L_1}{L_3 - L_2} = \frac{L_3 - L_2}{L_4 - L_3} = \alpha \quad (5-4)$$

where L_1 , L_2 , L_3 , L_4 are the values of the incremental inductance calculated in the respective iteration; then the final value of L will be:

$$L = L_1 + \frac{(L_2 - L_1)}{\alpha - 1} \quad (5-5)$$

Application of this technique decreases the number of the iterations for the inductance calculation. There are three solutions of the field required for the calculation of α (two of which require fewer iterations in the preconditioned gradient method), and one solution after the final value of the incremental inductance is calculated, so that the accuracy of it is checked and the field is solved for the final value of current so that eddy losses and torque can be calculated.

5.1.2 The Rotational Voltage

When the flux density is known in the machine, then the rotational voltage can be calculated for each conductor as:

$$V = B_r \cdot \omega \cdot r \cdot \ell \quad (5-6)$$

where B_r is the radial component of the flux, r the distance of the conductor from the axis of the machine, ℓ the length of the conductor and ω the angular velocity of the conductor. When the magnetic vector potential is known, B_r can be obtained from it as:

$$B_r = -\frac{1}{r} \cdot \frac{\partial A}{\partial \phi} \quad (5-7)$$

and the voltage induced in all the conductors will be

$$V = - \sum_{i=1}^n \left(\frac{\partial A}{\partial \phi} \right)_i \omega \cdot \ell \quad (5-8)$$

where n is the number of conductors in the armature and $\left. \frac{\partial A}{\partial \phi} \right|_i$ the derivative of the magnetic vector potential at the conductor. If the distribution of the winding is assumed linear over the armature, then:

$$V = - n \omega \ell \int_{\phi_1}^{\phi_n} \frac{\partial A}{\partial \phi} \cdot d\phi = - n \omega \ell (A_n - A_1) \quad (5-9)$$

where 1 and n are the first and last conductors of the uniform distribution of the winding and ϕ_1 and ϕ_n their respective angles.

5.1.3 The Voltage Input and External Connections of the Machine

The previously described method of handling the operation of a DC machine can be applied to any case where the waveform of the input voltage is complex. Here the case of a series traction motor is examined when driven from a set of batteries through a chopper controller of relatively low frequency (100-400 Hz). The connections of the machine are shown for this case in Figure 5-1.

The armature terminals are shunted by a reversely biased (freewheeling) diode, D2, and the armature plus series field shunted by D1. The first freewheeling diode, D2, does not carry any current in the

case that is being examined here, whereas the second diode, D_1 , conducts during the time that the chopper is not conducting.

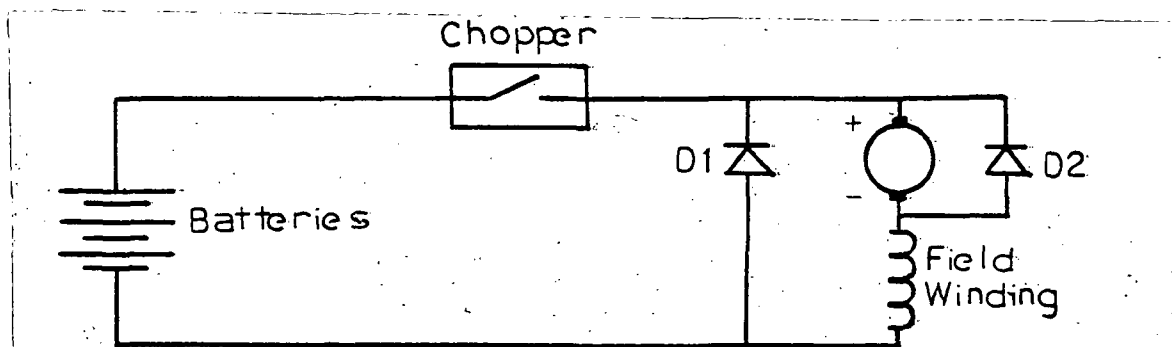


Figure 5-1 The external connections to a chopper controlled DC series motor.

The open circuited voltage of the batteries is known and is assumed to remain constant during the simulation, i.e. the batteries are not supposed to discharge significantly. The battery impedance cannot be generally considered a constant, but for the purposes of this simulation it was ignored, since its value does not greatly affect the performance of the machine.

5.1.4 The Algorithm

The algorithm that was used for the calculation of the currents in a DC machine makes repeated use of the procedures described previously

in this section. After every time step the value of the resulting current is injected into both the field and the armature windings and the field is calculated. From this solution the Maxwell stress tensor can be calculated in the air gap, and the torque computed. Then the procedure of calculating the inductance and change of current is repeated. The iteration stops after as many cycles as are needed for the current waveform to come to a quasi-steady state. The algorithm used is:

1. Start with an assumed current increment, I_{incr} , and an old value of current I_{old} :

$$I = I_{old} \quad (5-10)$$

2. Solve the electromagnetic field based on current in the armature and field, equal to I .
3. Calculate the voltage, V_{ind} , induced in the conductors due to the change ΔI in the time interval Δt and compute the incremental inductance:

$$L_{incr} = V_{ind} / \left(\frac{\Delta I}{\Delta t} \right) \quad (5-11)$$

4. Calculate a new change in current based on the new incremental inductance and a rotational voltage constant, K , calculated in the previous time step

where L_{ext} is the external and end turn inductance and R the resistivity of the winding

5. Repeat from steps 3 three times for $I = I_{old} + \Delta I$; calculate three values of incremental inductance and the final value from Equations (5-9) and (5-5) (Aitken Extrapolation)
6. Repeat steps 2, 3 and 4 for the new value of L_{incr}
7. Calculate the air gap torque and the eddy current losses in the iron.
8. Calculate from (5-9) the rotational voltage, V_{rot} and the constant K as:

$$K = V_{rot}/I$$

9. Repeat from step one using, as I_{old} , the new value of I and as the initial guess of ΔI , that one calculated last.

5.2 Application to an Electric Vehicle Motor

The algorithm of Section 5.1.3 was applied to a motor which was designed for operation in electric vehicles, operated from an 84 volt battery supply, utilizing a chopper with maximum frequency of operation of 400 Hz and a minimum time on of 1 ms to control the average voltage applied to the motor. The machine was connected to a dynamometer instrumented to measure the average current, output torque, and the revolutions per minute and loaded. Oscilloscope pictures were taken of the current

and voltage waveforms for various values of load, speed, chopper period and chopper conducting time.

5.2.1 Characteristics of the Motor

Prior to testing, the motor was dismantled and its dimensions measured and recorded. After reassembly, the friction and windage losses were measured and an interpolation technique applied to the results yielding the curve shown in Figure 5-2. Table 5-1 lists the main parameters of the motor.

The armature was wave wound and the pole windings series connected. The brush holder was moveable, allowing the brushes to be offset up to 30 electrical degrees from their neutral axis in either direction. The computer simulations presented here were with the two field windings connected in series and the brushes at the neutral position.

Figures 5-3 to 5-5 show the significant dimensions of the rotor, stator, field winding, armature slot and armature conductors.

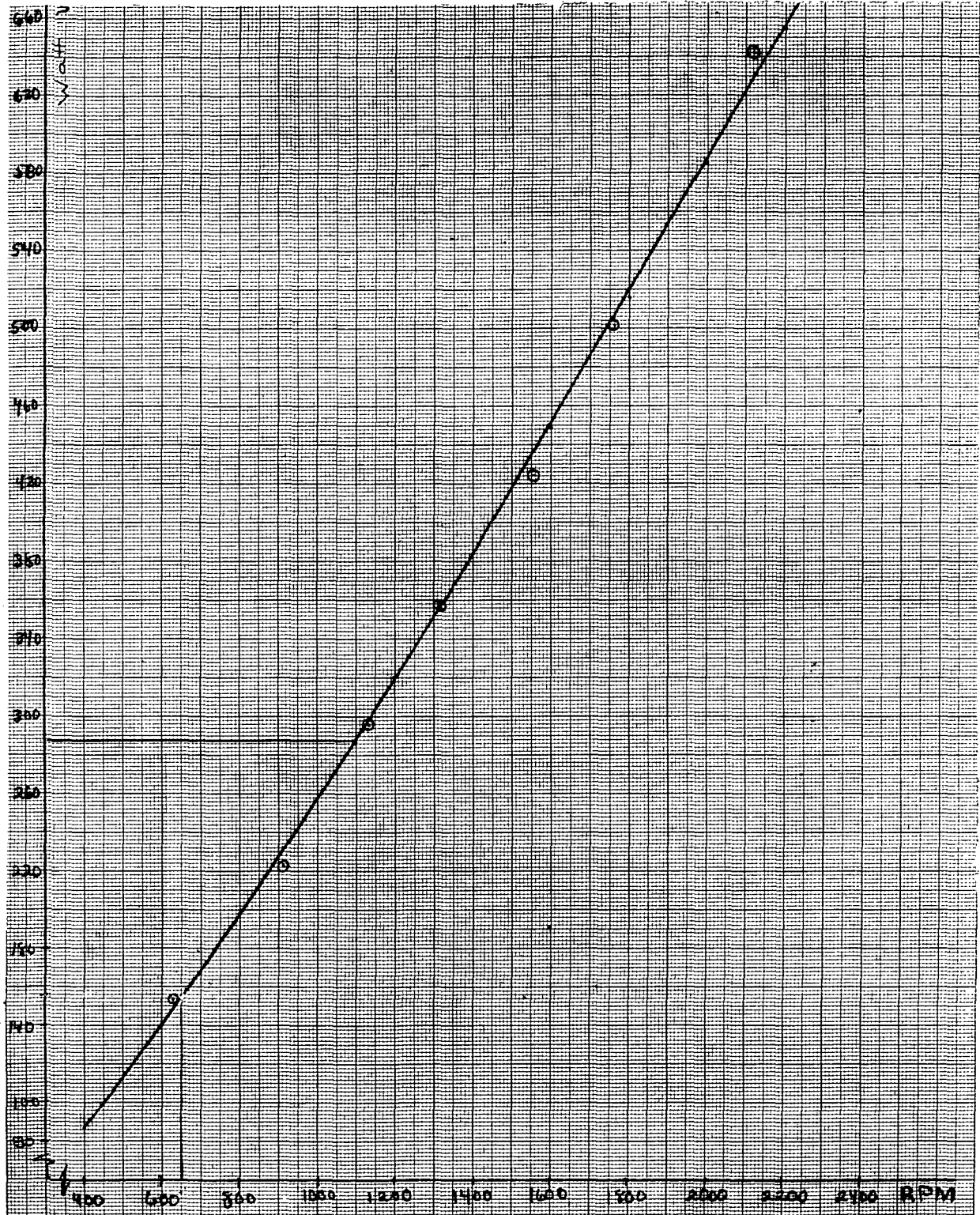


Figure 5-2 Friction and windage losses

No. of poles	4
Field winding turns/pole	20
No. of Slots	27
No. of conductors per slot	6
Length	96 mm.
No. of commutator bars	81
Frame material	wrought iron
Pole material	M 27, 0.47 mm Laminations
Armature Iron	M 27, 0.47 mm Laminations

Table 5-1 Parameters of the motor

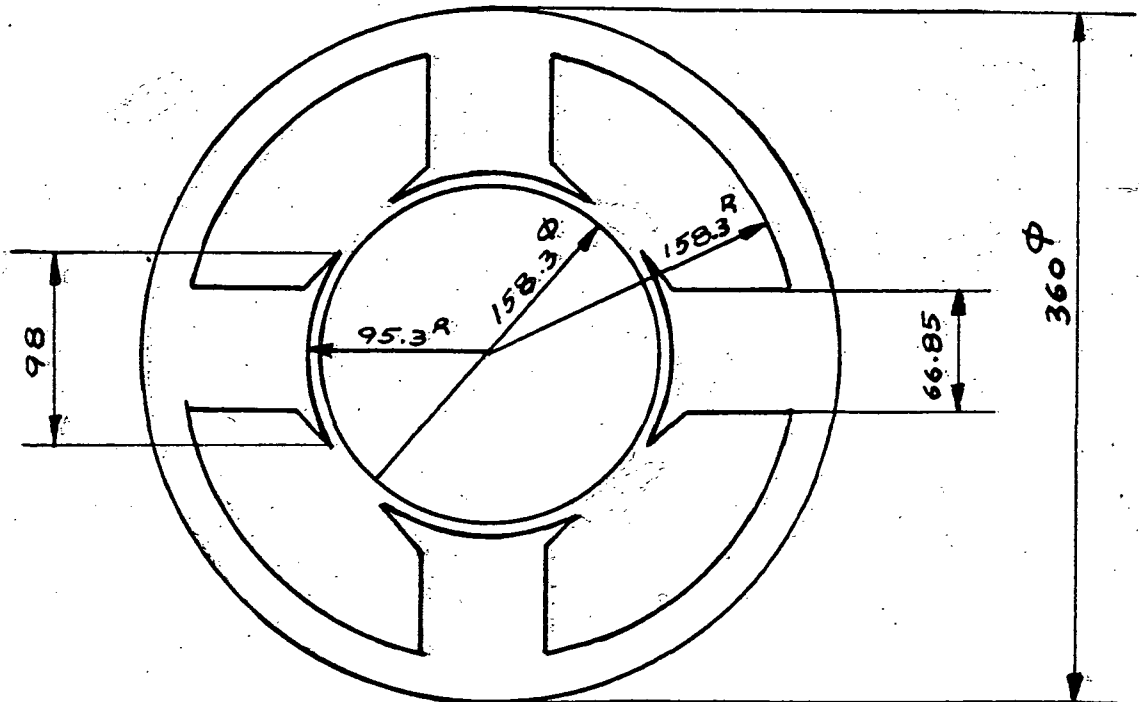


Figure 5-3 Dimensions of rotor and stator (in millimeters)

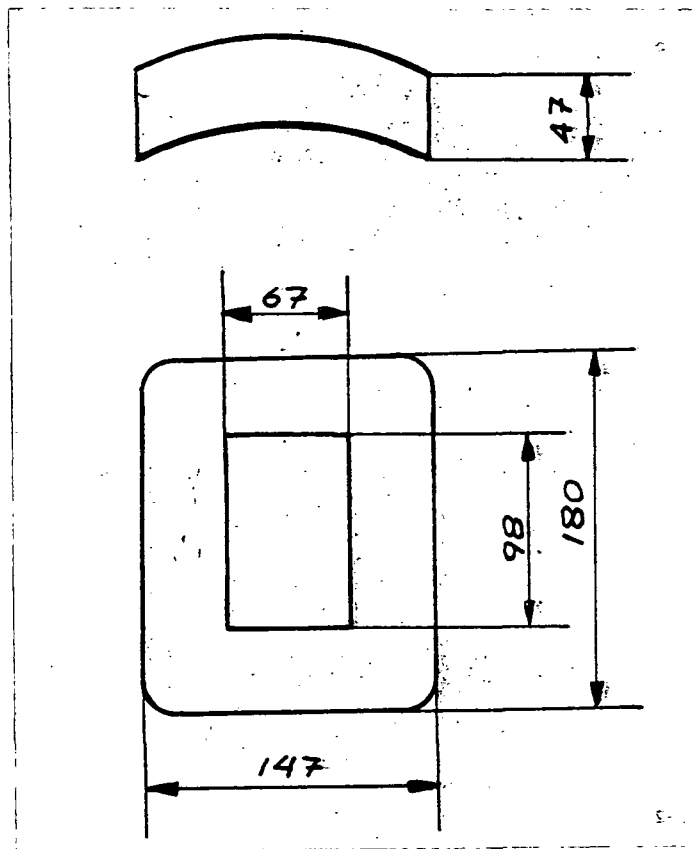


Figure 5-4 Dimensions of the field winding (in millimeters)

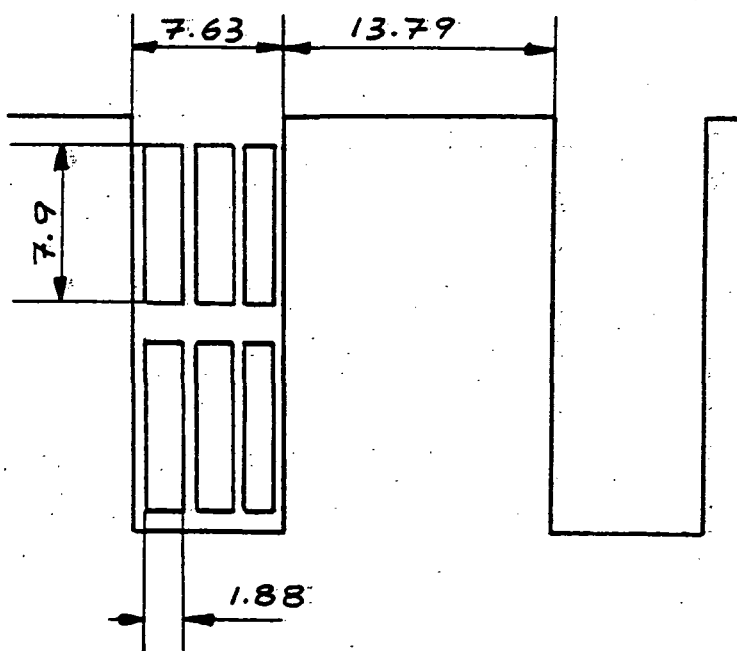


Figure 5-5 Dimensions of slot and armature conductors (in millimeters)

5.2.2 Approximations and Assumptions

The total number of slots in the armature of the machine is 27, making the number of slots per pole equal to 6.75. Since this number is not an integer, an accurate representation of the machine would be obtained only if the complete cross section was modeled. The accuracy would not be significantly decreased if only one pole was modeled using an integer number of slots, and keeping the ratio of the length of slot to tooth the same as in the actual machine.

In doing so, the number of Ampere-turns of the armature would be increased if the actual current of the machine was to be injected in the slot conductors. In order to simulate the field correctly and to maintain in the model the same magnetomotive force as in the real machine, the current in the armature winding should be multiplied by the ratio of the actual number of slots per pole to the number of slots in the model; in this case by $6.75/7.00$. This would ensure that the calculated values of the magnetic vector potential values and flux densities would be correct.

After the field is calculated, the voltages induced in the armature due to the field winding (and its self inductance) can be computed. These voltages will be the sum of the voltages induced in the conductors. A correction is needed here also, since the number of conductors in the model is larger than in the actual case. The corrected voltage induced in the armature, due either to rotation or self inductance should be the voltage calculated from the model, multiplied by $6.75/7.00$.

Commutation is a rather complicated phenomenon and it should be treated as such when it is studied alone. In that case the self inductances of the coils undergoing commutation are to be calculated, as well as their mutual inductance with each other and with the armature. Then, a model (consisting of differential equations) can be constructed based on these inductances and the resistivities of the various current paths. The problem is even more complicated by the fact that the brush resistivity is both nonlinear and dependent upon the brush pressure. On the other hand, if high resistivity commutation is assumed, its effect on the overall performance of the machine becomes minimal and can be neglected; i.e. the commutation assumed linear in the calculation of the currents of the coils undergoing commutation.

The conductor portions of the machine require more considerations. As described in section 3.2, when no eddy currents are anticipated, the real current densities can be assigned to the elements in the conductors and their conductivity assumed zero for the eddy currents. This is the case when a conductor is composed of many fine strands. When eddy currents and skin effects are anticipated, as is the case of solid conductors of relatively large cross sections, there are two possible ways to take their effect into account. One is to calculate the eddy currents in each individual conductor, by defining a relatively fine grid and applying equation (2-21) to all such conductors. The alternative procedure is to assume that all slots are going to behave similarly and solve, in a separate grid, the problem for only one slot at the same time that the main grid is solved, and from that solution calculate the changes of apparent resistance. In this investigation, the skin effect

was neglected and the apparent resistance of the windings used was the resistance that was measured at 100 Hz.

Figure 5-6 shows the discretization of one pole pitch. As can be noted, the discretization of the air gap is not shown. It is rather generated by the program as described in section 3.2.3. All conductors in the armature carry current in the same direction. Shifting of the brushes is accomplished by rotating the armature grid accordingly and letting the program define the airgap grid.

5.2.3 Results of the Computer Simulation

The program was run for various cases for which experimental results had been obtained previously. In Figure 5-7 the flux lines and the outline of the material boundaries are shown for the case of solid frame stator, where eddy currents are allowed to flow. In Figure 5-8 the same cross section is solved with the exception that the frame is assumed laminated. This is not the case of the motor discussed here, but the flux density distribution was examined because of interest in the characteristics between motors with laminated and those with solid frames.

In Figures 5-9, 5-10 and 5-11 the results of the simulation are presented for a sample case, where only ten points were used for one cycle. These results are presented here for comparison with experimental results.

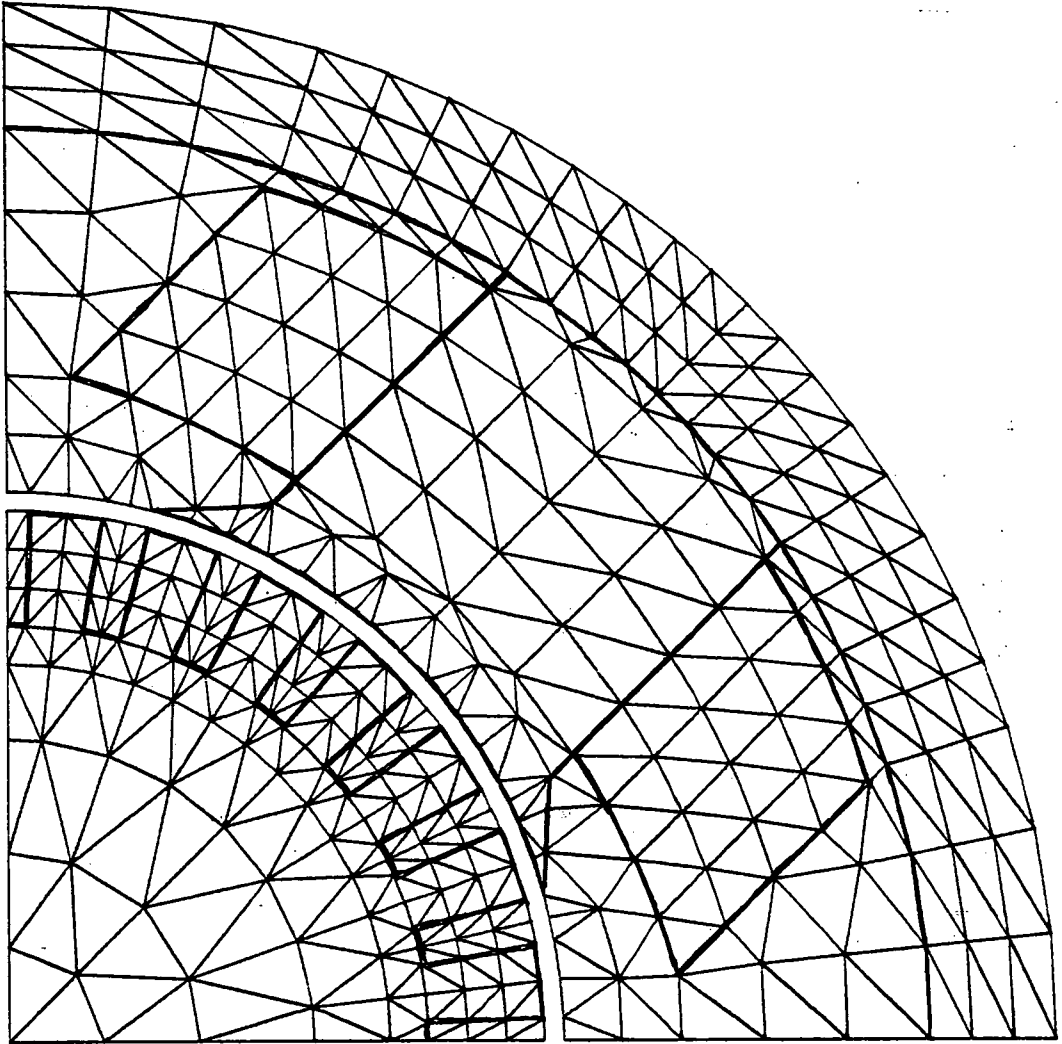


Figure 5-6 The grid for the electric vehicle motor

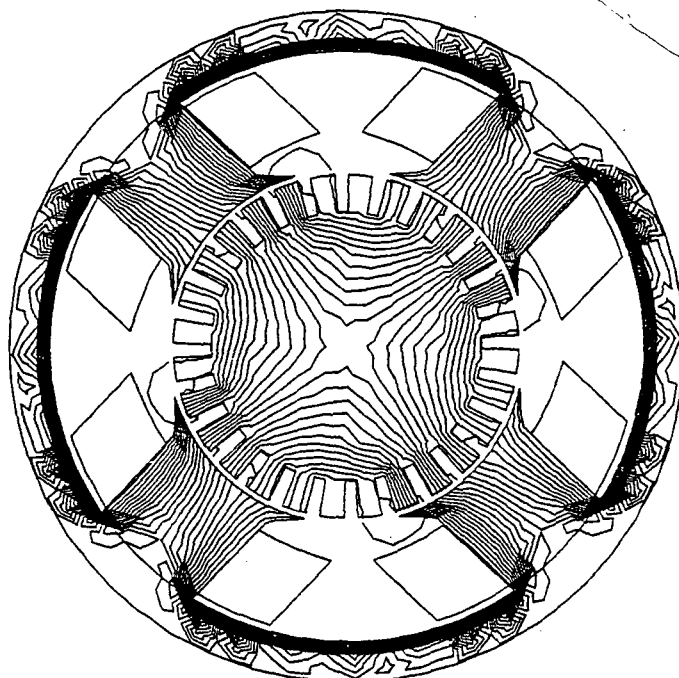


Figure 5-7 Solid Frame

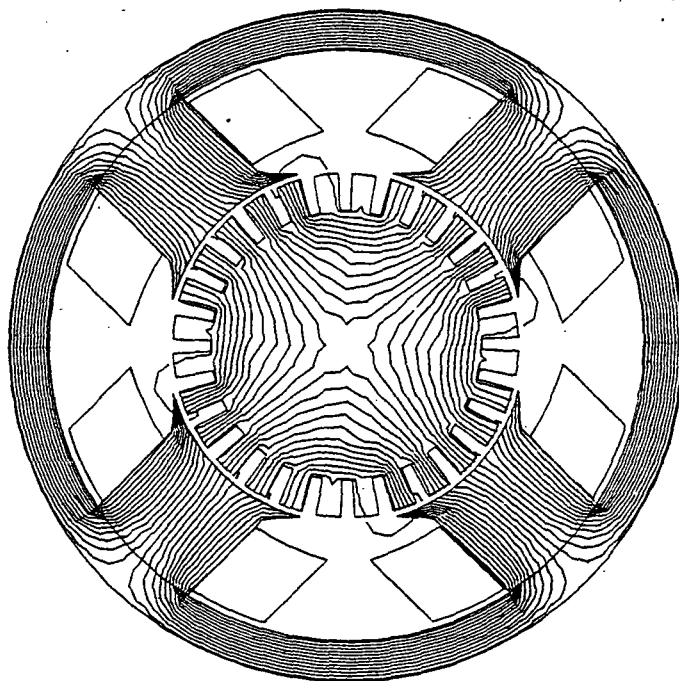


Figure 5-8 Laminated Frame

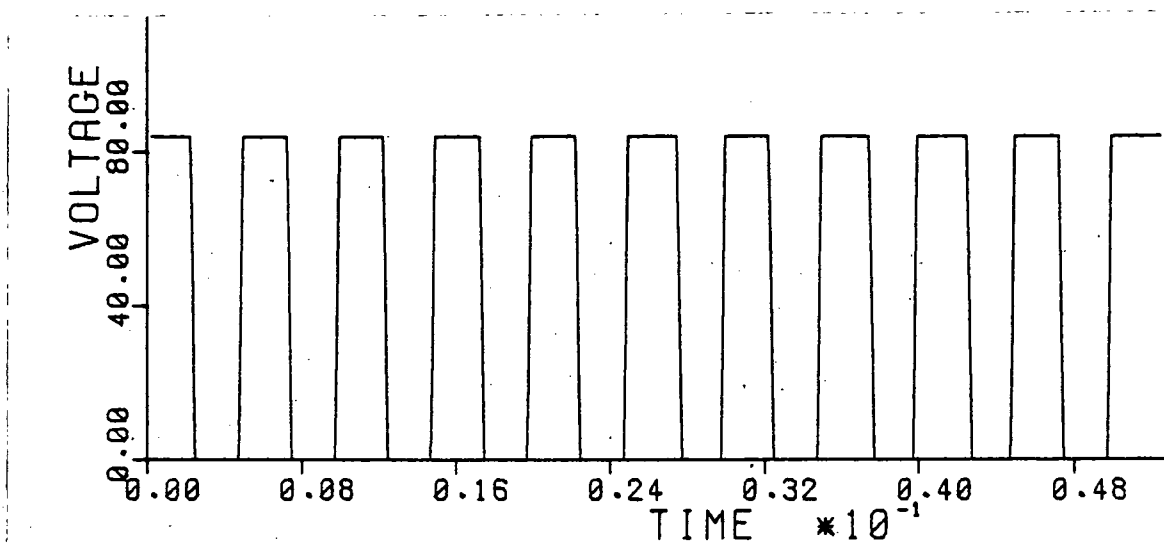


Figure 5-9 Voltage waveform

In Table 5-2 both observed test results and results of the simulation are given for a number of operating modes of the machine. The coarseness of the grid used does not seem to greatly affect the inductance and currents, but it obviously makes the eddy current calculation inaccurate, as can be observed from Figure 5-7. It also affects the accuracy of the torque as calculated from the Maxwell stress tensor.

The discrepancies between actual test data and results from the computer simulation can be attributed to the lack of knowledge of certain material parameters. The torque and current calculations depend not only on the coarseness of the grid, but they are also very sensitive to the resistivity and permeability of the frame. Typical values were used in the simulation from which the results of Table 5-2 were obtained, although significantly better results were obtained when other values of

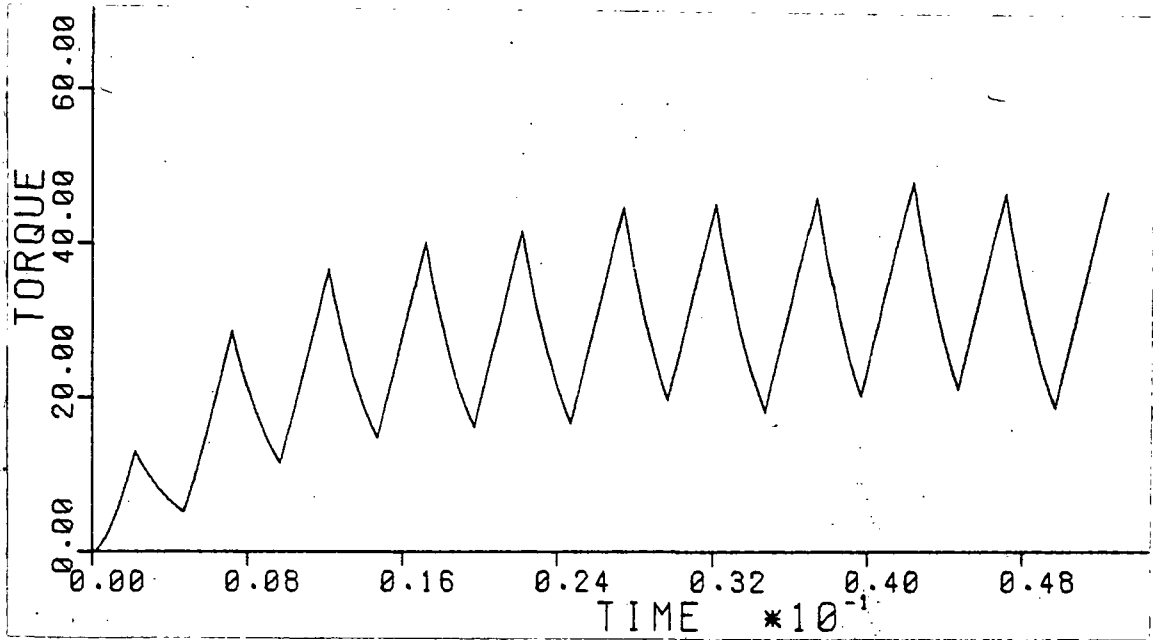


Figure 5-10 Torque waveform

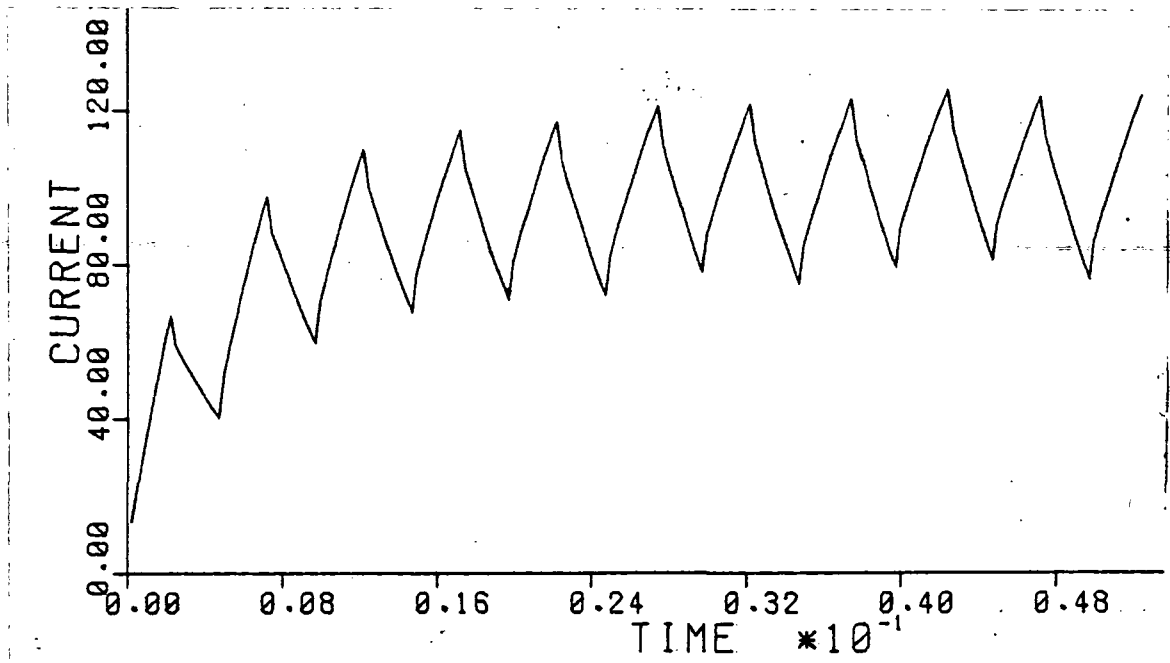


Figure 5-11 Current waveform

TEST					SIMULATION				
T (ms)	T _{on} /T	RPM (min)	I _{ave} A	$\Delta I/I_{ave}$	M _{sh} (N m)	M _{gap} (N m)	I _{ave} A	$\Delta I/I_{ave}$	M _{gap} (N m)
10	0.45	647	201.3	0.86	82.34	84.66	222.4	0.91	103.2
10	0.45	1102	104	1.18	28.93	31.43	115.2	1.205	40.6
5	0.45	1725	174.8	0.63	67.37	69.69	195.6	0.69	88.6
5	0.45	1120	120.4	0.66	29.51	32.02	127.3	0.704	42.8
5	0.45	1820	63.5	1.10	9.67	12.43	68.6	1.23	18.03

T: period of chopper

T_{on}: time on

I_{ave}: average value of current

ΔI : ripple current peak to peak

M_{sh}: shaft torque

M_{gap}: Air gap torque

*Calculated as the shaft torque plus friction and windage.

Table 5.2 Test and simulation results.

resistivity and permeability of the frame were used. Also the effect of the batteries was completely ignored, although battery characteristics affect markedly the performance of the machine.

5.2.4 Airgap Radial Flux - Brush Positioning

The magnetic field due to the field winding in a DC machine is symmetric around a pole center line and almost uniform under the pole face because of the constant reluctance of the air gap (provided that the slot effect is neglected). Outside the pole face, the radial flux density drops rapidly, becoming zero in the middle of the interpolar space. When the brushes are at the geometrical neutral axis, the armature cross field is also symmetric with respect to the point between the two brushes. The radial flux density of the airgap due to the field winding, the armature cross field and the resultant flux density are shown in Figure 5-12 a. As can be observed, a remaining flux density exists under the brushes. This flux induces a voltage in the coil undergoing commutation with the result that the commutation process is nonlinear. In order to achieve linear commutation this voltage should be equal and opposite to the direction of the voltage induced to the coil due to its self inductance, thereby achieving cancellation. Therefore, the brushes (and the cross field) must be shifted as shown in Figure 5-12 b. When the magnetic vector potential is known, at a cross section of the motor from a finite element or other numerical method, the radial flux density can be calculated, since:

$$B_r = -\frac{1}{r} \frac{\partial A}{\partial \phi} \quad (5-14)$$

In Figures 5-13 and 5-14 the magnetic vector potential and the radial flux density are shown for the rotor surface, Figures 5-15 and 5-16 show the same quantities for the stator surface. The reason the flux density curve is not smooth is the presence of teeth on the armature surface, which cause the concentration of flux in them. From these figures, the optimal location of the brushes can be calculated. In Figure 5-17 the field solution is shown for the brushes shifted 30 electrical degrees. In Figures 5-18 and 5-19 the magnetic vector potential values and the radial flux density on the rotor surface are presented for the 30° brush shift condition. The small amount of flux assisting the commutation can be observed (note arrows in Figure 5-19).

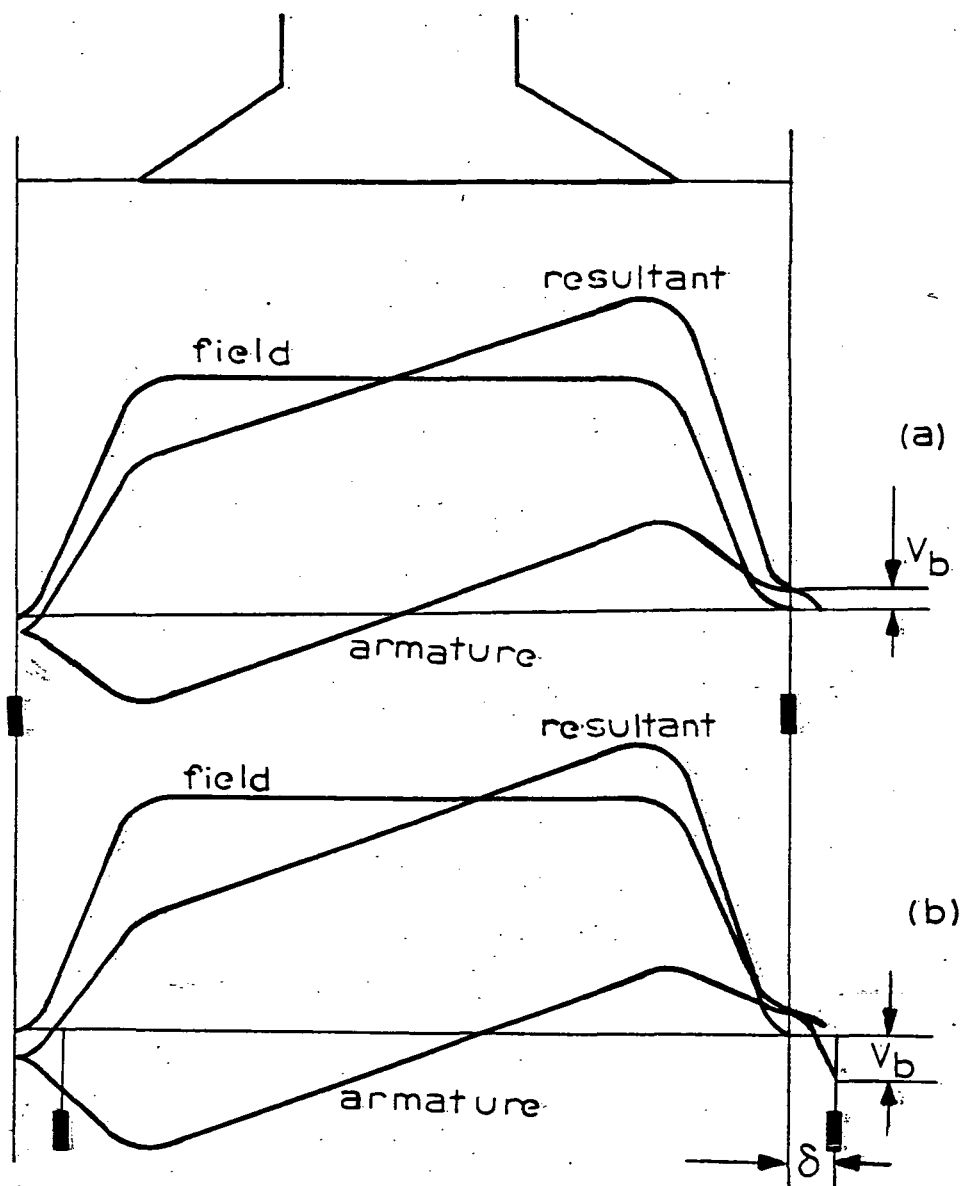


Figure 5-12 Effect of brush position on resultant field distribution
(a) brushes at neutral axis, (b) brushes shifted opposite to the rotation of the motor

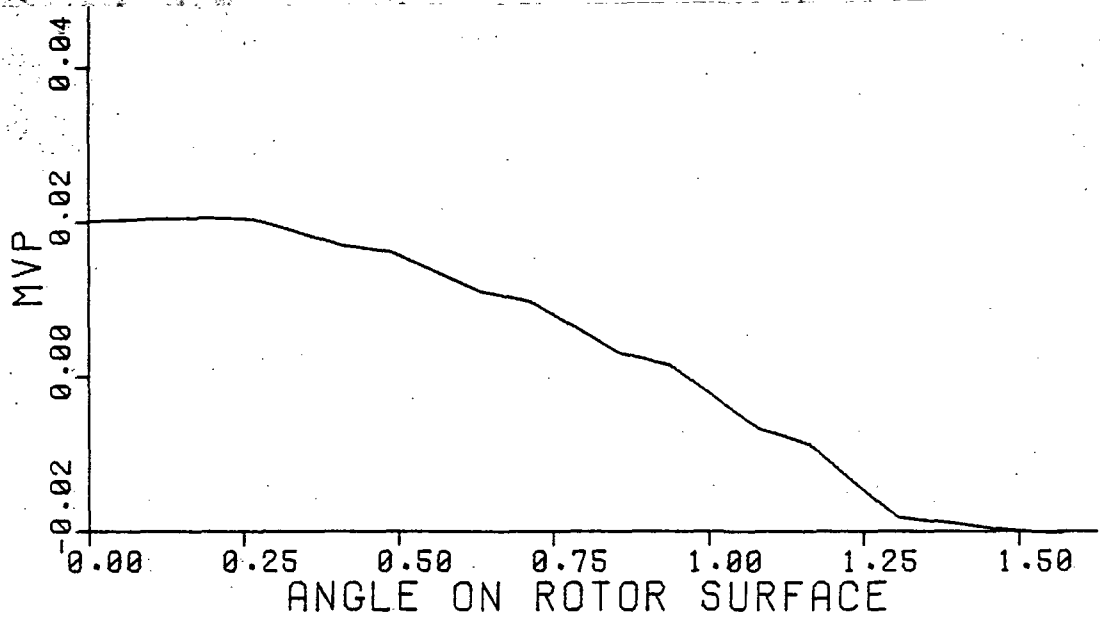


Figure 5-13 MVP on rotor surface brushes at 0°

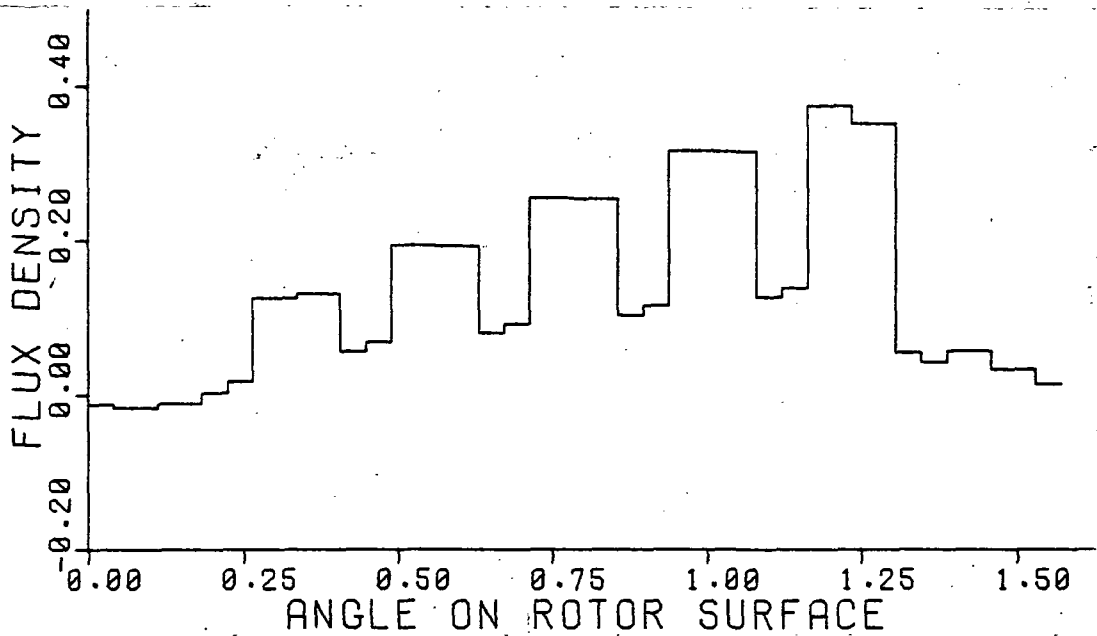


Figure 5-14 Flux density at rotor surface brushes at 0°

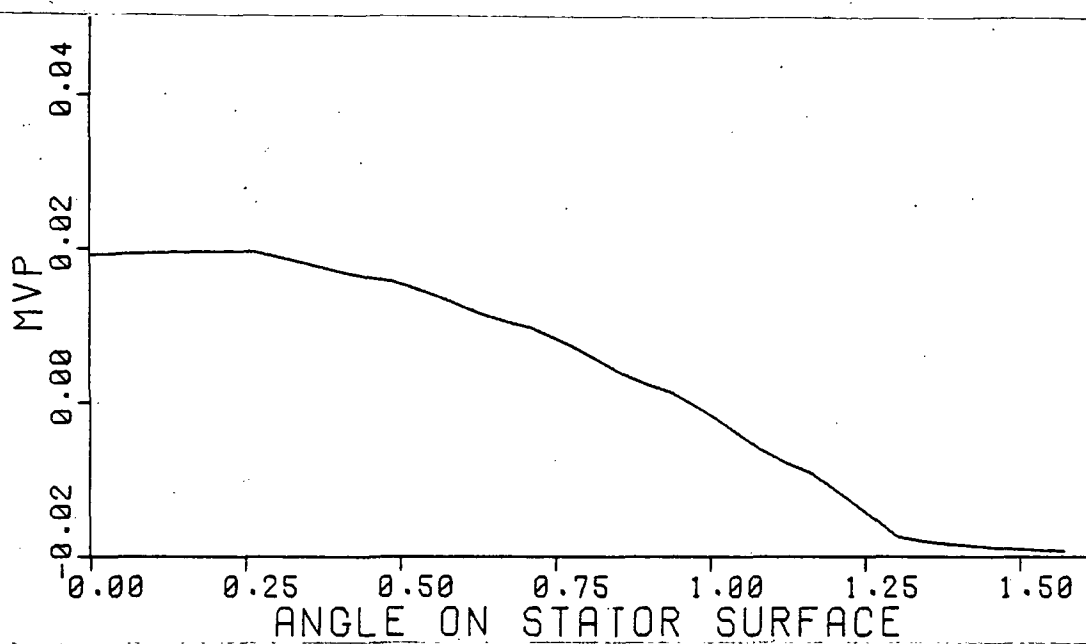


Figure 5-15 MVP at stator surface

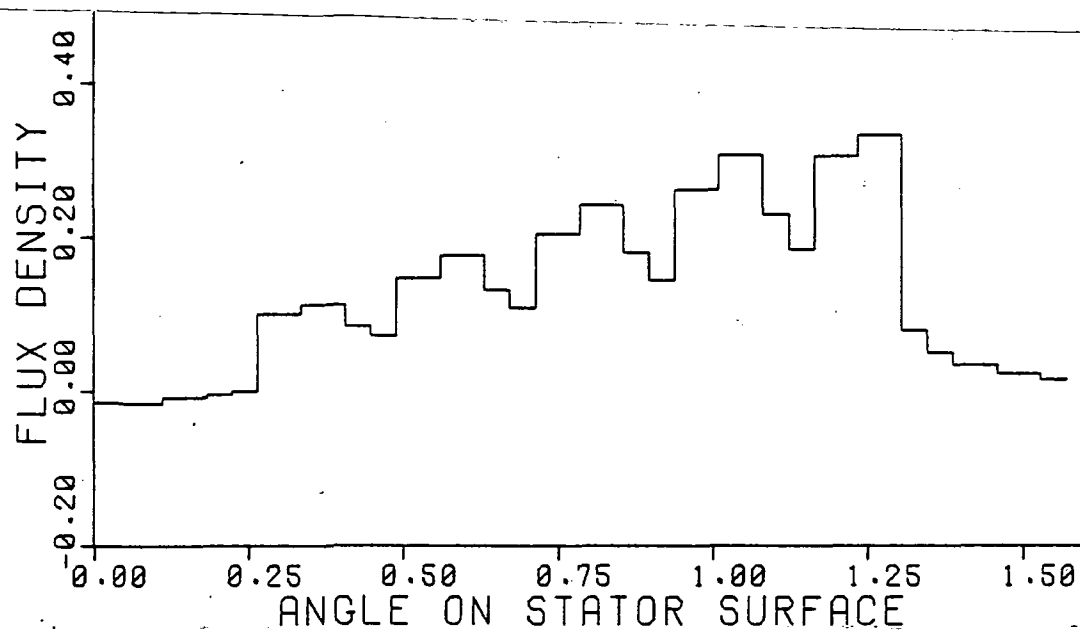


Figure 5-16 Flux density at stator surface

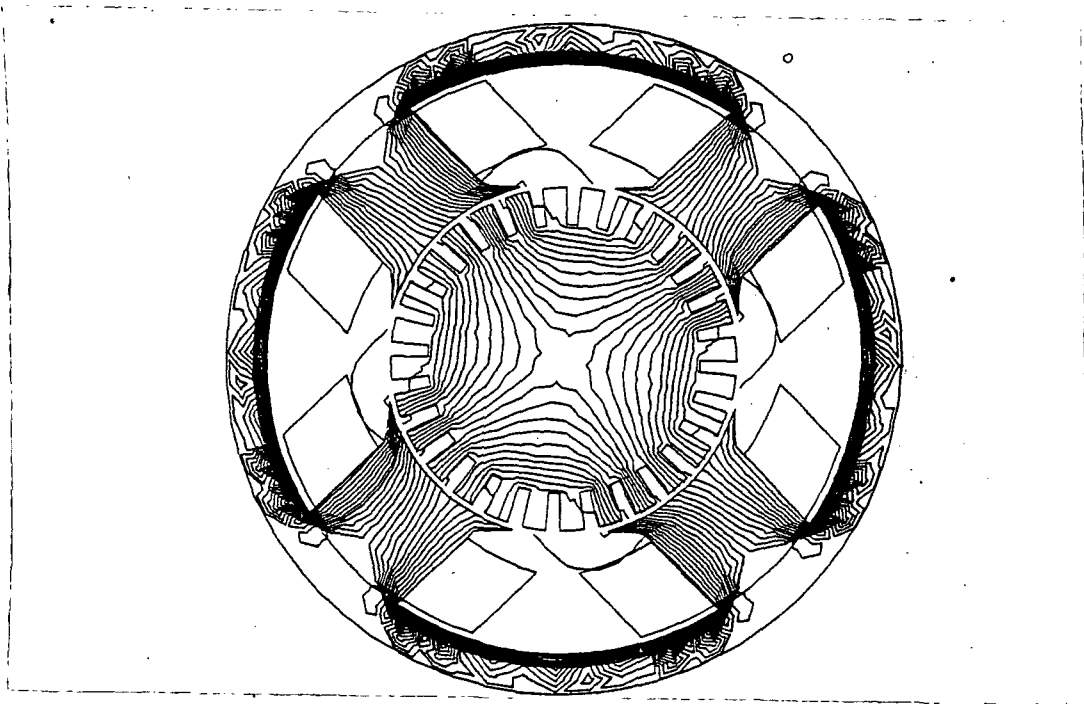


Figure 5-17 The magnetic field for brushes shifted 30 electrical degrees

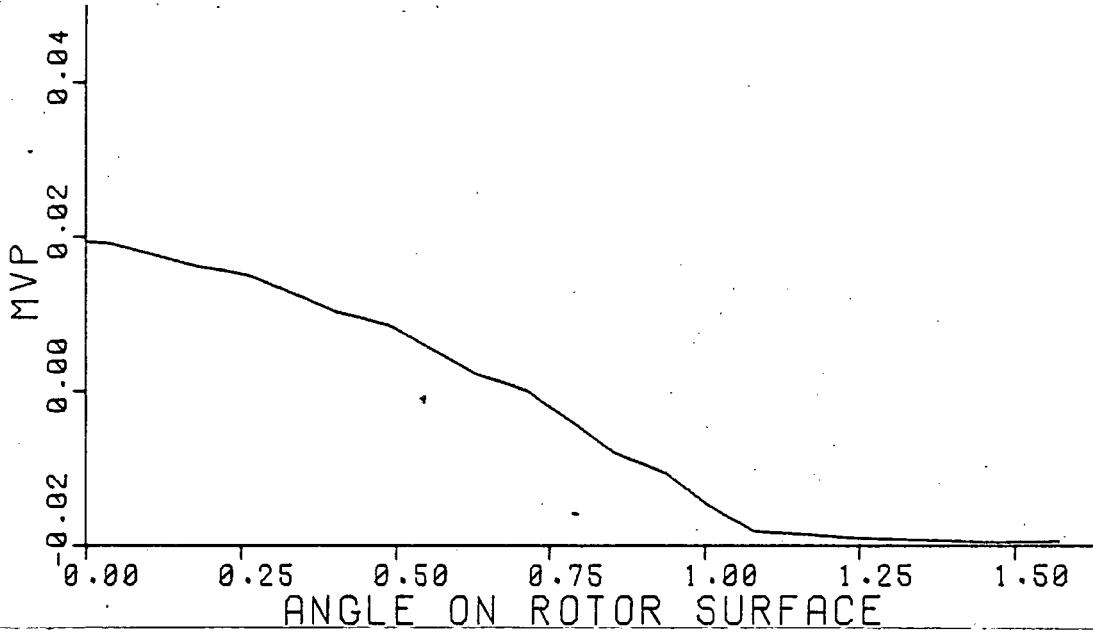


Figure 5-18 MVP at rotor surface. Brushes at 30 electrical degrees

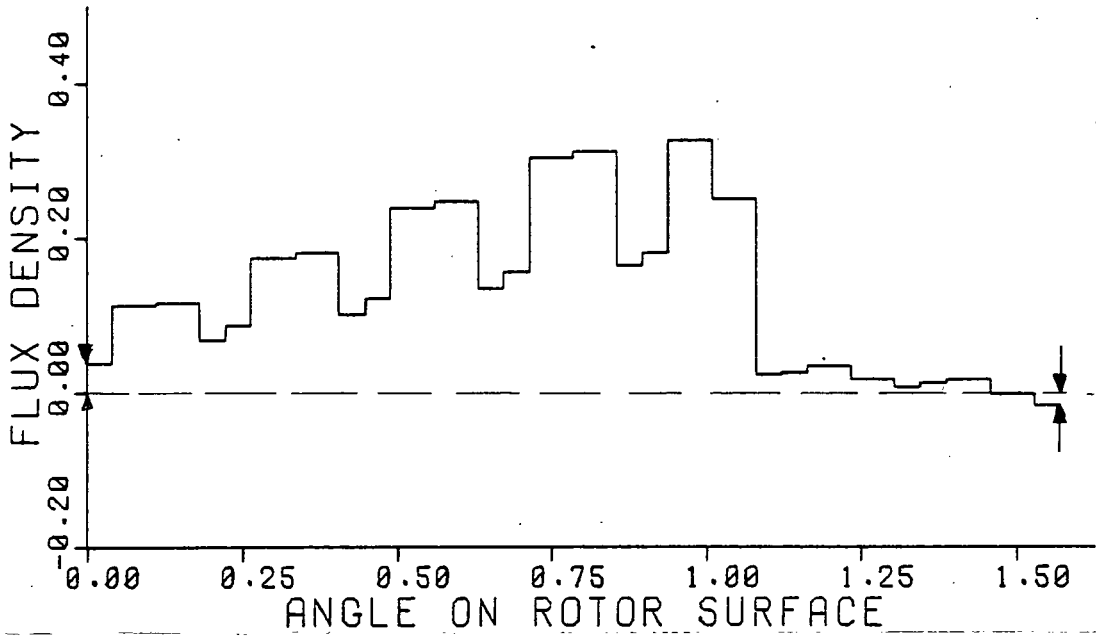


Figure 5-19 Flux density at rotor surface
Brushes at 30 electrical degrees

6.0 THE STARTING OF SALIENT POLE SYNCHRONOUS MOTORS WITH DAMPER BARS

The practical aspects of this problem are primarily the oscillatory torque and the sustained currents in the damper bars. Also of interest are the magnitude and waveform of phase currents and the possibility of the motor operating as a generator during the oscillatory cycle. The oscillatory torque can cause the destruction of gears and torsional failure of the shaft of the machine when the torque frequency coincides with one of the natural frequencies of the system. The currents in the damper bars, if sustained over a relatively long period, can increase the temperature of the pole face to levels which can result in mechanical damage. The complex waveform of the input current, and/or the operation of the machine as a generator can cause disturbances to the power circuit and possibly undesired operation of protective devices. The induced current in the field winding can cause elevated temperature, but the effect can be controlled by connecting a resistor across the field terminals. This resistor must be properly selected based on the problems of controlling the voltage across the field terminals and current heating effects, and the performance of the machine must be evaluated with this value of resistor.

6.1 The Electrical Equations of the Salient Pole Synchronous Machine

Let ω_0 be the synchronous electrical speed of the machine, i.e. the angular frequency of the voltage applied to the terminals:

$$\omega_o = 2\pi f \quad (6-1)$$

If the machine was not in the starting period but operating normally, the angular velocity of the rotor would be ω_{mo} :

$$\omega_{mo} = 2\pi f \frac{2}{p} \quad (6-2)$$

where P is the number of poles of the machine. During the starting of the machine, the rotor is revolving with a speed, ω_m , lower than ω_{mo}

$$\omega_m = \omega_{mo} (1-s) \quad 0 \leq s \leq 1 \quad (6-3)$$

where s is the slip. Defining ω_e the electrical speed of the rotor:

$$\omega_e = \frac{P}{2} \omega_m = \omega_o (1-s) \quad (6-4)$$

This quantity, ω_e , is fictitious and does not represent the mechanical angular velocity of an equivalent two pole machine operating at the same slip.

Figure 6-1 depicts the three phase salient pole synchronous machine with a field winding, f, and damper bars. In this investigation the number of bars per pole has been arbitrarily chosen as 9 without significant loss in generality.

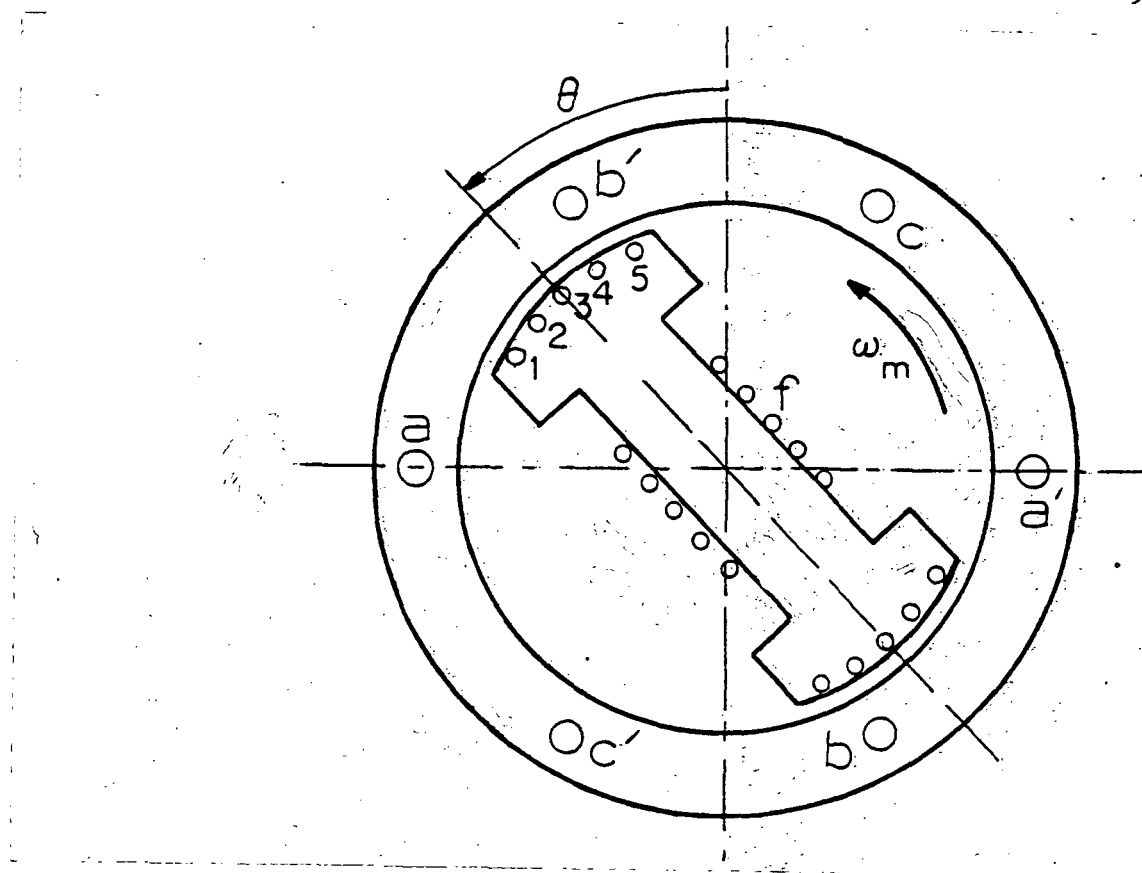


Figure 6-1 Salient pole synchronous machine

Kirchoffs equations⁽⁴⁶⁾ for the machine circuits are:

$$V = \psi + R \cdot I = L \cdot \dot{I} + L \cdot I + R \cdot I \quad (6-5)$$

where V is the vector of the voltages at the terminals of each of the 13 current paths (3 phases, 1 field, 9 damper bars), ψ is the vector of the flux linkages of the windings, L is the inductance matrix, R the resistance matrix and I the current vector.

The entries of the inductance matrix are denoted by L_{ij} and of the resistance matrix by R_{ij} , where $i, j = a, b, c, f, 1, \dots, 9$. The values of self and mutual inductance of the rotor circuits, L_{ij} , $i, j = f, 1, \dots, 9$, are constant, due to the fact that the stator is cylindrical, and the self and mutual coupling does not vary with the angle θ . However, the self and mutual couplings between the stator circuits and between the stator and rotor circuits vary with the angle θ due to the saliency of the rotor. These inductances can be expressed as:

$$\begin{aligned}
 L_{aa} &= L_{aao} + L_{aa2} \cos 2 \theta \\
 L_{bb} &= L_{aao} + L_{aa2} \cos 2 (\theta - 120^\circ) \\
 L_{cc} &= L_{aao} + L_{aa2} \cos 2 (\theta + 120^\circ) \\
 L_{ab} &= -[L_{abo} + L_{aa2} \cos 2 (\theta + 30^\circ)] \\
 L_{bc} &= -[L_{abo} + L_{aa2} \cos 2 (\theta - 90^\circ)] \\
 L_{ca} &= -[L_{abo} + L_{aa2} \cos 2 (\theta + 150^\circ)] \\
 L_{af} &= L_{afo} \cos \theta \\
 L_{bf} &= L_{afo} \cos (\theta - 120^\circ) \\
 L_{cf} &= L_{afo} \cos (\theta + 120^\circ) \\
 L_{ai} &= [L_{adi} \cos \theta - L_{aqi} \sin \theta] \\
 L_{bi} &= [L_{adi} \cos (\theta - 120^\circ) - L_{aqi} \sin (\theta - 120^\circ)] \\
 L_{ci} &= [L_{adi} \cos (\theta + 120^\circ) - L_{aqi} \sin (\theta + 120^\circ)] \\
 & \qquad \qquad \qquad i = 1, \dots, 9
 \end{aligned} \tag{6-6}$$

The terms L_{aao} , L_{abo} are the components of stator self and mutual inductance, and they are constant; L_{aa2} , L_{afo} are the maximum excursions

of inductances from their average values. L_{adi} and L_{aqi} do not represent actual inductances; they are constants which have to be evaluated together with L_{aao} , L_{abo} , L_{aa2} and L_{afo} .

The angle θ , as shown in Figure 6-1, is defined as the angle between the axis of the rotor and the axis of phase a in the equivalent two pole machine:

$$\theta = \omega_e t + \theta_0 = \omega_0(1-s) t + \theta_0 \quad (6-7)$$

where t is the time and θ_0 the initial value of θ .

From these definitions, the entries of matrix \dot{L} can be calculated:

$$\begin{aligned} \dot{L}_{aa} &= -2\omega_e L_{aa2} \sin 2\theta \\ \dot{L}_{bb} &= -2\omega_e L_{aa2} \sin 2(\theta-120^\circ) \\ \dot{L}_{cc} &= -2\omega_e L_{aa2} \sin 2(\theta+120^\circ) \\ \dot{L}_{ab} &= 2\omega_e L_{aa2} \sin 2(\theta+30^\circ) \\ \dot{L}_{bc} &= 2\omega_e L_{aa2} \sin 2(\theta-90^\circ) \\ \dot{L}_{ca} &= 2\omega_e L_{aa2} \sin 2(\theta+150^\circ) \\ \dot{L}_{af} &= -\omega_e L_{afo} \sin \theta \\ \dot{L}_{bf} &= -\omega_e L_{afo} \sin (\theta-120^\circ) \\ \dot{L}_{cf} &= -\omega_e L_{afo} \sin (\theta+120^\circ) \\ \dot{L}_{ai} &= -\omega_e [L_{adi} \sin \theta + L_{aqi} \cos \theta] \\ \dot{L}_{bi} &= -\omega_e [L_{adi} \sin (\theta-120^\circ) + L_{aqi} \cos (\theta-120^\circ)] \\ \dot{L}_{ci} &= -\omega_e [L_{adi} \sin (\theta+120^\circ) + L_{aqi} \cos (\theta+120^\circ)] \end{aligned} \quad (6-8)$$

The matrix R is a diagonal matrix, containing the resistivities of the circuits.

6.2 The Effect of the Damper Bar Connections

The damper bars in each pole are connected together at each end of the field pole so as to form a grill. Often this connection extends between poles to form a squirrel cage winding, similar to that of an induction motor. The type of connection has an effect on the starting and the transient performance of the synchronous machine, and the system of equations that describes it must be modified accordingly. In both cases the voltages of the terminals of the three phases are known and the voltage of the field winding terminals is zero since it is short circuited. The value of the field resistivity in matrix R , though, has to be increased by the value of the external resistor. Neglecting the resistance of the end ring between adjacent bars, the voltages across the damper bars, V_1, V_2, \dots, V_9 have the same value, V_d .

6.2.1 Closed End Rings (Cage Winding)

As shown in Figure 6-2, the currents and voltages at opposite poles are of opposite values.

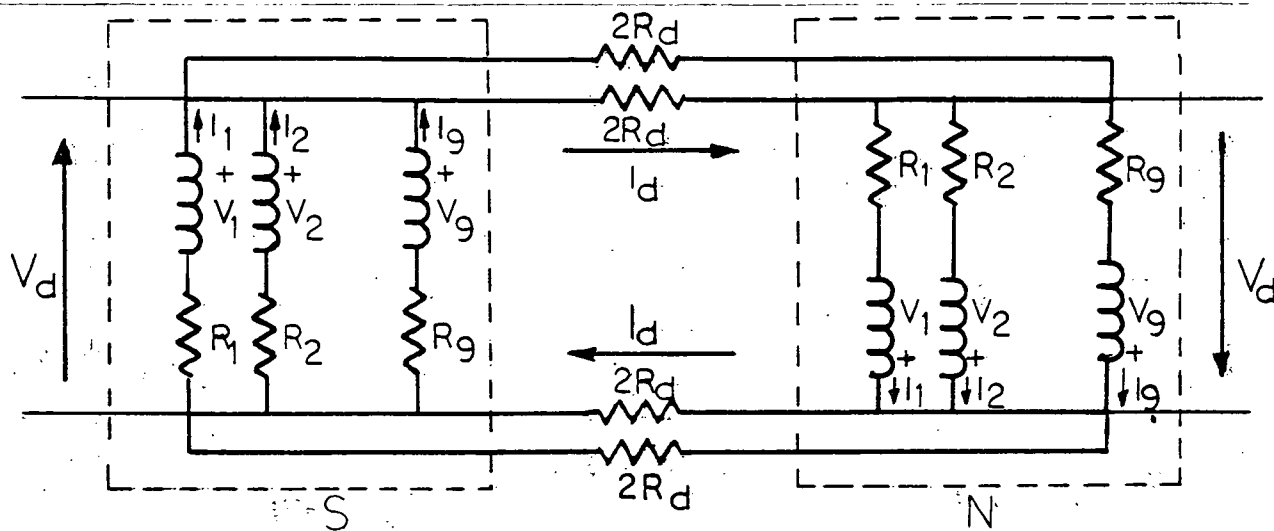


Figure 6-2 Damper winding with closed end rings

The resistance of the pole to pole connections is taken as $2R_d$, yielding a combined resistance of R_d . Thus, from Figure 6-2:

$$V_d = I_d R_d \quad (6-9)$$

$$V_d = (I_1 + I_2 + \dots + I_9) R_d \quad (6-10)$$

The voltages induced in the damper bars, V_i , are given by:

$$\begin{bmatrix} V_1 \\ \vdots \\ V_1 \end{bmatrix} = \begin{bmatrix} L_{1a} & L_{1b} & L_{1c} & L_{1f} & L_{11} & \dots & L_{19} \\ \vdots & \vdots & \vdots & \vdots & \vdots & \ddots & \vdots \\ L_{9a} & L_{9b} & L_{9c} & L_{9f} & L_{91} & \dots & L_{99} \end{bmatrix} \cdot i$$

$$+ \begin{bmatrix} \dot{L}_{1a} & \dot{L}_{1b} & \dot{L}_{1c} & 0 & \dots & \dots & \dots & 0 \\ \dot{L}_{9a} & \dot{L}_{9b} & \dot{L}_{9c} & 0 & \dots & \dots & \dots & 0 \end{bmatrix} \cdot I \quad (6-11)$$

Since $V_1 = V_2 = \dots = V_9 = V_d$, equation (6-11) can be substituted for equation (6-5), which becomes:

$$\begin{bmatrix} V_a \\ V_b \\ V_c \\ 0 \\ \vdots \\ 0 \end{bmatrix} = L \cdot \dot{I} + \dot{L} \cdot I + R' \cdot I \quad (6-12)$$

where the entries r'_{ij} of the modified matrix R' are given by

$$r'_{ij} = r_{ij} \quad i = a, b, c, f \quad \text{or } j = a, b, c, f$$

and

$$r'_{ij} = r_{ij} + R_d \quad i, j = 1, \dots, 9$$

(6-13)

6.2.2 Open End Rings

The case of open end rings presents a more complicated problem. The determination of the voltage across the damper bars is based on the fact that the total current of the damper bars in each pole sums to zero.

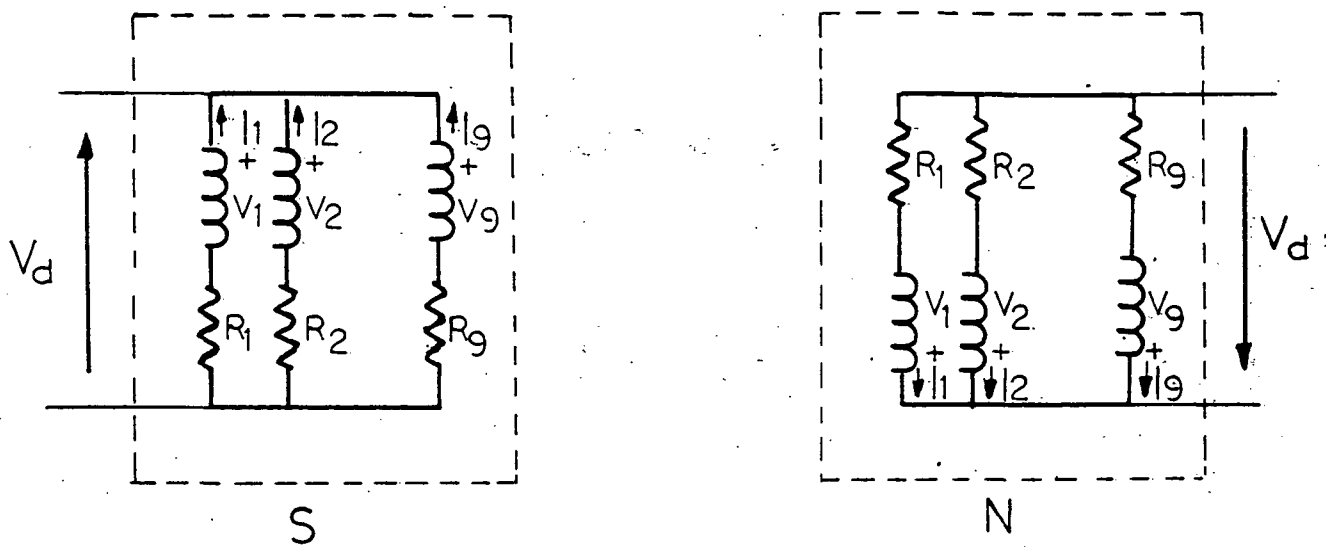


Figure 6-3 Damper windings with open end rings

Neglecting again the resistivity between adjacent bars and assuming the same voltage V_d , across all the damper bars of a pole, equation (6-5) can be written as:

$$V^* = \begin{bmatrix} V_a \\ V_b \\ V_c \\ 0 \\ \vdots \\ 0 \end{bmatrix} = L \cdot \dot{I} + L \cdot I + R \cdot I - \begin{bmatrix} 0 \\ 0 \\ 0 \\ V_d \\ \vdots \\ V_d \end{bmatrix} \quad (6-14)$$

Denoting:

$$I = I^* - L^{-1} \cdot \begin{bmatrix} 0 \\ 0 \\ 0 \\ 0 \\ \vdots \\ V_d \end{bmatrix} \quad (6-15)$$

then, \dot{I}^* can be calculated from (6-14) which is modified to:

$$\dot{V}^* = L \cdot \dot{I}^* + \dot{L} \cdot I + R \cdot I \quad (6-16)$$

$$\dot{I}^* = L^{-1} [\dot{V}^* - (\dot{L} + R) \cdot I] \quad (6-17)$$

Since the currents of all the damper bars in each pole sum to zero:

$$\sum_{i=1}^9 I_i = 0 \quad (6-18)$$

the voltage V_d can be calculated from (6-15) as:

$$V_d = \frac{\sum_{i=1}^9 I_i^*}{\sum_{i=1}^9 \sum_{j=1}^9 \lambda_{ij}} \quad (6-19)$$

where λ_{ij} are the entries of the matrix L^{-1} . Finally the vector I can be calculated as:

$$I = \dot{I}^* + L^{-1} \begin{bmatrix} 0 \\ 0 \\ 0 \\ 0 \\ V_d \\ \vdots \\ V_d \end{bmatrix} \quad (6-20)$$

6.3 Calculation of Constants

The constant entries of the matrices L and \dot{L} and the constants in equations (6-6) can be calculated from flux plots and from analytical considerations.

6.3.1 External Connections

The machine is connected to the electrical network considered an infinite bus through an equivalent line and a power transformer. The inductances of these components can be calculated from the per unit impedance of the transformer and the short circuit apparent power at the end of the line.

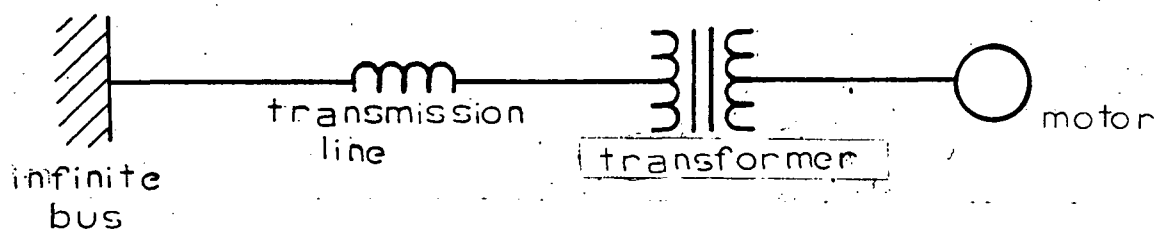


Figure 6-4. Equivalent circuit for the supply of the motor.

The value of the inductance of the transmission line and the transformer must be added to the value of L_{aao} which is calculated from the flux maps of the machine.

6.3.2 Self and Mutual Inductances of the Salient Pole Machine

In order to calculate the constants of the machine inductances, the electromagnetic field must be solved for several excitations at various operating conditions. Initially the field is solved for a certain rotor position and the actual currents in the phase windings, the field and the damper bars. The solution, besides giving the magnetic vector potential at every point, also yields the permeabilities of all the

elements in magnetic portions of the machine. Then, the rotor is moved so that its axis coincides with the axis of phase a. By applying current to phase a and calculating the electromagnetic field without changing the permeabilities assigned to each element, the self inductance of phase a and its mutual inductances with the other circuits can be calculated for that position of the rotor and for the saturation of the current paths due to the actual currents.

The inductances thus calculated are the inductances in equations (6-8) corresponding to angle $\theta=0$.

The rotor is then revolved by 90 electrical degrees and the previous process repeated again without changing the saturation levels. The same parameters are calculated again, this time corresponding to the angle $\theta=90^\circ$. Always keeping the permeabilities of the elements the same as resulted from the initial field calculation, current is applied to the field winding and each damper bar, and the field solved for each case. From the information gathered from the field solutions, the constant values of the self and mutual inductances are then calculated for the specific operating condition defined by the original current vector.

In addition to the external inductance, L_{ext} , the end turn inductance should be added to the calculated value of L_{aao} , and the field and damper bar end inductances added to the corresponding inductances. These inductances were obtained for the case investigated here, from Kilgore's formulae⁽⁴⁷⁾. It is understood that they are not accurately determined, but their value is too small for a significant error to be introduced.

The procedure described above was applied to a 300 HP, 6 pole synchronous generator with open end ring (grill). Figure 6-5 shows the grid used for the solution of the magnetic vector potential and Figures 6-6 to 6-13 show the equipotential lines for currents applied to the field, the damper bars and phase a at zero and ninety electrical degrees. Due to symmetry, the field was solved for current applied to only five of the nine damper bars since the parameters of the rest would be the same.

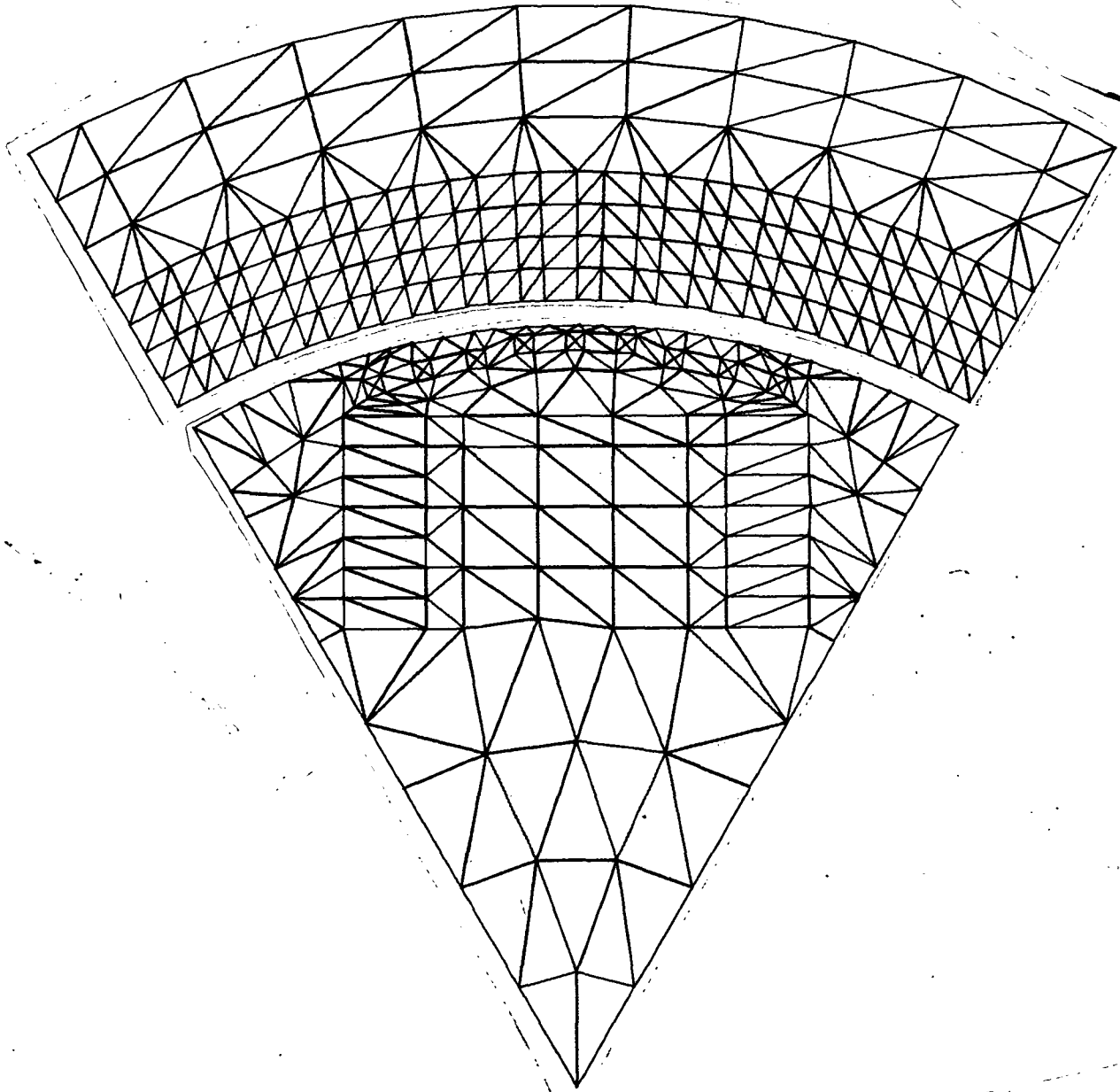


Figure 6-5 The grid for a six generator

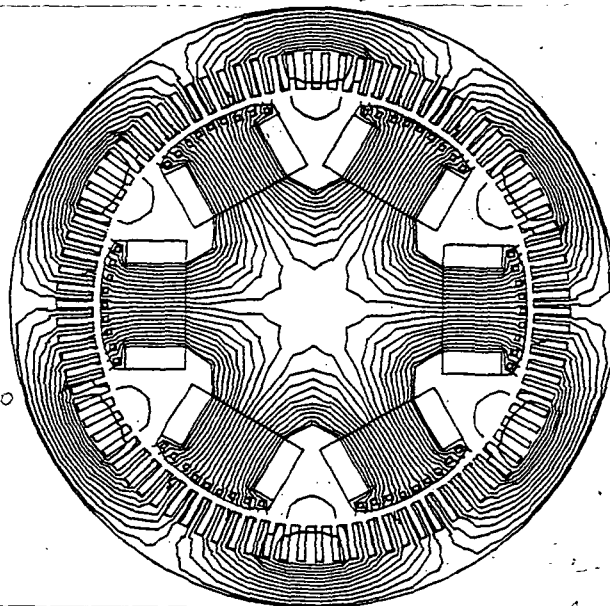


Figure 6-6 Current in phase a, $\theta = 0$

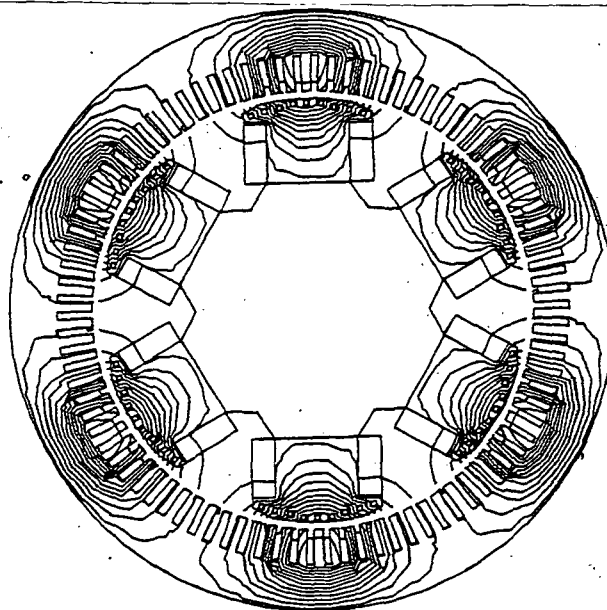


Figure 6-7 Current in phase a, $\theta = 90^\circ$

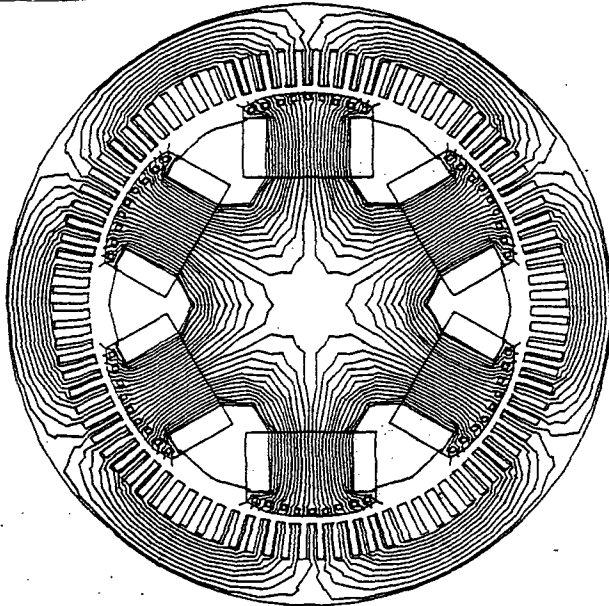


Figure 6-8 Current in field

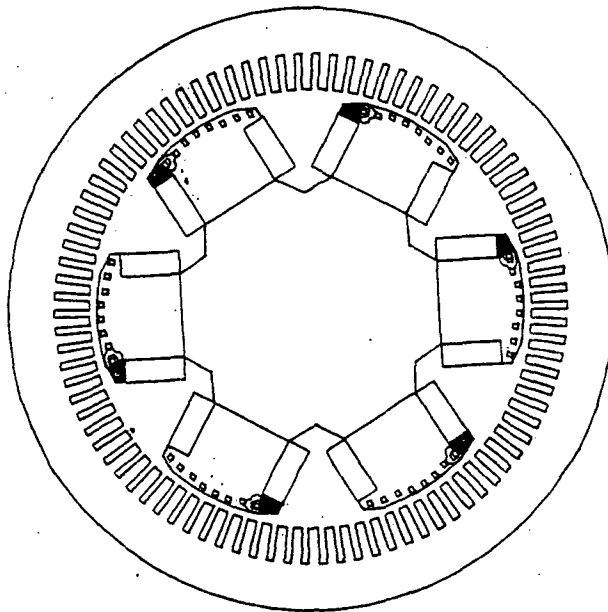


Figure 6-9 Current in damper bar No. 1

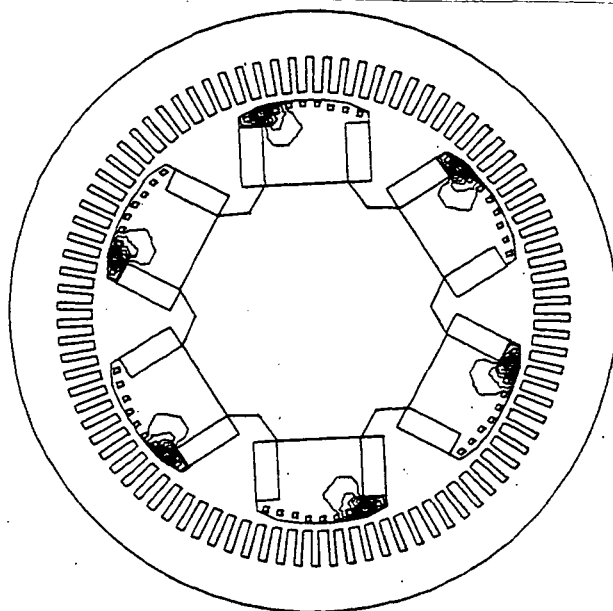


Figure 6-10 Current in damper bar No. 2

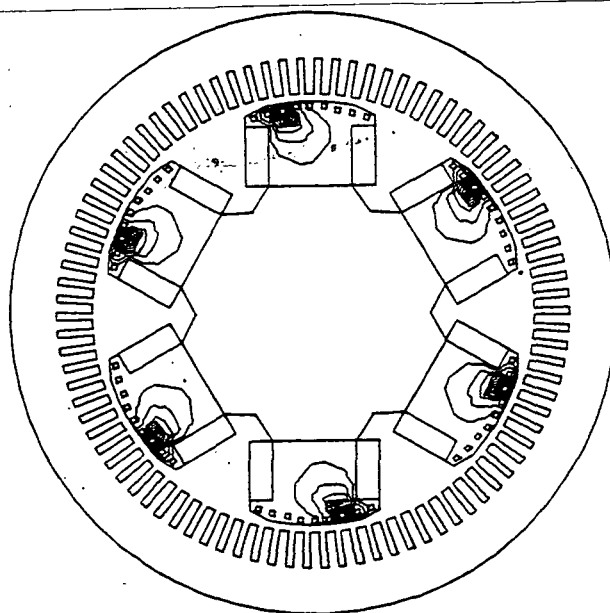


Figure 6-11 Current in damper bar No. 3

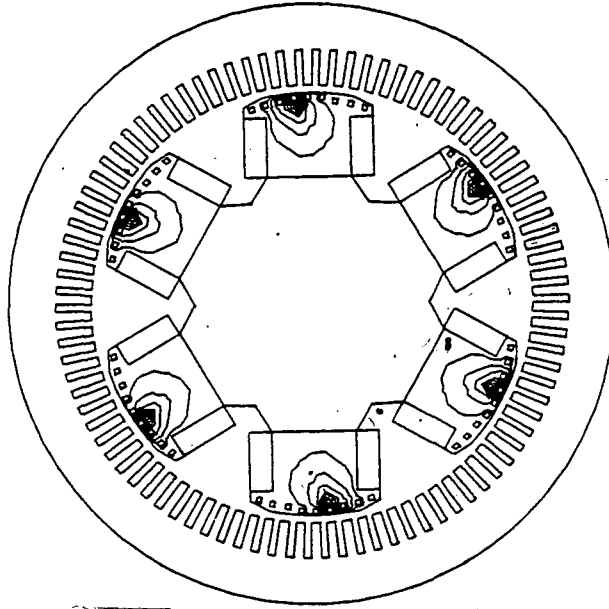


Figure 6-12 Current in damper bar No. 4

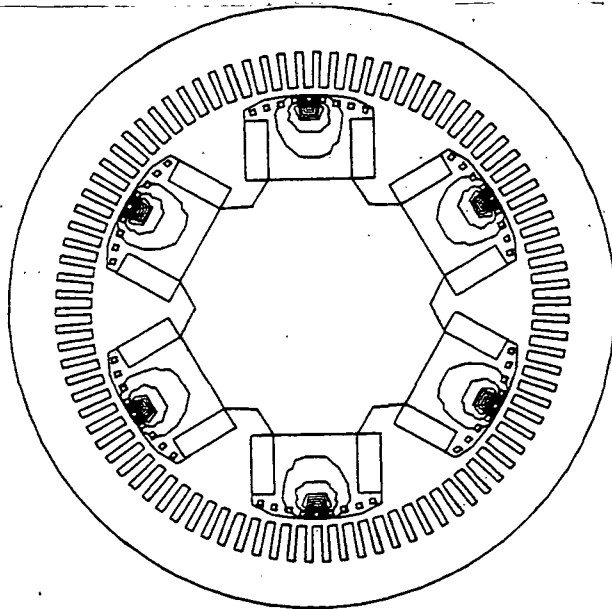


Figure 6-13 Current in damper bar No. 5

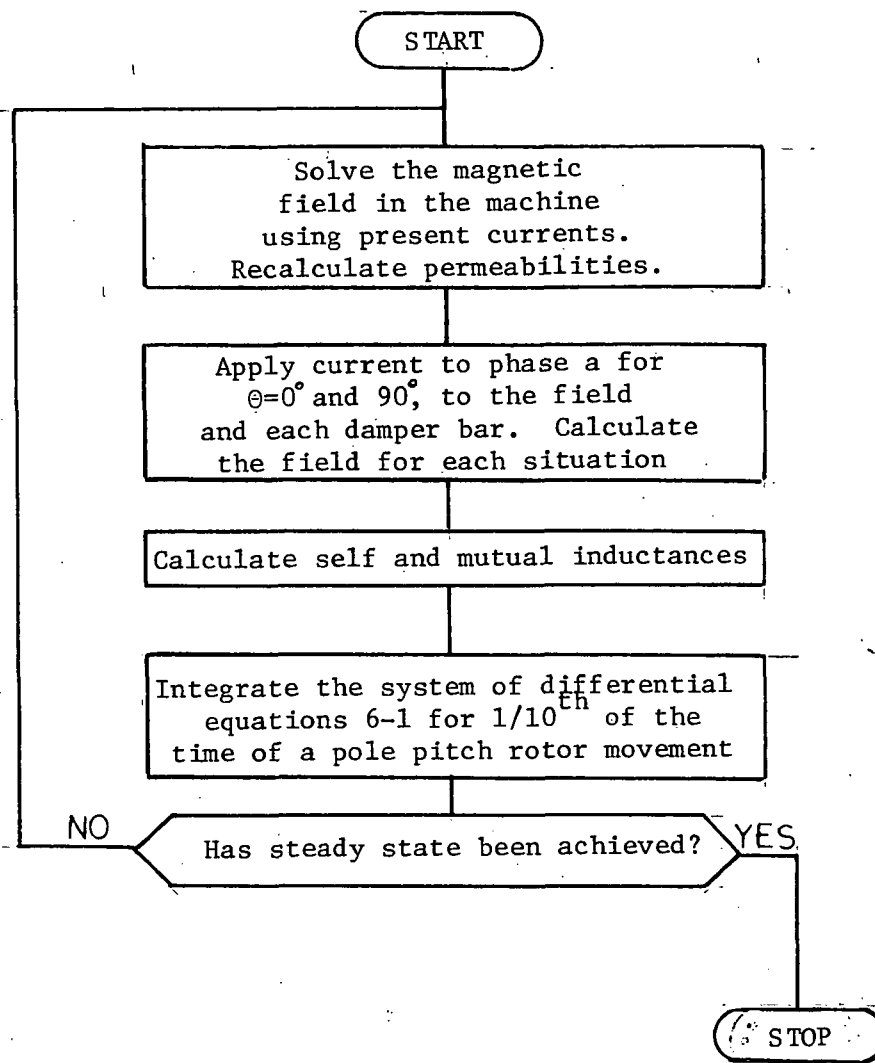


Figure 6-14 The algorithm for the starting of a synchronous machine

6.4 The Algorithm and the Integration Scheme

The saturation levels in the machine must be evaluated several times within a cycle, since, as is shown in Figures 6-23 to 6-31 the flux densities within the machine vary significantly during the movement of the rotor over one pole pitch. After the determination of the saturation levels, the self and mutual inductances must again be calculated as described in section 6.3. The system of differential equations (6.5) as modified in 6.3.1 or 6.3.2 to account for the voltage at the end rings is solved in the time domain using a predictor corrector method⁽⁴⁸⁾. At each time step the currents are printed and prepared for plotting, and the integral of their square calculated. The integration is stopped when steady state is reached.

Since there are no eddy currents in the iron portions of the machine, the torque, M , can be calculated faster and accurately by taking the partial derivatives of the coenergy of the field with respect to the angle:

$$M = \frac{\partial W}{\partial \theta} = \frac{1}{2} \sum_i \sum_j \frac{\partial L_{ij}}{\partial \theta} I_i I_j \quad (6-21)$$

and finally

$$i, j = a, b, c, f, 1, \dots, 9$$

$$M = \frac{1}{2} \frac{1}{\omega_s} \sum_i \sum_j \dot{L}_{ij} I_i I_j \quad (6-22)$$

The flow chart of this algorithm is given in Figure 6-14.

The currents and torque computed using this algorithm were compared to the results of a simulation of a start up of the same machine, based

on test data by J.R. Misage⁽⁴⁹⁾. The phase currents and torque from this simulation and results of sample runs are shown in Figures 6-15 and 6-16.

In Figures 6-17 to 6-20, the steady state currents in the phases the field and the damper bars are plotted as functions of time. They compare favorably with the current waveforms published by Jovanovski in 1969⁽²⁷⁻³⁰⁾, from test data and analytical calculations.

Figures 6-24 to 6-31 show the field in the machine for consecutive time instants when the angular velocity of the magnetomotive force is not the same as the angular velocity of the rotor; rather the machine is operating at a slip of 0.5. The time between two consecutive instants is one tenth of a cycle.

Figure 6-32 shows the torque oscillations for this case and for other slip values.

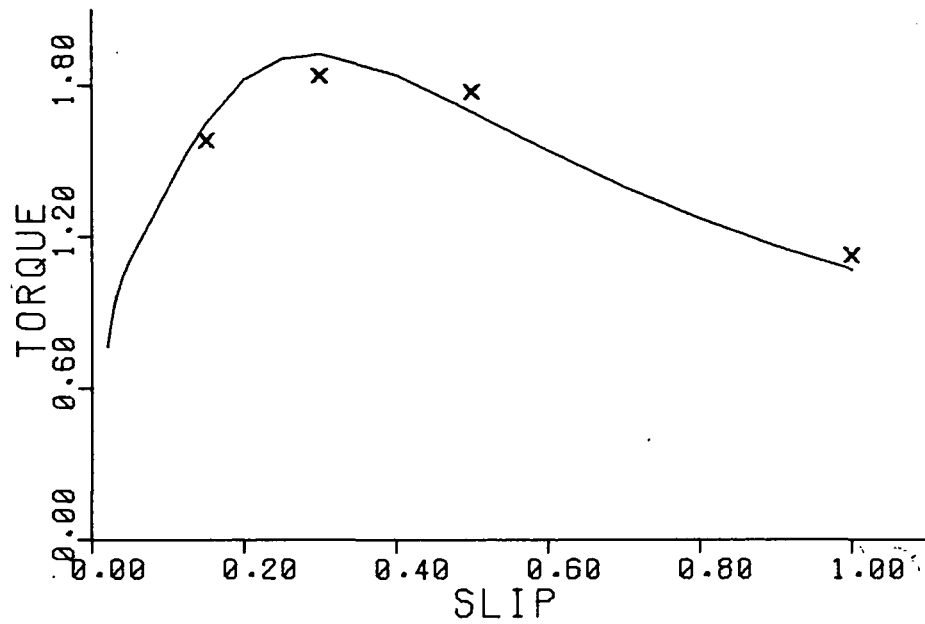


Figure 6-15 RMS values of current. The solid line depicts current calculated from a computer simulation based in test data, and x points resulting from this study

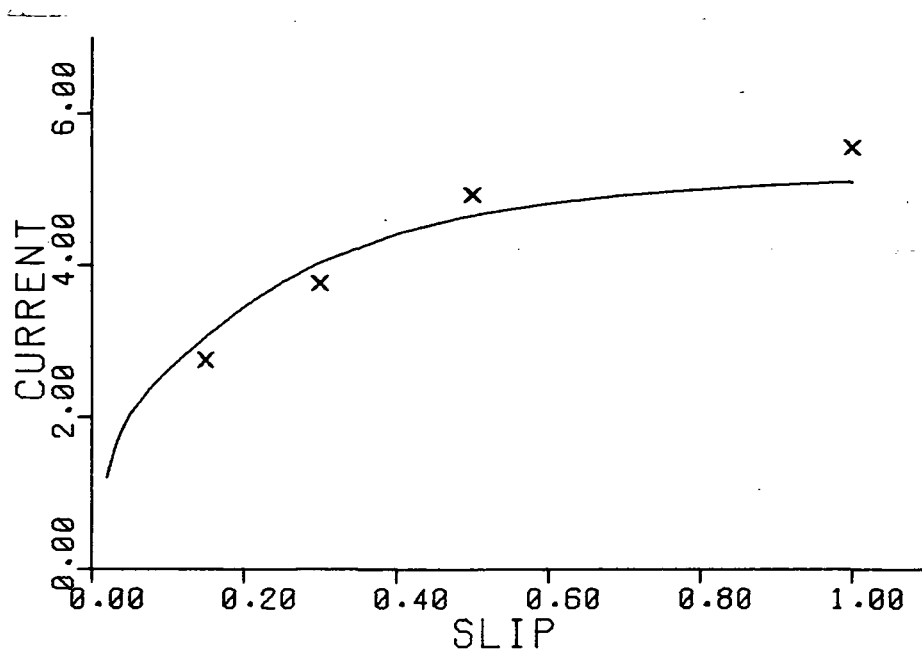
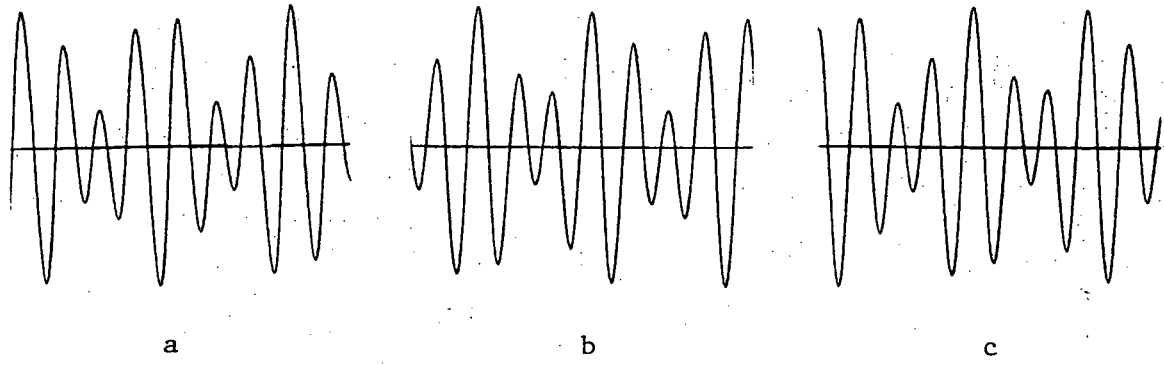
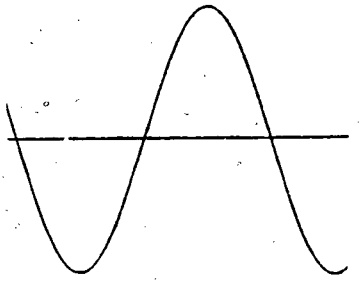
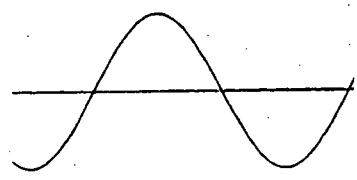


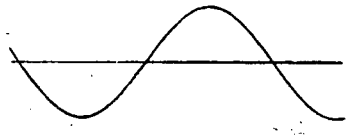
Figure 6-16 Average value of torque



.05 sec.



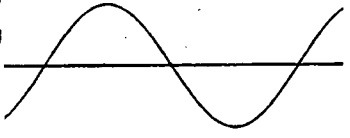
1



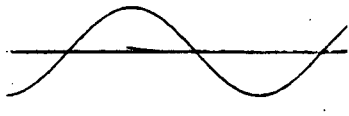
2



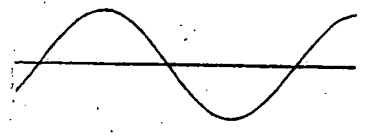
3



4



5



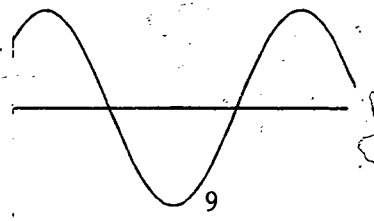
6



7



8



9

Figure 6-17 Currents in all 13 circuits
Slip = 0.15

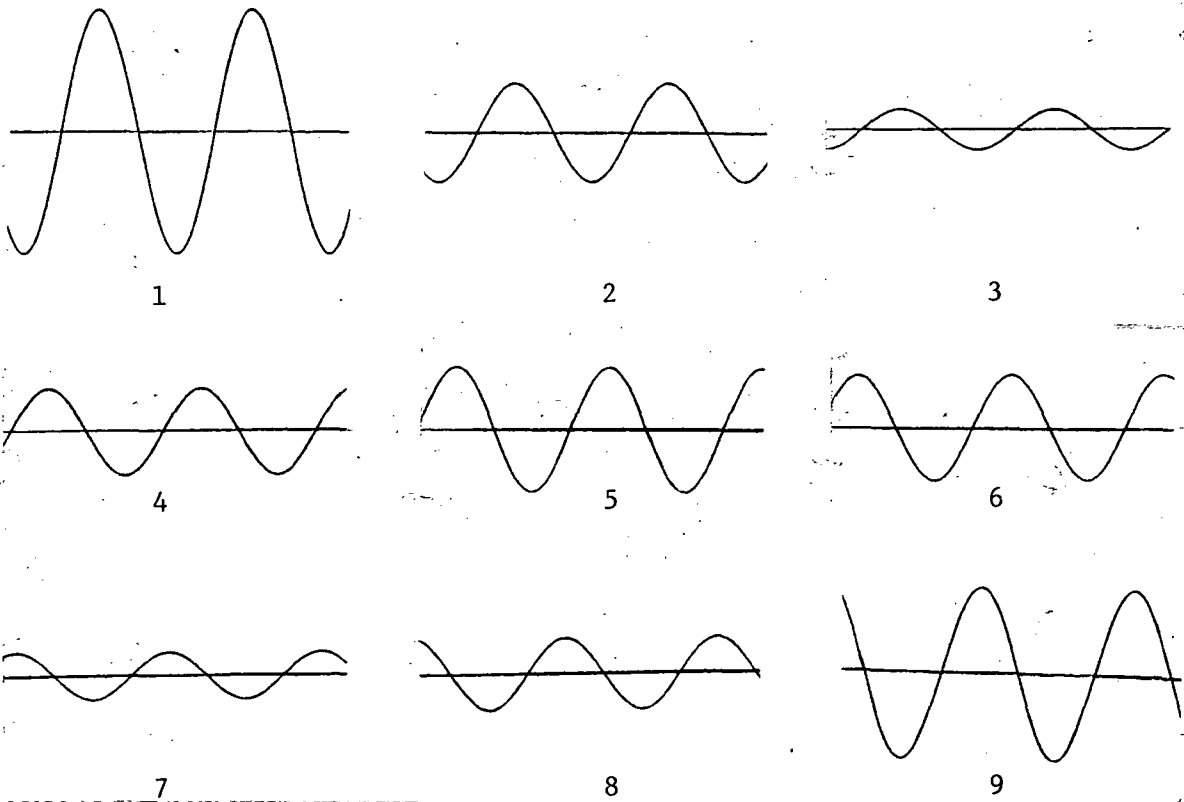
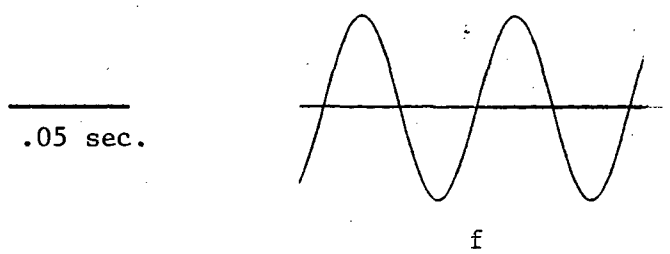
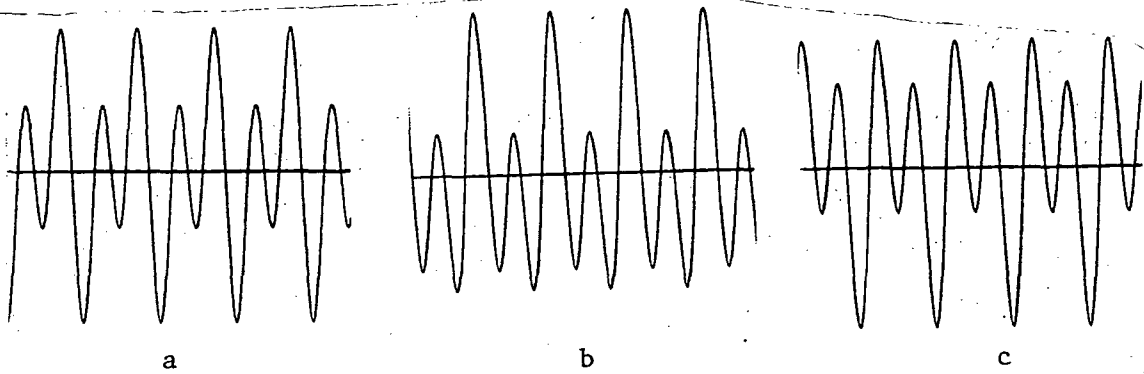


Figure 6-18 Currents in all 13 circuits
Slip = 0.25

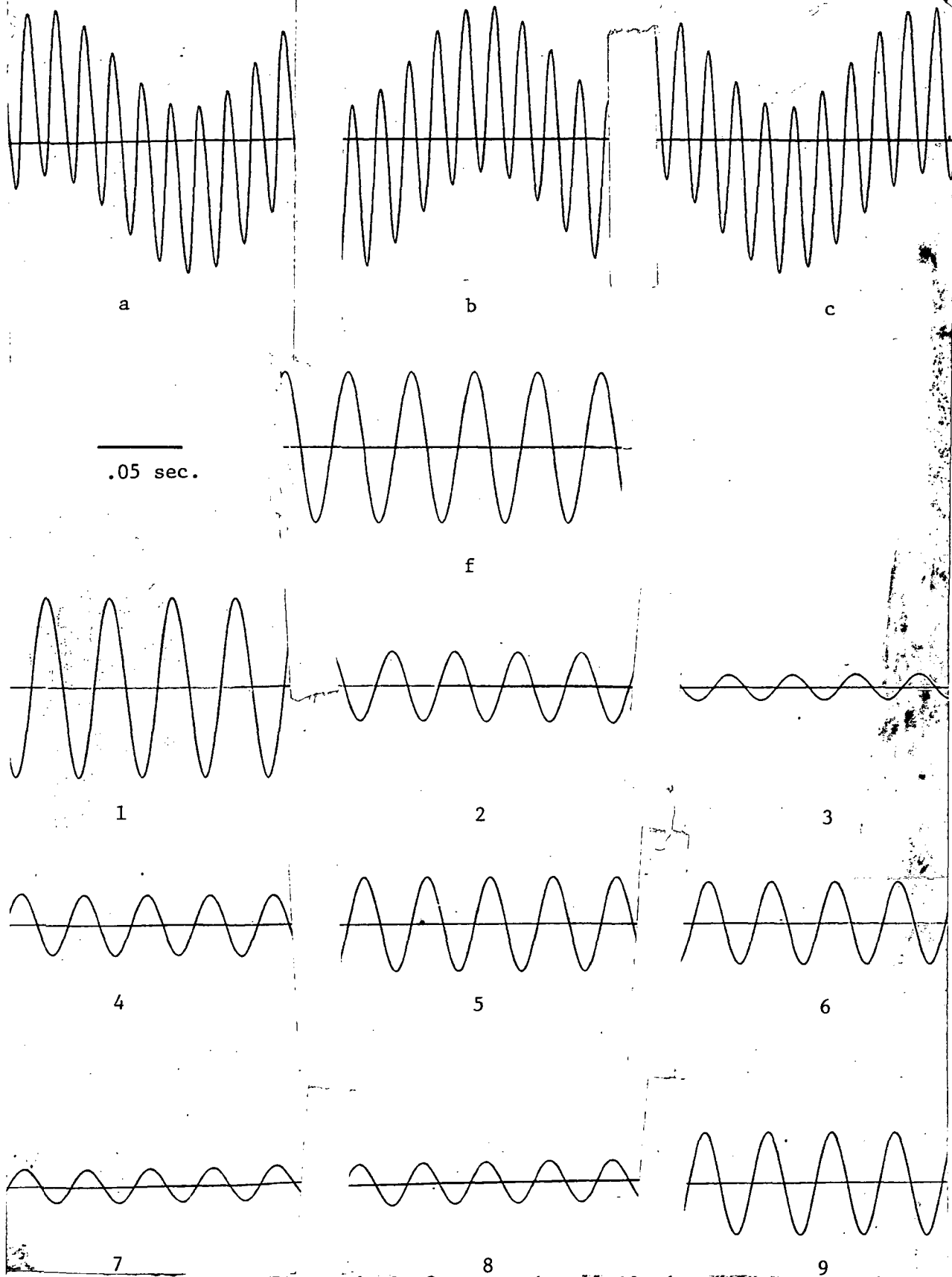


Figure 6-19 Currents in all 13 circuits
Slip = 0.45

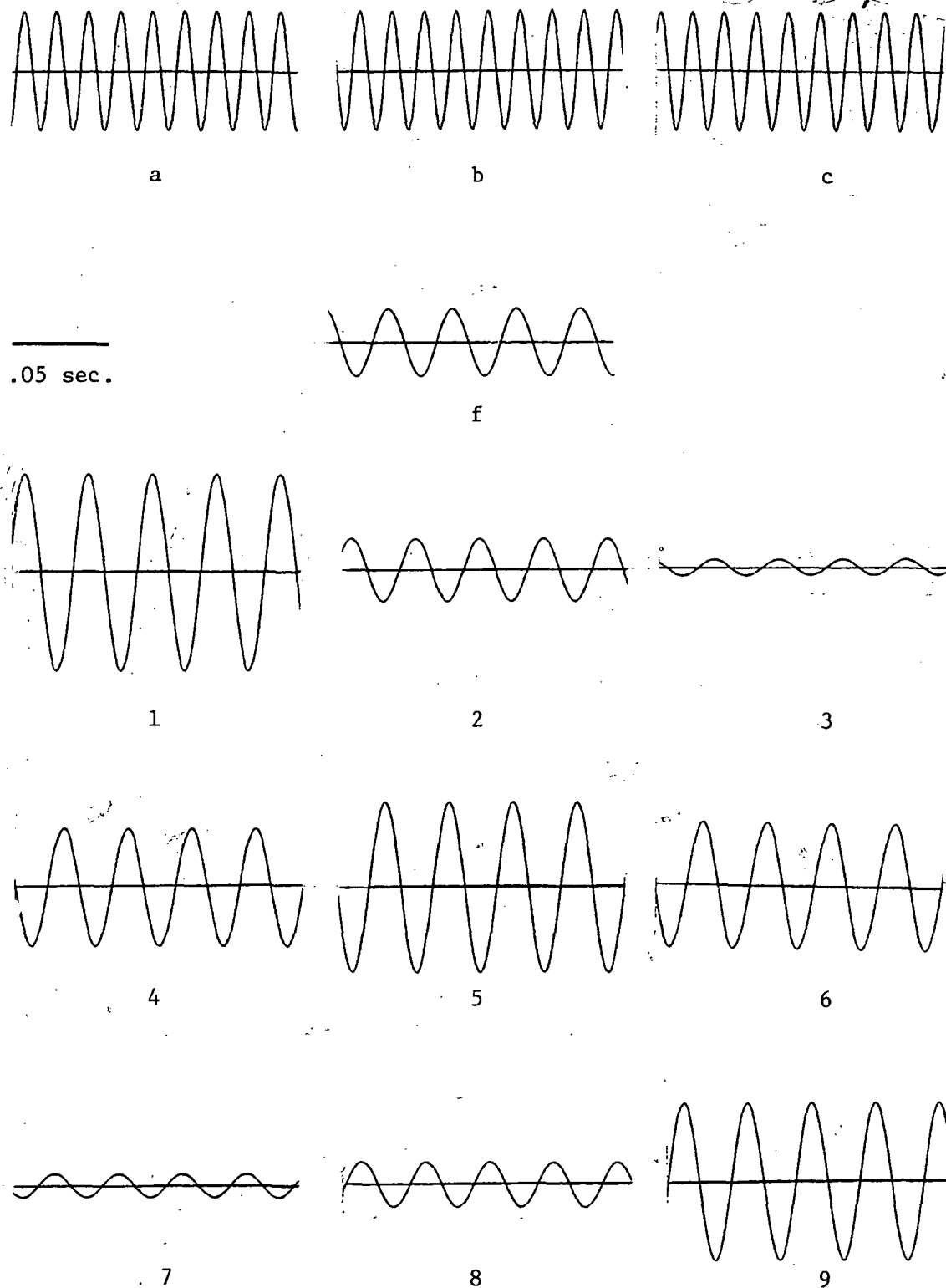


Figure 6-20 Currents in all 13 circuits
Slip = 0.5

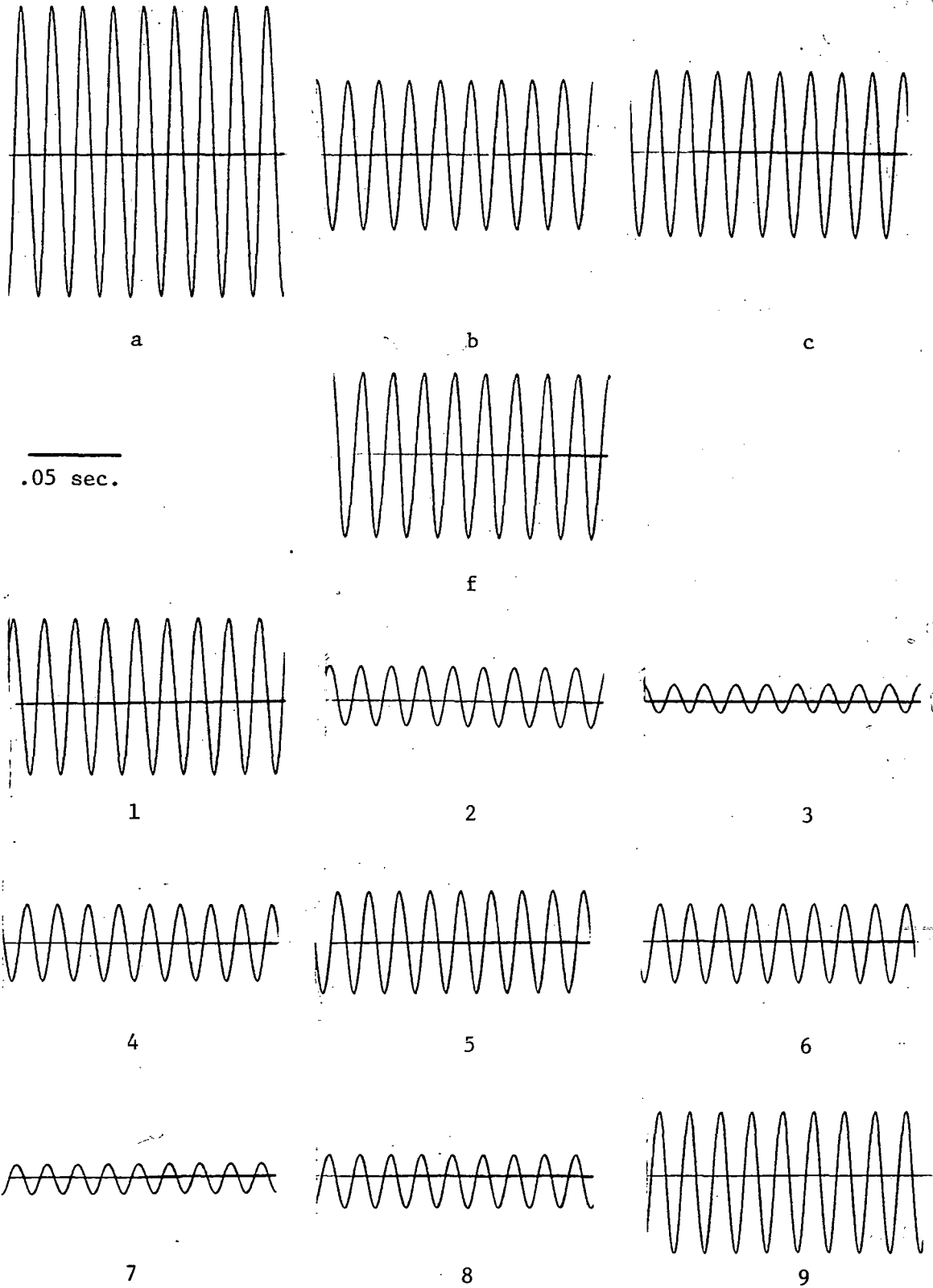


Figure 6-21 Currents in all 13 circuits
Slip = 1.00

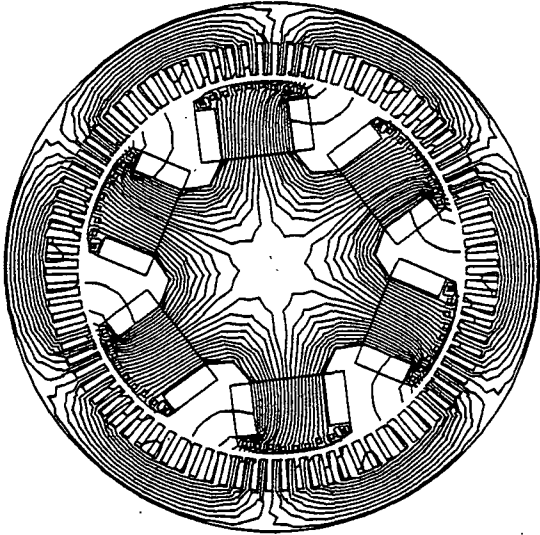


Figure 6-22
The field at a cross section. Step 1

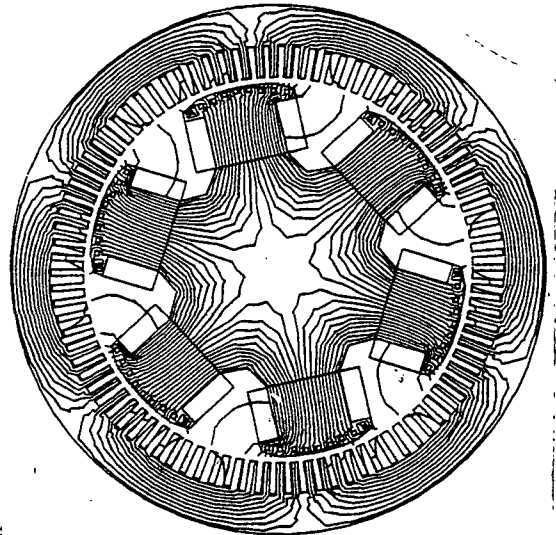


Figure 6-23
Step 2

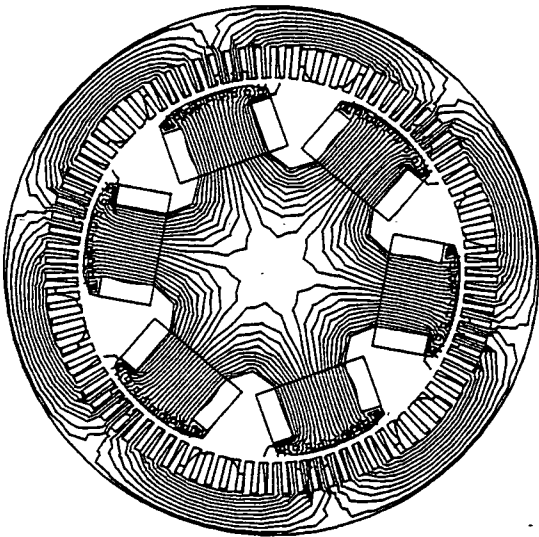


Figure 6-24
Step 3

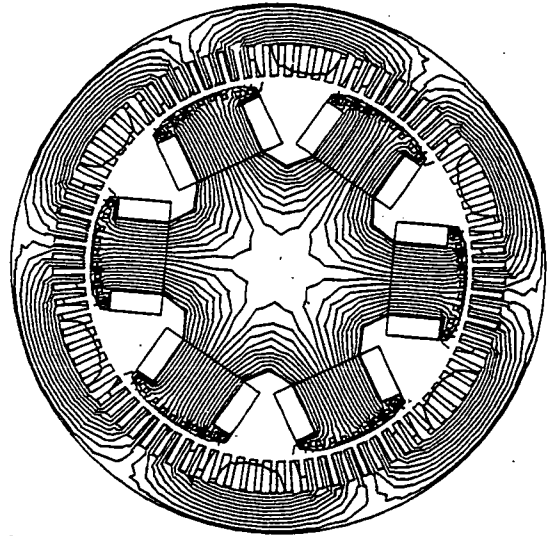


Figure 6-25
Step 4

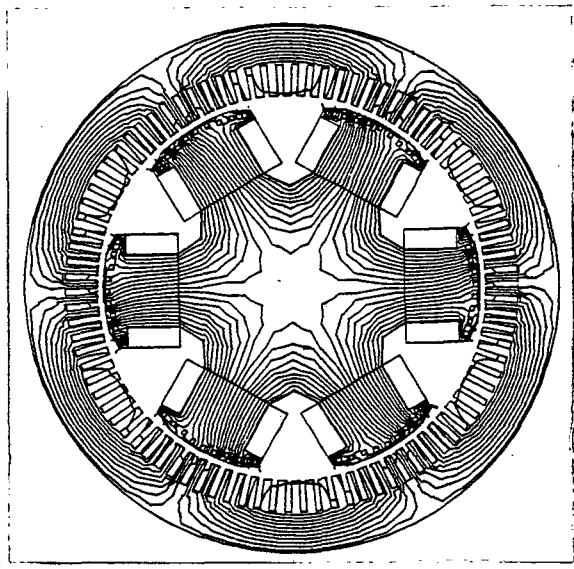


Figure 6-26
Step 5

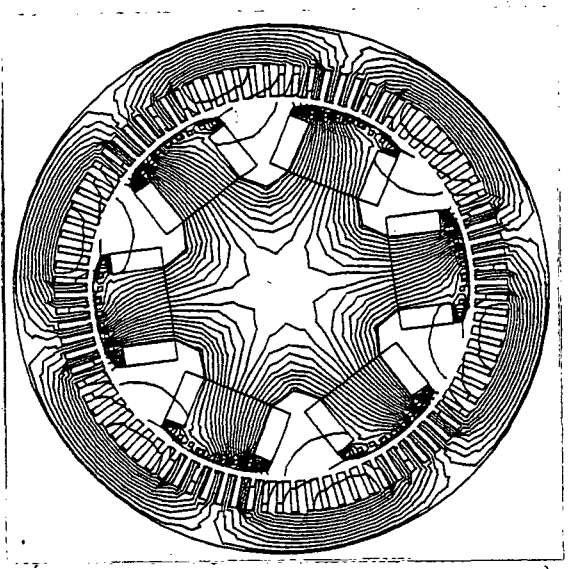


Figure 6-27
Step 6

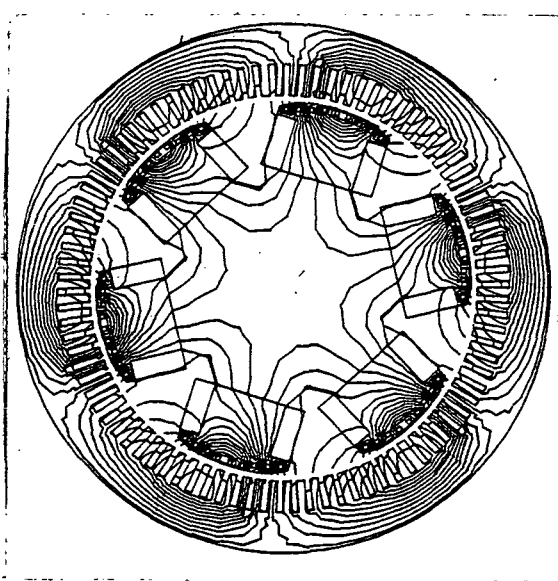


Figure 6-28
Step 7

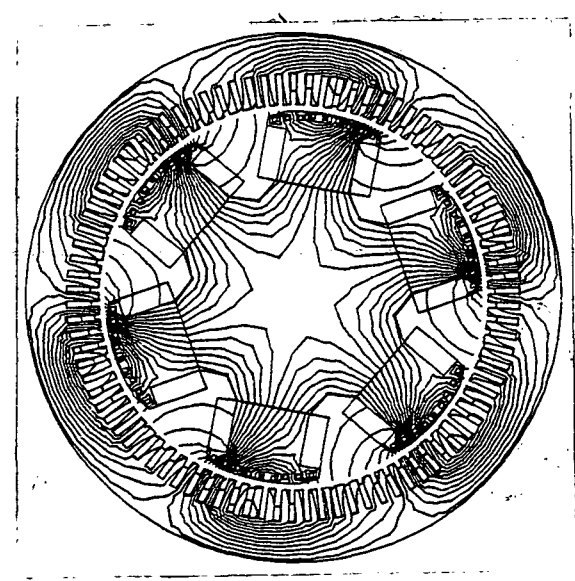


Figure 6-29
Step 8

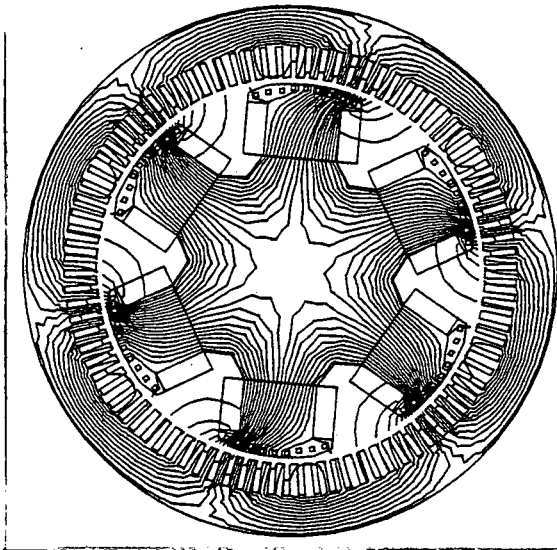


Figure 6-30
Step 9

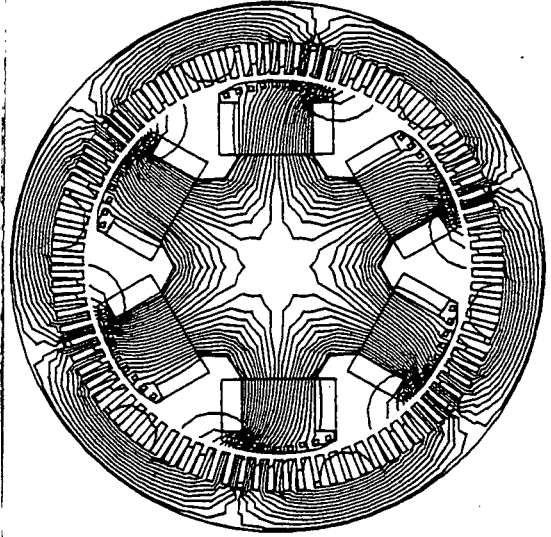


Figure 6-31
Step 10

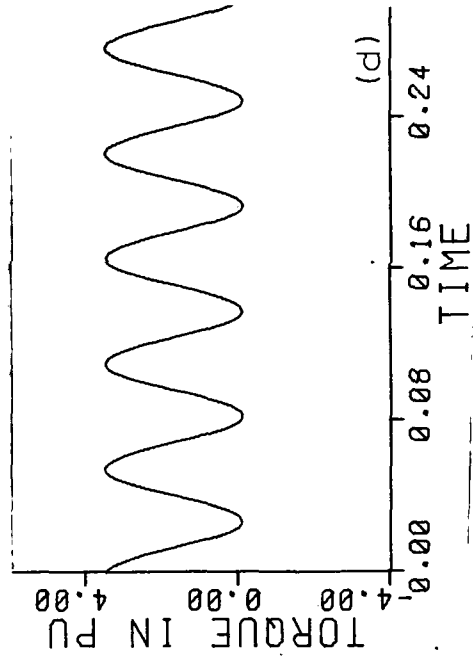
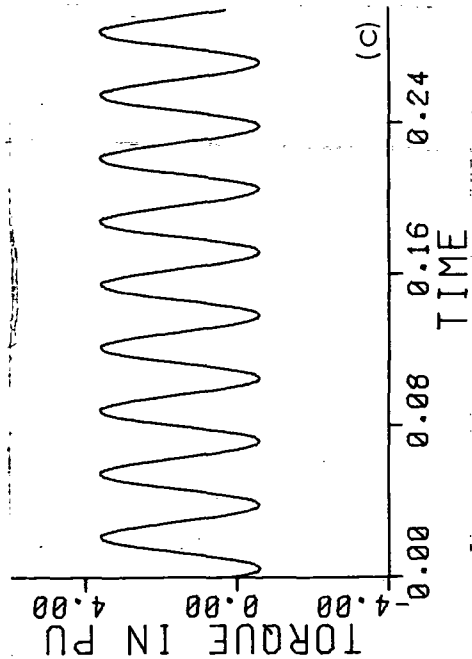
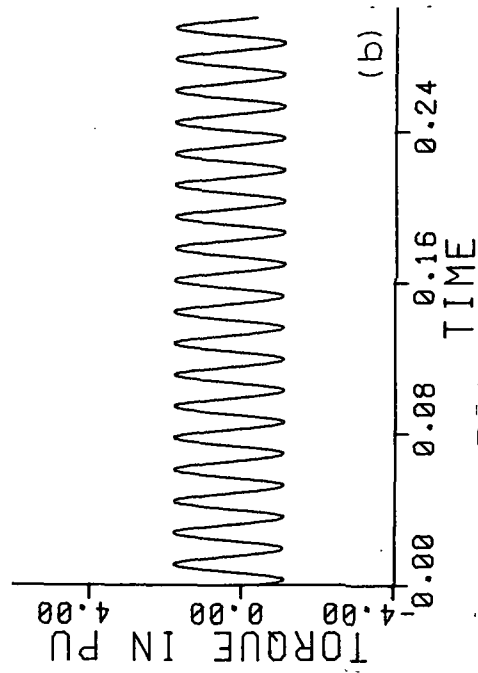
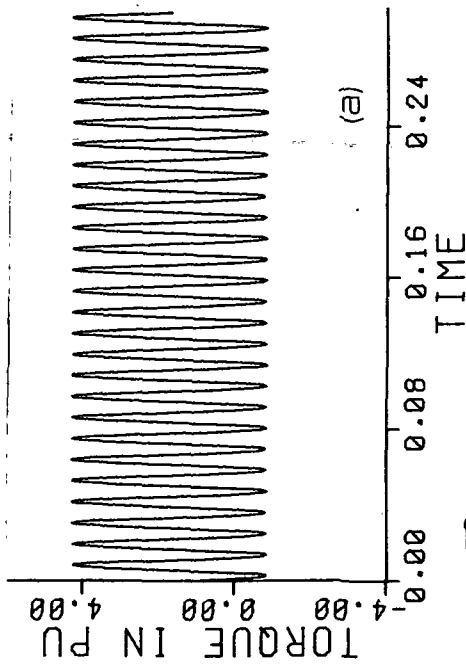


Figure 6-32 Torque at various slips.

7.0 CONCLUSIONS

The effects of saturation and eddy currents in magnetic materials render the conventionally defined inductances and other parameters of electrical machines inadequate to describe and predict the machine performance for modes of operation which cannot be categorized as steady state. The time dependent solution of the magnetic field was introduced in this investigation as a method for accounting for the variation, in time, of the machine parameters in predicting and analyzing the performance of the electrical machines.

In order to continuously model the electromagnetic field in the cross section of a machine, the method of time dependent finite element method was used, combined with an also time dependent construction of a grid for the air gap region. The Maxwell stress tensor was used to calculate the airgap torque from the magnetic vector potential distribution. Incremental inductances were defined and calculated as functions of time, depending on both eddy currents and saturation. The currents in all the machine circuits were calculated in the time domain based on these inductances, which were continuously updated. The method was applied to a chopper controlled DC series motor used for electric vehicle drive, and to a salient pole synchronous motor with damper bars. The simulation results were compared to experimentally obtained ones.

This technique, of continuously modeling the electromagnetic field in electrical machines was shown to provide an insight in the operation of machines and account for the effect of the eddy currents and saturation on the overall performance. The cases examined here do not exhaust

the capabilities of the method; neither do they define its limitations. The time dependent finite element method, although it requires repetitive solution of a system of linear equations, was shown to be a very powerful tool in taking into account nonlinearities and complex waveforms, and becomes more attractive when combined with a fast iterative solution scheme which reduces the overall computer time.

The application and suitability of such a scheme, i.e. the pre-conditioned conjugate gradient method, was investigated. The method was applied to the system of linear equations resulting from the finite element method and it was shown that it combines both the speed required for the solution of time dependent problems and the ability to handle the ill conditioned matrices resulting from elements in iron and air domains.

This work, as noted earlier, does not cover all the possible applications and aspects of the continuous modeling of the electromagnetic field. The accuracy of the solutions for the cases already examined can be increased by using a finer grid, both in the solid iron regions, to improve the calculation of eddy currents, and in the airgap to provide a finer distribution of the flux densities resulting in a more accurate evaluation of the torque through the Maxwell stress tensor.

The techniques used here can be applied to the skin and eddy current effects in solid conductors, either by constructing a finer grid for each of them, or by solving separately a small grid for one conductor bundle or one slot, every time the larger grid is solved. Application to separately excited or shunt DC machines and to the study of commutation, would be a further extension of this work, since two or more

circuits inductively coupled would be involved. Another possible application would be the case of solid salient pole machines during starting or transient mode. The calculation of the field, in many small machines in which neither the rotor is cylindrical nor the stator uniform, would be an interesting application of the time dependent computer generated grid for the airgap.

A final improvement to the techniques described here, would be the application of the Newton-Raphson method to the calculation of the permeability of the iron. The underrelaxation method was preferred here merely because of the simplicity of the involved programming, but at the expense of computational time.

BIBLIOGRAPHY

1. E.A. Erdelyi and E.F. Fuchs, "Nonlinear Magnetic Analysis of DC Machines - Part I: Theoretical Fundamentals," IEEE Transactions on Power Apparatus and Systems, September-October 1970, pp. 1546-1554.
2. E.F. Fuchs and E.A. Erdelyi, "Nonlinear Magnetic Analysis of DC Machines - Part II: Application of the Improved Treatment," IEEE Transactions on Power Apparatus and Systems, September-October 1970 pp. 1555-1564.
3. E.F. Fuchs and E.A. Erdelyi, "Determination of Waterwheel Alternator Inductances from Flux Plots," IEEE Transactions on Power Apparatus and Systems, November-December 1972, pp. 2510-2517.
4. E.F. Fuchs and E.A. Erdelyi, "Nonlinear Theory of Turboalternators - Part I: Magnetic Fields at No Load and Balanced Loads," IEEE Transactions on Power Apparatus and Systems, March-April 1973, pp. 583-591.
5. E.F. Fuchs and E.A. Erdelyi, "Nonlinear Theory of Turboalternators - Part II: Load Dependent Synchronous Reactances," IEEE Transactions on Power Apparatus and Systems, March-April 1973, pp. 592-599.
6. N.A. Demerdash and H.B. Hamilton, "Simulation for Design Purposes of Magnetic Fields in Turbogenerators with Symmetrical and Asymmetrical Rotors - Part II: Model Calibration and Applications," IEEE Transactions on Power Apparatus and Systems, September-October 1972, pp. 1992-1999.
7. N.A. Demerdash and H.B. Hamilton, "Simulation for Design Purposes of Magnetic Fields in Turbogenerators with Symmetrical and Asymmetrical Rotors - Part III: Flux Distribution Under Load," IEEE Transactions on Power Apparatus and Systems, November-December 1979, p. 1729.
8. S.J. Salon, "The Use of Distributed Parameter Rotor Models in AC Machine Analysis," (unpublished Ph.D. Dissertation, School of Engineering, University of Pittsburgh, 1976).
9. M.V.K. Chari and P. Silvester, "Analysis of Turbo-alternator Magnetic Field by Finite Elements," IEEE Transactions on Power Apparatus and Systems, March-April 1971, pp. 454-469.
10. N.A. Demerdash and T.W. Nehl, "An Evaluation of the Methods of Finite Elements and Finite Differences in the Solution of Nonlinear Electromagnetic Fields," IEEE Paper F 78020-0, 1977.

11. A. Foggia, J.C. Sabonnaidiere and P. Silvester, "Finite Element Solution of Saturated Travelling Magnetic Field Problems," IEEE Transactions on Power Apparatus and Systems, May-June 1975, pp. 866-871.
12. S. Douglas, Jr. and T. DuPont, "Galerkin Methods for Parabolic Equations," SIAM Journal of Numerical Analysis, Vol. 7, No. 4, December 1970, pp. 575-626.
13. T.M. Linville, "Starting Performance of Salient Pole Synchronous Motors," AIEE Transactions, April 1930, pp. 531547.
14. G.O. Goodwin, "The Nature of A.C. Machine Torques," IEEE Transactions on Power Apparatus and Systems, Vol. PAS-95, No. 1, January-February 1976, p. 145-153.
15. E.D. Goodman, "Steady state and transient torque of a synchronous motor," (unpublished doctoral thesis, McGill University, Montreal, Canada, 1975).
16. K. Kato and K. Tsuboi, "Asynchronous Starting Characteristics of Salient Pole Synchronous Machines with Damper Windings - Effect of Conductor Bars Between Poles," Electrical Engineering in Japan, Vol. 91, No. 2, 1971, pp. 127-134.
17. G. Pasqualini, "Etude general du regime transitoire au demarrage d'une machine synchrone," Revue General de Electricite Tome 84, No. 12, Dec., 1975.
18. F. Notelet, "Courants et couple transitoires lors du demarrage du moteur synchrone avec inducteur ouvert," Revue General de Electricite Tome 84, No. 12, Dec. 1975.
19. A. Horrath, "Fluctuating Torsional Vibrations when Running up a Turbo-Compressor Asynchronously, by Means of a Salient-Pole Synchronous Motor," The Brown Boveri Review, June-July 1963, p. 417.
20. E. Alwers, K. Baltisberger, R. Grabirz, "Asynchronous Starting of Synchronous Machines for Pumped Storage Schemes," The Brown Boveri Review, 59, 1972, pp. 6167.
21. M. Canay, "Asynchronous Starting of Synchronous Machines With or Without Rectifiers in the Field Circuit," Proceedings IEEE, 119, 1972, p. 1701.
22. M. Canay, "Asynchronous Starting of a 230 MVA Synchronous Machine in 'Vianden 10' Pumped Storage Station," The Brown Boveri Review, Vol. 61, No. 7, 1974, p. 313.

23. P.K. Sattler, "Erwärmung der massiven Polschuhe von Synchronmotoren bei Asynchronen Anlauf," Electrotechnische Zeitschrift-A Bd83, #24, 1962, pp. 807-811.
24. E.Alwers, "Das Anfahren von Gasturbinen in Frequenzanlauf nach Unger," Electrotechnische Zeitschrift-A, Bd92 (1971) H.10 p. 563-566.
25. P.H. Barret, "Computation of Electromagnetic, Thermal and Mechanical Quantities During Asynchronous Starting of Solid Salient Pole Synchronous Machines," IEEE-PES Paper, F80 172-7, presented at the Winter Power Meeting, 3-8 Feb. 1980, New York.
26. E.D. Goodman, "Steady State and Transient Torque of a Synchronous Motor," (unpublished Ph.D. Dissertation, McGill University, Montreal, Canada, 1975).
27. S.B. Jovanovski, "Calculation and Testing of Damper Winding Current Distribution in a Synchronous Machine with Salient Poles," IEEE Transactions on Power Apparatus and Systems, November 1969, pp. 1611-1619.
28. S.B. Jovanovski, "The Quadrature-Axis Equivalent Circuit of a Synchronous Machine with a Grill," IEEE Transactions on Power Apparatus and Systems, November 1969, pp. 1620-1624.
29. S.B. Jovanovski, "Contribution to the Theory of Asynchronous Performance of Synchronous Machines with Salient Poles: Part I - Analysis of MMF and Magnetic Field Space Variations and Armature Current Time Pulsations," IEEE Transactions on Power Apparatus and Systems, July 1969, pp. 1150-1161.
30. S.B. Jovanovski and S.A.A. Hamman, "Contribution to the Theory of Asynchronous Performance of Synchronous Machines with Salient Poles: Part II - Analysis of MMF and Magnetic Field Angular Velocity - Power and Torque Calculations," IEEE Transactions on Power Apparatus and Systems, March-April 1971, pp. 418-426.
31. E. Arnold, J.L. LaCour, A. Fränkel, Wechselstrom-Kommutator Maschinen (Berlin: Springer-Verlag 1912).
32. P.W. Franklin, "Theory of the DC Motor Controlled by Power Pulses. Part I - Motor Application," IEEE Transactions on Power Apparatus and Systems, January-February 1972, pp. 249-255.
33. P.W. Franklin, "Theory of the DC Motor Controlled by Power Pulses. Part II - Breaking Methods, Commutation and Additional Losses," IEEE Transactions on Power Apparatus and Systems, January-February 1972, pp. 256-262.
34. F.T. DeWolf, "Measurement of Inductance of DC Machines," IEEE Transactions on Power Apparatus and Systems, September-October 1972, pp. 1636-1644.

35. H.B. Hamilton and E. Strangas, "Series Rotor Parameter Variations as a Function of Frequency and Saturation," IEEE PES Paper, F80 151-1 presented in the Winter Power Meeting, New York, Feb. 3-8, 1980.
36. W.K.H. Panofski and M. Phillips, Classical Electricity and Magnetism, (Addison-Wesley 1962).
37. M.V.K. Chari, "Finite Element Solution of Magnetic and Electric Field Problems in Electrical Machines and Devices," GE Report No. 76 CRD-12, May 1976.
38. J.T. Oden and J.N. Reddy, An Introduction to the Mathematical Theory of Finite Elements, (Wiley Interscience, 1976).
39. R.S. Varga, Matrix Iterative Analysis (Prentice Hall 1962).
40. J.R. Whitman, ed., The Mathematics of Finite Elements and Applications, "The Analysis and Application of Sparse Matrix Algorithms in the Finite Element Method by D.J. Evans" (Academic Press, 1973), pp. 427-447.
41. D.J. Evans, "The Use of Pre-conditioning in Iterative Methods for Solving Linear Equations with Symmetric Positive Definite Matrices," J. Inst. Maths. Applics., 1967, 4, pp. 295-314.
42. David G. Luenberger, Introduction to Linear and Nonlinear Programming (Addison Wesley, 1965), pp. 133-178.
43. J.K. Reid, ed., Large Sparse Sets of Linear Equations, "On the Method of Conjugate Gradients for the Solution of Large Sparse Systems of Linear Equations, by J.K. Reid" (Academic Press, 1971).
44. G. Dahlquist and A. Björk, Numerical Methods (Prentice Hall, 1967), p. 235.
45. A.S. Langsdorf, Principles of Direct Current Machines, (McGraw Hill, 1959).
46. C. Concordia, Synchronous Machines, Theory and Performance (J. Wiley and Sons, 1951).
47. L.A. Kilgore, "Calculation of Synchronous Machine Constants," Transactions of AIEE, Vol. 50, 1931, pp. 1201-1213.
48. C.W. Gear, "The Automatic Integration of Ordinary Differential Equations," Communications of the AClI, March 1971, Vol. 14, No. 3.
49. J.R. Misage, "Transient Torque Buildups During Starting of Excavator MG Sets," Presented at the thirtieth annual meeting, Open Pit Mining Association, June 6, 1974, Louisville, Kentucky.